ROLE OF ELECTRON-LATTICE INTERACTION IN LATTICE DYNAMICS AND SUPERCONDUCTIVITY OF PHOSPHORUS

MASATO AOKI

February 1987

Abstract

Recent success in growing large single-crystal of black phosphorus has been motivating many intensive investigations of the physical properties of phosphorus. Particuraly the pressure-induced frequency-softening of a particular phonon mode (LAx mode) observed in the orthorombic black phosphorus and the fairly high superconducting transition temperature, as well as its pressure dependence, observed in the simple-cubic phosphorus have been received considerable attention. These characteristic phenomena are expected to be related with the strong electron-lattice interaction.

In part I a role of the electron-lattice interaction in the lattice dynamics of black phosphorus, which is a narrow gap semiconductor, has been studied from the microscopic point of view. The electron-lattice coupling constants are derived on the basis of tight-binding calculations of the electronic band structure and the generalized electronic susceptibility is calculated. From these results the interplanar forces are evaluated. Reflecting the narrow gap of this substance, the interplanar forces take significant values even for far neighboring planes. Further, owing to considerable decrease of the energy gap induced by pressure, the interplanar forces reveal characteristic pressure dependences. These effective forces combined with short range repulsive forces appropriately chosen explain qualitatively the observed pressure dependence of the phonon dispersion curves. Particularly we emphasize that the

effective interplanar forces caused by the electron-lattice ineraction are important to explain the pressure-induced frequency-softening of the LAx mode as observed.

In part II a role of the electron-lattice interaction in the superconductivity observed in the simple-cubic phosphorus, which is stabilized above 110 kbar, has been studied. First we calculate the electronic band by the self-consistent augmented plane wave (APW) method. The density of states (DOS) and the Fermi surfaces are calculated and pressure effects on them are studied. As pressure increases from 132 kbar to 304 kbar, a change of the total DOS at the Fermi level, $D(E_F)$, is found to be quite small, but a remarkable change is found for some particular Fermi surfaces. The small value of $D(E_F)$ and fairly high superconducting transition temperature, such as 5∿11 K, suggest that the simple-cubic phosphorus is a system having the strong electron-phonon interaction. Therefore we have calculated the electron-lattice matrix elements on the basis of the rigid muffin-tin approximation, using the electronic band structure calculated by APW method. By averaging the electron-lattice matrix elements over the Fermi surface, we have evaluated Tc in accordance with McMillan-Allen-Dynes equation. Tc is obtained to be 3∿10 K for 132 kbar and 4∿11 K for 304 kbar. The order of magnitude of Tc is in good agreement with the observed one. As for the pressure effect on Tc, the calculated result shows rather small pressure dependence of T_c compared with that observed by Akahama et al. This disagreement might be due to a rough estimation of the phonon frequencies.

Acknowledgements

The author would like to express his sincere thanks to Professor K. Motizuki, under whose guidance this work was done, for valuable discussions and suggestions and to Dr. N. Suzuki for helpful and stimulative discussions and valuable comments. Also he thanks for their help in preparing the manuscript. Without their help and contiuous encouragements, this work would not have been completed. Thanks are also due to Professor Y. Yamada and Professor Y. Fujii for their preprint on the inelastic neutron scattering measurements of black phosphorus. He also thanks Professor S. Endo and Dr. Y. Akahama for some valuable comments and data of the superconductivity of simple-cubic phosphorus. He is grateful to Dr. K. Katoh for useful comments on the APW calculations.

We wish to thank Professor A. Yanase for providing us the computer programs for APW calculation and for drawing Fermi surfaces developed by him.

CONTENTS

PART II. ELECTRONIC BAND STRUCTURE AND SUPERCONDUCTIBITY IN SIMPLE-CUBIC PHOSPHORUS

PART I

ELECTRON-LATTICE INTERACTION AND LATTICE DYNAMICS IN BLACK PHOSPHORUS

§1. Introduction

Recent success in growing relatively large single crystals of black phosphorus (BP)[1,2] has stimulated many experimental and theoretical studies of its physical properties. BP is an interesting material from various points of view:

(1) it is an elemental semiconductor of narrow gap ($E_g \simeq$ 0.3 eV)[3,4],

(2) it is a layered system consisting of puckered layers[5,6],

(3) as pressure is increased, it shows a successive phase transition such as semiconductor (orthorhombic, A11) to semimetal (rhombohedral, A7) and to metal (simple cubic).[6-8]

(4) in its cubic phase it becomes a superconductor with a fairly high transition temperature Tc= 5∿11 K.[9-12]

BP is an attractive system also from the lattice dynamical point of veiw. According to inelastic neutron scattering measurements at normal and at high pressure,[13] the whole of the longitudinal acoustic mode (LAx mode) along the [100] direction shows definite softening with increasing pressure, as shown in Fig.1-1, whereas the other acoustic phonon branches show hardening in the pressure range of (0-15) kbar. This LAx acoustical mode corresponds to the accordion motion of the puckered layer and affects strongly the bond angle of P atoms. Hence, this mode is expected to be strongly coupled with electrons. Thus it is speculated that the softening of the LAx mode with increasing pressure is related with the electron-lattice interaction.

Thus far, lattice dynamical calculation at normal pressure

has been performed by Kaneta, Katayama-Yoshida and Morita[14] on the basis of the valence force field model, and by Kaneta and Morita[15] on the basis of the adiabatic bond charge model. The results obtained from the latter model can explain well the data obtained by inelastic neutron scattering,[13] infrared absorption [16], Raman scattering[16,17], and specific heat measurements.[18] However, there has been no attempt to explain the characteristic pressure dependence of the phonon frequencies mentioned above. The aim of the present study is to investigate microscopically the coupling between the electrons and the lattice and to clarify the origin of the softening of the LAx mode caused by pressure.

In §2 the crystal structure and the Brillouin zone of BP are described and the electronic band structure is calculated on the basis of the tight-binding method with use of the extended Hückel approximation. We discuss also effects of pressure on the band structure.

In §3 the electron-lattice interaction is derived microscopically on the basis of the tight-binding method and the generalized electronic susceptibility, $\chi^{\alpha\beta}(ij,q)$, is calculated for BP. A possible origin of the softening of the LAx mode is discussed.

In §4 the interplanar forces along the [100] direction caused by the electron-lattice interaction are evaluated from the generalized electronic susceptibility obtained in §3.

In §5 lattice dynamics is studied for 15 kbar as well as for normal pressure. The origin of softening of the LAx mode caused by pressure is discussed in detail.

Finally, §6 is devoted to some remarks and conclusion.

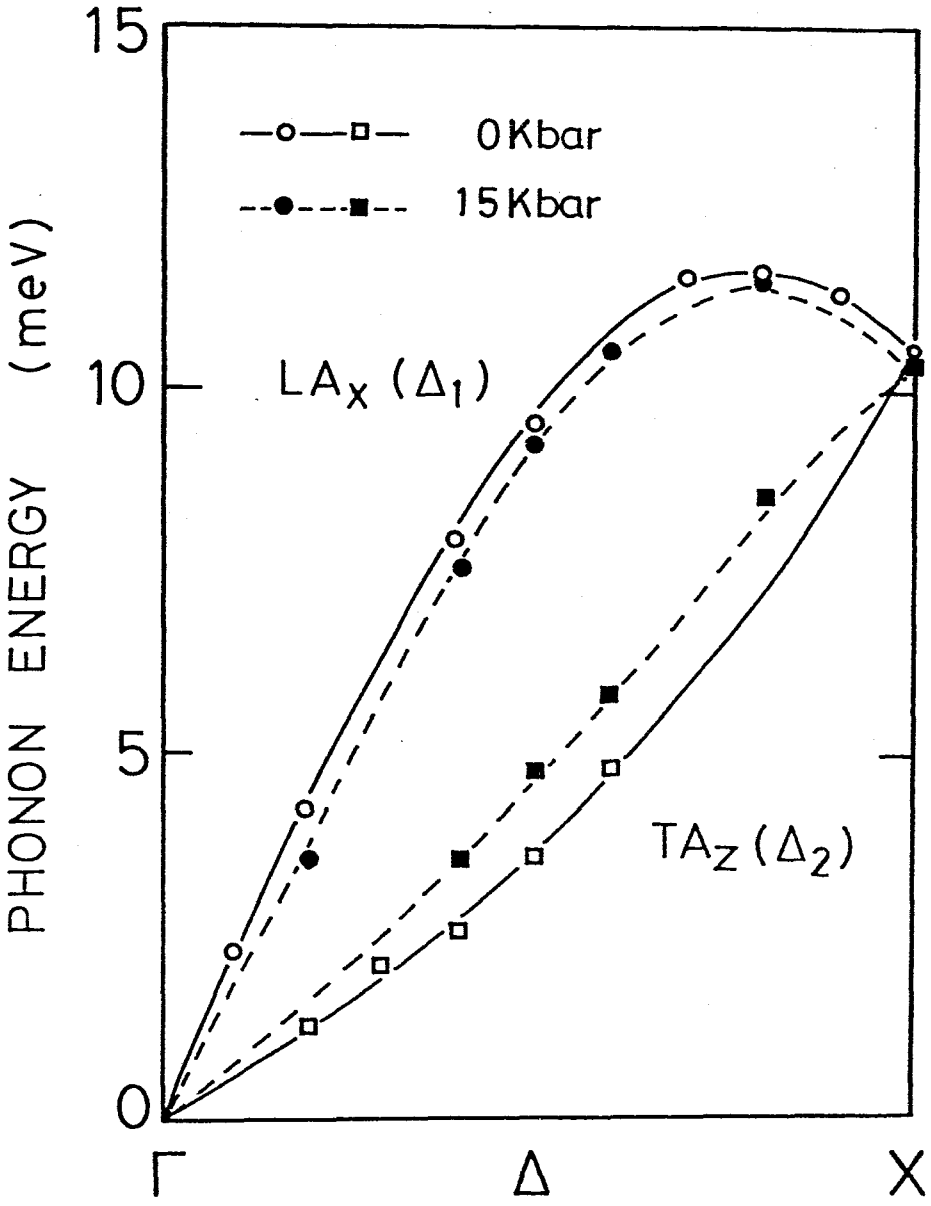

Fig.1-1 Phonon dispersion of two acoustic modes, LAx(Δ_1) and TAz(Δ_2), observed by inelastic neutron scattering.[13] The full and broken curves are drawn only for the guide to eye.

§2. Tight-Binding Calculation of Electronic Band Structure

2-1 Crystal Structure

The crystal structure of BP is orthorhombic (space group D_{2h}^{18}) and consists of puckered layers as shown in Fig.2-1. Atomic positions in this orthohombic lattice are specified by three latttice constants, a, b,and c, and two structure parameters, u and v. The primitive translational vectors are

$$\mathbf{a}_1=(c,0,0), \tag{2.1a}$$
$$\mathbf{a}_2=(0,a/2,b/2), \tag{2.1b}$$
$$\mathbf{a}_3=(0,-a/2,b/2). \tag{2.1c}$$

Four atoms in the primitive unit cell are located at the following points:

$$\tau_1=(uc,0,vb), \qquad \tau_2=-\tau_1,$$
$$\tau_3=(c/2-uc,a/2,vb), \quad \tau_4=-\tau_3. \tag{2.2}$$

Here the inversion center is chosen as the origin.

The point group of this crystal is D_{2h} with eight operations: $E,C_{2x},C_{2y},C_{2z},I,\sigma_x,\sigma_y,\sigma_z$. Half of these operations, namely C_{2x},C_{2z},σ_x,and σ_z, are accompanied by non-primitive translation

$$\tau=(c/2,0,b/2). \tag{2.3}$$

Within a layer, P atoms are covalently bonded each other through the 3p electrons to form the zig-zag chain along the y-direction and puckered arrangements along the x-direction. The layers are loosely bound by weak van der Waals forces. Cartz et al. have determined the crystal structure parameters from the neutron diffraction measurements.[19] Their values at normal pressure (at 15 kbar) are

a=3.3133 (3.3116) A, b=10.473 (10.260) A, c=4.374 (4.289) A
u=0.0806 (0.0782), v=0.1034 (0.1050).

Reflecting the covalent bonding of the zig-zag chain, compressibility with respect to the y-direction is fairly small.[19] The change of the lattce constant c with increasing pressre arises mainly from the change of the distance between the zig-zag chains, and the width of a zig-zag chain itself remains almost unchanged.

The reciprocal lattice vectors, $\mathbf{a}_1^*$,$\mathbf{a}_2^*$, and $\mathbf{a}_3^*$, are given by

$$\mathbf{a}_1^*=2\pi(1/c,0,0), \tag{2.4a}$$
$$\mathbf{a}_2^*=2\pi(0,1/a,1/b), \tag{2.4b}$$
$$\mathbf{a}_3^*=2\pi(0,-1/a,1/b). \tag{2.4c}$$

The first Brillouin zone of BP is a six-sided prism as shown in Fig.2-2. The electronic states specified by wave vectors on the

hexagonal face must be two-fold degenerate on acount of the properties of the irredusible representation of the non-symmorphic space group.[20] From now on we represent the x, y, and z components of wave vectors in units of $2\pi/c$, $2\pi/a$, and $2\pi/b$, respectively. For example,

$$\Gamma=(0,0,0), \quad X=(1/2,0,0), \quad Z=(0,0,1), \quad L=(1/2,0,1).$$

Symmetry lines which connect Γ and X, Γ and Z, and Z and L are denoted as Δ, Σ, and U, respectively.

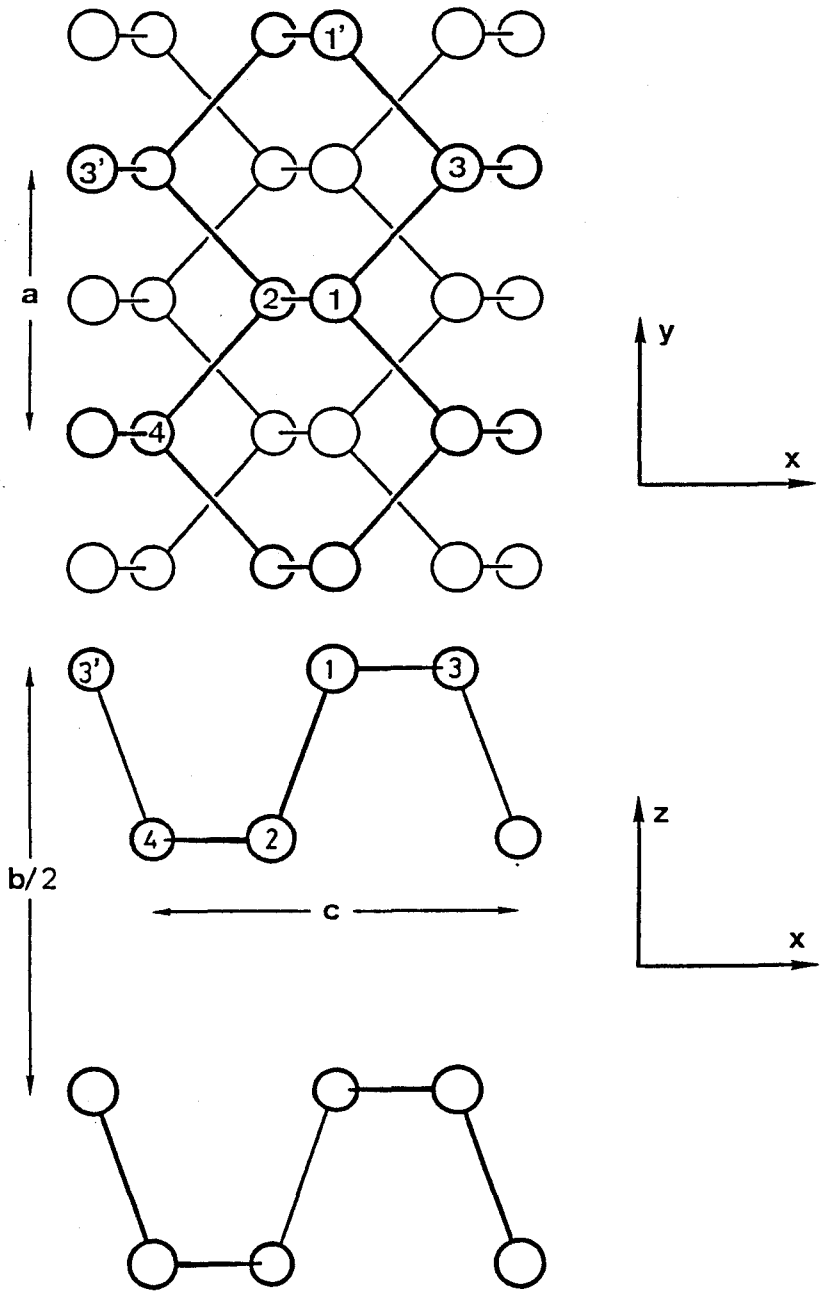

Fig.2-1 The crystal structure of black phosphorus. The upper figure shows the projection of two successive puckered layers on to the xy-plane. The lower figure shows that on to the xz-plane.

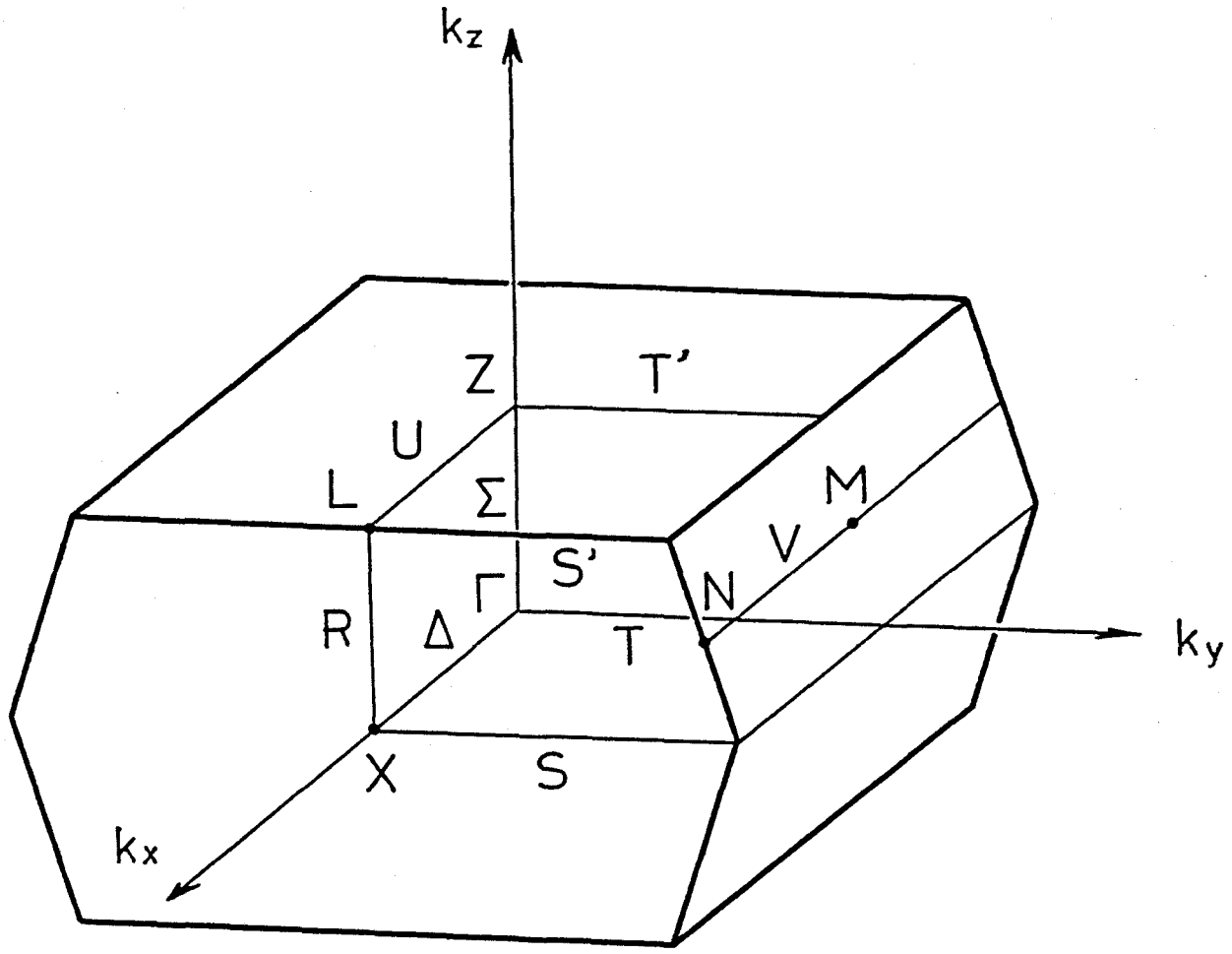

Fig.2-2 The Brillouin zone of black phosphorus.

2-2 Electronic Band Sturcture

The electronic band structure and the electronic properties of BP have been extensively investigated in recent years. There have been calculations of the energy bands of BP using the self-consistent pseudopotential (SCP) method[21] and the tight-binding (TB) method.[22]

In the SCP calculation, Appelbaum-Hamann type core potential, which is determined so that the calculated 3s and 3p levels of P^{4+} ion could well reproduce the experimental values, has been used and the X_α method with $\alpha=0.8$ was adopted for the exchange potential. The results of the SCP calculation are in good agreement with the XPS spectrum,[23] the partial density of states measured by soft X-ray spectroscopy,[24] and the valence band structure measured by angle-resolved photoemission spectroscopy.[25]

In the TB calculation, Slater-type atomic wave functions with Clementi's exponents for 3s and 3p orbitals and the extended Hückel approximation (EHA) have been used. The qualitative features of the electronic density of states as well as the dispersion curves of the lowest conduction band and the highest valence band are in good agreement with those obtained by the SCP calculation.

The TB method has an advantage that it can be extended easily to calculations of the electron-lattice interaction even in complex systems. Thus, we adopt the TB method to study the electron-lattice interaction of BP. We first illustrate the

TB method with use of the EHA, and then the calculated band structures are presented.

Slater-type wave functionsfor 3s and 3p orbitals are expressed as

$$\phi_{3s}(\mathbf{r}) = C_{3s} r^2 \exp(-\alpha_{3s} r), \tag{2.5a}$$

$$\phi_{3p_x}(\mathbf{r}) = C_{3p} x r \exp(-\alpha_{3p} r), \tag{2.5b}$$

$$\phi_{3p_y}(\mathbf{r}) = C_{3p} y r \exp(-\alpha_{3p} r), \tag{2.5c}$$

$$\phi_{3p_z}(\mathbf{r}) = C_{3p} z r \exp(-\alpha_{3p} r), \tag{2.5d}$$

where C_{3s} and C_{3p} are the normalization constants and α_{3s}= 1.8806 and α_{3p}=1.6288 (atomic unit) are Clementi's exponents. Bloch functons are written in the form of linear combinations of the atomic orbitals:

$$\psi_{i\mu}(\mathbf{k},\mathbf{r}) = \frac{1}{\sqrt{N}} \sum_{\ell} \phi_{\mu}(\mathbf{r}-\mathbf{R}_{\ell i}) \exp(i\mathbf{k}\cdot\mathbf{R}_{\ell i}), \tag{2.6}$$

where $\mathbf{R}_{\ell i}=\mathbf{R}_{\ell}+\tau_i$ represents the position vector of the i-th ion (i=1,2,3,4) in a primitive cell at a lattice point R_{ℓ}, and μ denotes the atomic orbitals 3s,$3p_x$,$3p_y$,and $3p_z$.

The electronic band energies $E^0_{n\mathbf{k}}$ are obtained by solving the secular equation

$$\det|T_{i\mu,j\nu}(\mathbf{k},\mathbf{k}) - ES_{i\mu,j\nu}(\mathbf{k},\mathbf{k})| = 0, \tag{2.7}$$

where $\{T_{i\mu,j\nu}(\mathbf{k},\mathbf{k})\}$ and $\{S_{i\mu,j\nu}(\mathbf{k},\mathbf{k})\}$ are transfer and overlap

matrices, respectively. Elements of the overlap matrix are defined by

$$S_{i\mu,j\nu}(\mathbf{k},\mathbf{k}')=\int \psi^{*}_{i\mu}(\mathbf{k},\mathbf{r})\psi_{j\nu}(\mathbf{k}',\mathbf{r})d^3r$$

$$=\delta_{\mathbf{k},\mathbf{k}'}\sum_{\ell} S_{\mu\nu}(R_{\ell i}-\mathbf{R}_{0j})\exp[-i\mathbf{k}\cdot(R_{\ell i}-\mathbf{R}_{0j})], \qquad (2.8)$$

where

$$S_{\mu\nu}(R_{\ell i}-\mathbf{R}_{0j})=\int \phi_{\mu}(\mathbf{r}-\mathbf{R}_{\ell i})\phi_{\nu}(\mathbf{r}-\mathbf{R}_{0j})d^3r \qquad (2.9)$$

are overlap integrals which can be calculated analytically using eq.(2.5) for arbitrary $(R_{\ell i}-\mathbf{R}_{0j})$. Elements of the transfer matrix are defined by

$$T_{i\mu,j\nu}(\mathbf{k},\mathbf{k}')=\int \psi^{*}_{i\mu}(\mathbf{k},\mathbf{r})H\,\psi_{j\nu}(\mathbf{k}',\mathbf{r})d^3r$$

$$=\delta_{\mathbf{k},\mathbf{k}'}\sum_{\ell} T_{\mu\nu}(R_{\ell i}-\mathbf{R}_{0j})\exp[-i\mathbf{k}\cdot(R_{\ell i}-\mathbf{R}_{0j})], \qquad (2.10)$$

with

$$T_{\mu\nu}(R_{\ell i}-\mathbf{R}_{0j})=\int \phi_{\mu}(\mathbf{r}-\mathbf{R}_{\ell i})H\phi_{\nu}(\mathbf{r}-\mathbf{R}_{0j})d^3r. \qquad (2.11)$$

where H represents the one-electron Hamiltonian which is assumed to include screening, exchange, and correlation in some appropriate way in a one-electron approximation.

The wave function $\Phi_n(\mathbf{k},\mathbf{r})$ which corresponds to $E^{0}_{n\mathbf{k}}$ can be expressed in the form of linear combination of the basis Bloch functions $\psi_{i\mu}(\mathbf{k},\mathbf{r})$:

$$\Phi_n(\mathbf{k},\mathbf{r})=\sum_{i\mu} A_{i\mu,n}(\mathbf{k})\psi_{i\mu}(\mathbf{k},\mathbf{r}), \tag{2.12}$$

where $A(\mathbf{k})$ is the transformation matrix and it satisfies the following relations:

$$A^{\dagger}(\mathbf{k})T(\mathbf{k},\mathbf{k})A(\mathbf{k})=E^{d}(\mathbf{k}), \tag{2.13}$$

$$A^{\dagger}(\mathbf{k})S(\mathbf{k},\mathbf{k})A(\mathbf{k})=1, \tag{2.14}$$

where $E^{d}(\mathbf{k})$ is the diagonal matrix with elements $E^{0}_{n\mathbf{k}}$. When a set of Bloch functions forms an orthonormal basis, contribution from an atomic orbital μ of the i-th ion to the electronic state $(n\mathbf{k})$ is given by $W(i\mu,n\mathbf{k})\equiv|A_{i\mu,n}(\mathbf{k})|^2$. In case of non-orthognal basis, on the other hand, this relation is not valid in general. However, if $W(i\mu,n\mathbf{k})$ is significantly large for particular $i\mu=j\nu$ compared with other $W(i\mu,n\mathbf{k})$'s $(i\mu\neq j\nu)$, it is reasonable to say that the atomic orbital ν of the j-th ion mainly contributes to the electronic state $(n\mathbf{k})$.

After Takao et al.[22] we adopt the EHA to evaluate the transfer integrals. In the EHA transfer integrals are assumed to be proportional to overlap integrals:[26]

$$T_{\mu\nu}(R_{\ell i}-R_{0j})=\begin{cases}\frac{1}{2}K_{\mu\nu}(I_{\mu}+I_{\nu})S_{\mu\nu}(R_{\ell i}-R_{0j}), & \text{for } R_{\ell i}\neq R_{0j},\\ I_{\mu}\delta_{\mu\nu}, & \text{or } R_{\ell i}=R_{0j},\end{cases} \tag{2.15}$$

where I_{μ} denotes the ionization energy and $K_{\mu\nu}$ represents a parameter chosen appropriately. In actual calculations the

ionization energies are taken from the values calculated by Harman and Skillman[27] (I_{3s}=-1.2588 Ryd., I_{3p}=-0.6139 Ryd.) and as to the values of K_{ss} and K_{pp} we use the commonly chosen value 1.75 which reproduces fairly well the energy bands of Si or Ge obtained on the basis of the emprical pseudopotential method. The remaining parameter K_{sp} may be chosen so as to reproduce the band gap at normal pressure.

In actual calculations overlap integrals are taken into consideration up to the tenth neighbours. The minimum energy gap E_g between the valence and conduction bands appears at Z point and is given by $E_g=E(Z_4^-)-E(Z_2^+)$, where Z_4^- and Z_2^+ denote the irreducible representations of the space group. Fig.2-3 shows the K_{sp}-dependence of E_g. The energy gap, 0.3eV, at normal pressure can be obtained if we take K_{sp}=1.379, which is slightly different from that determined by Takao et al.[22] who used the crystal structure parameters different from ours. In our calculations crystal structure parameters are taken from the measurements by Cartz et al.[19] (see §2-1).

The energy dispersion curves along the U line and the Σ line in the first Brillouin zone at noraml pressure are shown by solid curves in Fig.2-4. The region of the energy gap is shaded. The dispersion curves of the highest valence band (HVB) and the lowest conduction band (LCB) are quite similar to those obtained by Asahina et al. on the basis of the SCP method. It is noted that the character of the wave functions is $3p_z$-like in HVB and LCB.

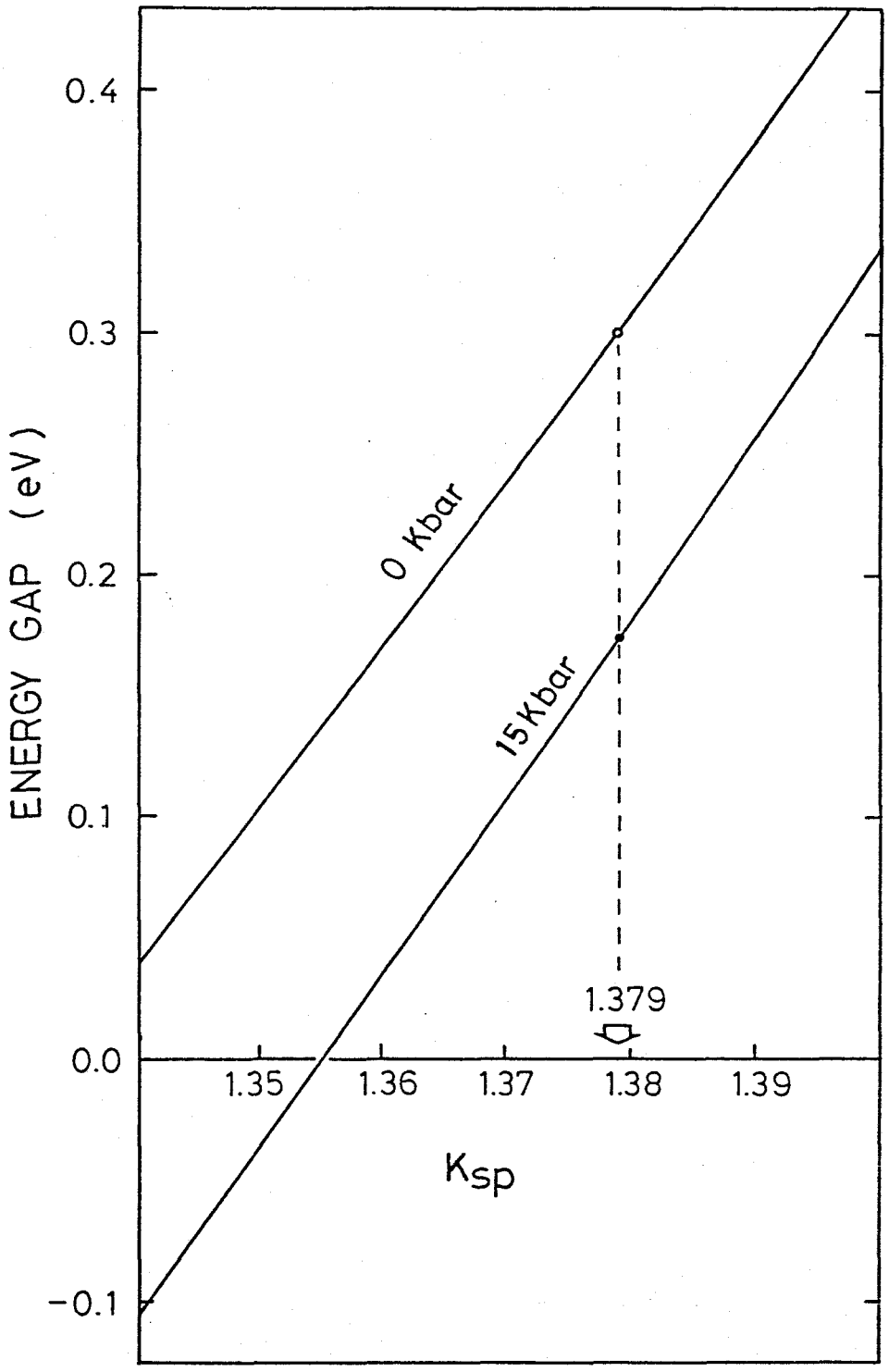

Fig.2-3 K_{sp}-dependence of the minimum energy gap at the Z point for 0 kbar (normal pressure) and for 15 kbar.

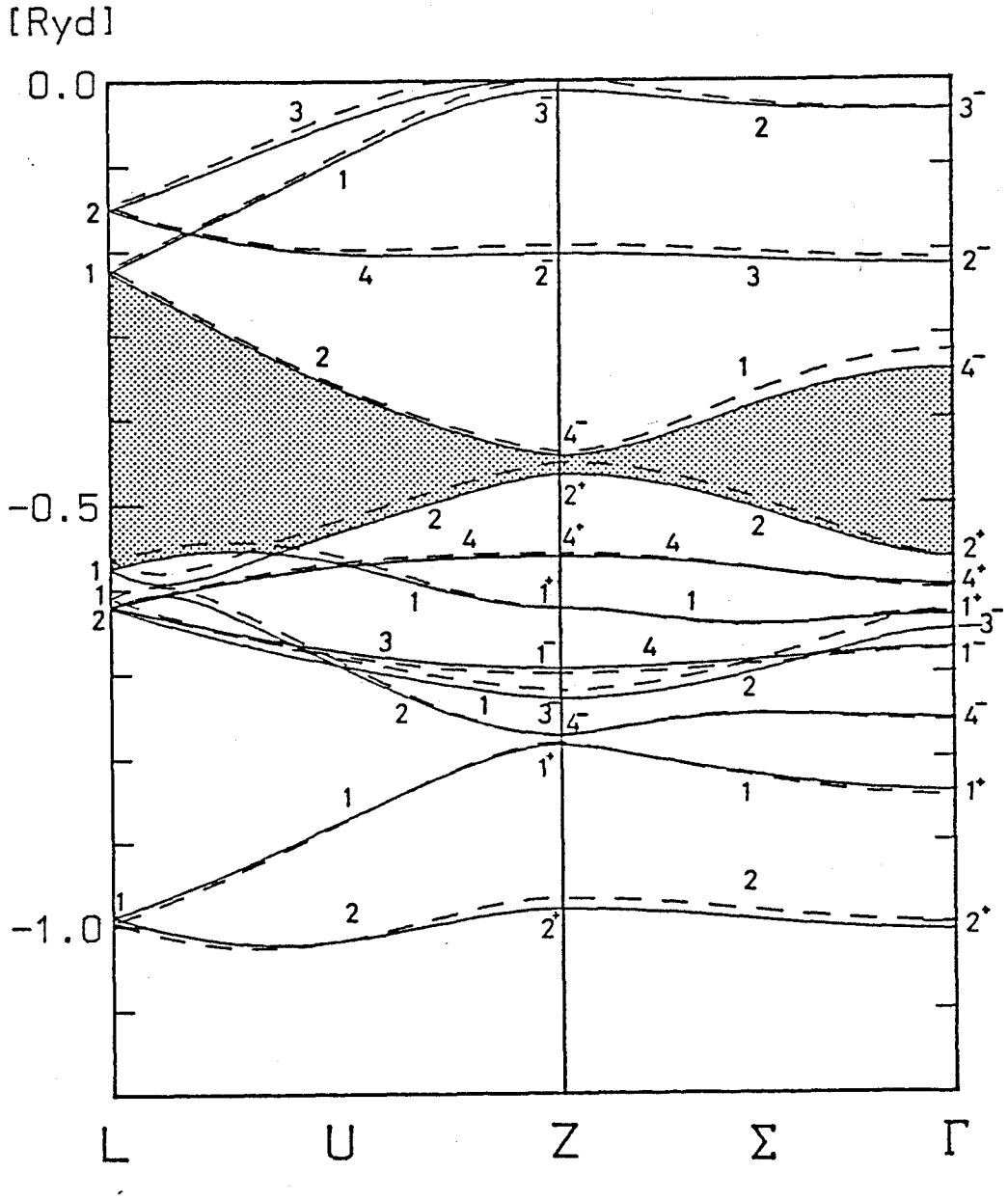

Fig.2-4 The energy dispersion curves along the U and Σ lines. Full curves: at 0 kbar (normal pressure). Broken curves: at 15 kbar. The gap region is shaded.

2-3 Pressure effects

The electronic band structure of BP at 15kbar has been calculated in the same way as at normal pressure. We used crystal structure parameters a, b, c, u, and v at 15kbar determined by Cartz et al.[19] But, no modification were made for the values of EHA parameters, K_{ss}, K_{pp}, and K_{sp}.

At 15kbar, the minimum energy gap, which appears also at Z point, is 0.17eV as shown in Fig.2-3 and Fig.2-4. The calculated pressure coefficient of energy gap dE_g/dP has negative value of -8.5 meV/kbar: this is about a half of the experimental value, -16.7 meV/kbar, which has been determined by electrical resistivity measurements.[28] In spite of the simplified treatments for the transfer integrals, our calculations well reproduce the pressure dependence of the energy gap.

The energy dispersion curves along the U and Σ lines at 15 kbar are shown by dashed curves in Fig.2-4. It should be noted that as pressure is applied the energies of HVB (Z_2^+-U_2-L_1) considerablly shift up whereas the energies of LCB (Z_4^--U_2-L_1) are almost unchanged. Hence the direct or indirect energy gap between HVB and LCB along the U line decreases considerably when pressure is applied.

From group theoretical consideration, the electron-phonon matrix elements between two electronic states with U_2-symmetry on the U line do not vanish only for Δ_1-phonons, to which the LAx-phonon belongs. Therefore, these facts suggest that the remarkable narrowing of the energy gap along the U line could be responsible for the pressure-induced softening of the LAx-phonon.

§3 Electron-Lattice Interaction

3-1 Generalized electronic susceptibility

In the adiabatic approximation the ions in the crystal vibrate in the instantaneous potential given by the sum of (i) electrostatic potential produced by ions themselves and (ii) adiabatic potential which is the electronic free energy when the ions rest at their instantaneous positions. If displacements of the ions $\delta R_{\ell i}$ from their equilibrium position $R_{\ell i}$ are assumed to be sufficiently small, we can treat the problem within the harmonic approximation. Then, the change of the total potential energy due to the displacements can be generally expressed as

$$\Delta V = \frac{1}{2} \sum_{\alpha\beta} \sum_{\ell\ell' ij} F^{\alpha\beta}(\ell i, \ell' j) \delta R^{\alpha}_{\ell i} \delta R^{\beta}_{\ell' j} , \tag{3.1}$$

where $F^{\alpha\beta}(\ell i, \ell' j)$ represents force constant. Introducing Fourier transform of the displacement, $u^{\alpha}_{i}(\mathbf{q})$, defined by

$$u^{\alpha}_{i}(\mathbf{q}) = \frac{1}{\sqrt{N}} \sum_{\ell} \delta R^{\alpha}_{\ell i} \exp(i\mathbf{q}\cdot\mathbf{R}_{\ell i}), \tag{3.2}$$

eq.(3.1) can be expressed as

$$\Delta V = \frac{1}{2} \sum_{\mathbf{q}} \sum_{i\alpha} \sum_{j\beta} D^{\alpha\beta}(ij,\mathbf{q}) u^{\alpha}_{i}(\mathbf{q}) u^{\beta}_{j}(-\mathbf{q}), \tag{3.3}$$

where $D^{\alpha\beta}(ij,\mathbf{q})$ is the so-called dynamical matrix defined by

$$D^{\alpha\beta}(ij,q) = \sum_{\ell} F^{\alpha\beta}(\ell i,\ell' j)\exp\{iq\cdot(R_{\ell i}-R_{\ell' j})\}. \qquad (3.4)$$

In general the electronic free energy can be expressed as $F_{bs}-F_{e-e}$. Here F_{bs} denotes the contribution from the band structure (effective one-electron energy part) and F_{e-e} represents the sum of the Hartree potential energy and the correlation-exchange energy. The term $-F_{e-e}$ must be necessary so that the electron-electron interaction energy is not counted twice. Consequently, within the adiabatic and harmonic approximation we can express the dynamical matrix as follows:

$$D^{\alpha\beta}(ij,q) = D^{\alpha\beta}_{bs}(ij,q) + R^{\alpha\beta}(ij,q) \qquad (3.5)$$

where $D^{\alpha\beta}_{bs}(ij,q)$ is the contribution arising from the change of F_{bs} due to lattice distortion, ΔF_{bs}, and $R^{\alpha\beta}(ij,q)$ represents the contribution from the change of ion-ion Coulomb energy and $-F_{e-e}$. It should be noted that the forces correponding to $R^{\alpha\beta}(ij,q)$ are short-ranged in general.[29)]

ΔF_{bs} can be obtained on the basis of the TB method extended to the displaced structure. In calculating the energy bands of the displaced structure we have two choices. One is the Frölich approach and the other is the Bloch approach. In the Frölich approach, the atomic wave functions are moving adiabatically with the ions. In the Bloch approach, the electron-lattice matrix element is taken with respect to electronic states of the undistorted structure. It has been shown by Ashkenazi et al.[30)] that within the harmonic approximation both approaches lead to

the same physical results. In the present study we adopt the Frölich approach and express the basis functions in the displaced structure as

$$\psi_{i\mu}(\mathbf{k},\mathbf{r}) = \frac{1}{\sqrt{N}} \sum_{\ell} \phi_{\mu}(\mathbf{r}-\mathbf{R}_{\ell i}-\delta\mathbf{R}_{\ell i})\exp(i\mathbf{k}\cdot\mathbf{R}_{\ell i}). \tag{3.6}$$

Overlap and Transfer matrices are defined by

$$S_{i\mu,j\nu}(\mathbf{k},\mathbf{k}') = \int \psi^{*}_{i\mu}(\mathbf{k},\mathbf{r})\psi_{j\nu}(\mathbf{k}',\mathbf{r})d^{3}r, \tag{3.7}$$

$$T_{i\mu,j\nu}(\mathbf{k},\mathbf{k}') = \int \psi^{*}_{i\mu}(\mathbf{k},\mathbf{r})H\psi_{j\nu}(\mathbf{k}',\mathbf{r})d^{3}r, \tag{3.8}$$

and the band energies of the distorted structure are determined by solving the secular equation

$$\det|T(\mathbf{k},\mathbf{k}')-ES(\mathbf{k},\mathbf{k}')|=0. \tag{3.9}$$

It is noted that overlap and transfer matrices are not diagonal in $\mathbf{k}$. In the harmonic approximation it is sufficient to take into account the change of overlap and transfer integrals up to the second order of $\delta R^{\alpha}_{\ell i}$. Then, the band energies of the distorted structure are calculated by using the first and the second order perturbation theory for the non-orthogonal representation. The results are as follows:

$$E_{n\mathbf{k}} = E^{0}_{n\mathbf{k}} + E^{(2)}_{n\mathbf{k}}, \tag{3.10}$$

$$E^{(2)}_{n\mathbf{k}} = \frac{1}{N} \sum_{\mathbf{q}} \sum_{i\alpha} \sum_{j\beta} g_{2}^{i\alpha,j\beta}(n\mathbf{k},\mathbf{q})u^{\alpha}_{i}(\mathbf{q})u^{\beta}_{j}(-\mathbf{q})$$

$$+\frac{1}{N}\sum_{q}\sum_{i\alpha}\sum_{j\beta}\frac{g^{i\alpha}(nk,n'k-q;E^0_{nk})g^{j\beta}(nk,n'k-q;E^0_{nk})^*}{E^0_{nk}-E^0_{n'k-q}}u^{\alpha}_i(q)u^{\beta}_j(-q). \tag{3.11}$$

Here g and g_2 are defined by

$$g^{i\alpha}(nk,n'k-q;E) = \xi^{i\alpha}(nk,n'k-q)-E^0_{nk}\eta^{i\alpha}(nk,n'k-q), \tag{3.12}$$

$$g_2^{i\alpha,j\beta}(nk,q) = \xi_2^{i\alpha,j\beta}(nk,nk,q)-E^0_{nk}\eta_2^{i\alpha,j\beta}(nk,nk,q), \tag{3.13}$$

where

$$\xi^{i\alpha}(nk,n'k')=\sum_{\mu i'\nu j'}A^*_{i'\mu,n}(k)\dot{T}^{\alpha}_i(i'\mu k,j'\nu k')A_{j'\nu,n'}(k'), \tag{3.14}$$

$$\eta^{i\alpha}(nk,n'k')=\sum_{\mu i'\nu j'}A^*_{i'\mu,n}(k)\dot{S}^{\alpha}_i(i'\mu k,j'\nu k')A_{j'\nu,n'}(k'), \tag{3.15}$$

$$\xi_2^{i\alpha,j\beta}(nk,n'k',q)=\sum_{\mu i'\nu j'}A^*_{i'\mu,n}(k)\dot{T}^{\alpha\beta}_{ij}(i'\mu k,j'\nu k')A_{j'\nu,n'}(k'), \tag{3.16}$$

$$\eta_2^{i\alpha,j\beta}(nk,n'k',q)=\sum_{\mu i'\nu j'}A^*_{i'\mu,n}(k)\dot{S}^{\alpha\beta}_{ij}(i'\mu k,j'\nu k')A_{j'\nu,n'}(k'). \tag{3.17}$$

$\dot{S}^{\alpha}_i$ and $\dot{S}^{\alpha\beta}_{ij}$ are expressed in terms of derivatives of overlap integrals as follows:

$$\dot{S}^{\alpha}_i(i'\mu k,j'\nu k')=\delta_{ii'}S'^{\alpha}_{i'\mu,j'\nu}(k')-\delta_{ij'}S'^{\alpha}_{i'\mu,j'\nu}(k), \tag{3.18}$$

$$\dot{S}^{\alpha\beta}_{ij}(i'\mu k,j'\nu k',q)=\delta_{ii'}\delta_{ji'}S'^{\alpha\beta}_{i'\mu,j'\nu}(k')-\delta_{ij'}\delta_{jj'}S'^{\alpha\beta}_{i'\mu,j'\nu}(k)$$

$$- \delta_{ij'}\delta_{ji'}S'^{\alpha\beta}_{i'\mu,j'\nu}(\mathbf{k}'+\mathbf{q}) - \delta_{ii'}\delta_{jj'}S'^{\alpha\beta}_{i'\mu,j'\nu}(\mathbf{k}-\mathbf{q}), \quad (3.19)$$

where

$$S'^{\alpha}_{i'\mu,j'\nu}(k) = \sum_{\ell} S'^{\alpha}_{\mu\nu}(R_{\ell i'}-R_{\ell' j'})\exp\{-i\mathbf{k}\cdot(R_{\ell i'}-R_{\ell' j'})\}, \quad (3.20)$$

$$S'^{\alpha\beta}_{i'\mu,j'\nu}(k) = \sum_{\ell} S'^{\alpha\beta}_{\mu\nu}(R_{\ell i'}-R_{\ell' j'})\exp\{-i\mathbf{k}\cdot(R_{\ell i'}-R_{\ell' j'})\}, \quad (3.21)$$

with

$$S'^{\alpha}_{\mu\nu}(R) = \frac{\partial}{\partial R_\alpha} S_{\mu\nu}(R), \quad (3.22)$$

$$S'^{\alpha\beta}_{\mu\nu}(R) = \frac{\partial^2}{\partial R_\alpha \partial R_\beta} S_{\mu\nu}(R). \quad (3.23)$$

$\dot{T}^{\alpha}_{i}$ and $\dot{T}^{\alpha\beta}_{ij}$ are expressed in the same forms as those of $\dot{S}^{\alpha}_{i}$ and $\dot{S}^{\alpha\beta}_{ij}$ in terms of $T'^{\alpha}_{\mu\nu}$ and $T'^{\alpha\beta}_{\mu\nu}$. The first and the second order derivatives of the overlap integral, eqs.(3.23) and (3.24), can be represented in terms of Slater-Koster's two center integrals and their derivatives. Their expressions for s and p orbitals are given in Appendix A. In a framework of the EHA the derivatives of transfer integrals are evaluated as follows:

$$T'^{\alpha}_{\mu\nu}(R) = \frac{1}{2} K_{\mu\nu}(I_\mu+I_\nu)S'^{\alpha}_{\mu\nu}(R), \quad (3.24)$$

$$T'^{\alpha\beta}_{\mu\nu}(R) = \frac{1}{2} K_{\mu\nu}(I_\mu+I_\nu)S'^{\alpha\beta}_{\mu\nu}(R). \quad (3.25)$$

$g^{i\alpha}(n\mathbf{k},n'\mathbf{k}-\mathbf{q};E^{0}_{n\mathbf{k}})$, which is called the electron-lattice interction

coefficient, represents the strength of coupling between the electronic states (nk) and (n'k-q) caused by the displacement $u_i^\alpha(q)$.

The free energy associated with the electronic bands is given by

$$F_{bs} = -k_B T \sum_{nk} \log[1+\exp\{-(E_{nk}-\mu_e)/k_B T\}] + \mu_e N_e, \tag{3.26}$$

and the chemical potential μ_e is determined from

$$N_e = 2 \sum_{nk} f(E_{nk}), \tag{3.27}$$

where

$$f(E_{nk}) = \frac{1}{1+\exp\{(E_{nk}-\mu_e)/k_B T\}} \ . \tag{3.28}$$

In the harmonic approximation the change of F_{bs} due to lattice distortions is simply given by

$$\Delta F_{bs} = 2 \sum_{nk} E^{(2)}_{nk} \ f^0(E^0_{nk}) \ , \tag{3.29}$$

where $f^0(E_{nk})$ is the Fermi distribution function for the undistorted structure. Substituting eq.(3.11) into eq.(3.29) we obtain the final expression for ΔF_{bs} as follows:

$$\begin{aligned} \Delta F_{bs} &\equiv \frac{1}{2} \sum_{q} \sum_{i\alpha j\beta} D^{\alpha\beta}_{bs}(ij,q) u^\alpha_i(q) u^\beta_j(-q) \\ &= \frac{1}{2} \sum_{q} \sum_{i\alpha j\beta} [\chi^{\alpha\beta}(ij,q) + D^{\alpha\beta}_2(ij,q)] u^\alpha_i(q) u^\beta_j(-q), \end{aligned} \tag{3.30}$$

where

$$\chi^{\alpha\beta}(ij,q) = 2 \sum_{nn'\mathbf{k}} \sum \frac{1}{E^0_{n\mathbf{k}} - E^0_{n'\mathbf{k}-\mathbf{q}}}$$

$$\times[g^{i\alpha}(n\mathbf{k},n'\mathbf{k}-\mathbf{q};E^0_{n\mathbf{k}})g^{j\beta}(n\mathbf{k},n'\mathbf{k}-\mathbf{q};E^0_{n\mathbf{k}})^* f^0(E^0_{n\mathbf{k}})$$

$$-g^{i\alpha}(n\mathbf{k},n'\mathbf{k}-\mathbf{q};E^0_{n'\mathbf{k}-\mathbf{q}})g^{j\beta}(n\mathbf{k},n'\mathbf{k}-\mathbf{q};E^0_{n'\mathbf{k}-\mathbf{q}})^* f^0(E^0_{n'\mathbf{k}-\mathbf{q}})], \tag{3.31}$$

$$D_2^{\alpha\beta}(ij,q) = 2 \sum_{n\mathbf{k}} 2g^{i\alpha,j\beta}(n\mathbf{k},q)f^0(E^0_{n\mathbf{k}}). \tag{3.32}$$

$\chi^{\alpha\beta}(ij,q)$ is called the generalized electronic susceptibility and represents the contribution to the dynamical matrix arising from the linear electron-lattice interaction. Forces correponding to $\chi^{\alpha\beta}(ij,q)$ are usually long-ranged in metals and narrow-gap semiconductors. On the other hand, forces coorresponding to $D_2^{\alpha\beta}(ij,q)$ can be treated as short-range and the term $D_2^{\alpha\beta}(ij,q)$ can be included safely into $R^{\alpha\beta}(ij,q)$. Thus, from now on we express the total dynamical matrix as

$$D^{\alpha\beta}(ij,q) = \chi^{\alpha\beta}(ij,q) + R^{\alpha\beta}(ij,q). \tag{3.33}$$

The phonon frequencies are determined from diagonalization of $D^{\alpha\beta}(ij,q)$.

3-2 Eigenvalues of $\chi^{\alpha\beta}(ij,q)$

We have calculated $\chi^{\alpha\beta}(ij,q)$ for the narrow gap semiconductor BP at zero temperature. The summation over the first Brillouin zone has been carried out by dividing the 1/8 irreducible zone into 234 rectangular meshes. The relative weights have been correctly considered for meshes which are truncated by the zone boundary plane perpendicular to $a^*=(0,1,1)$. The accuracy of numerical evaluation of $\chi^{\alpha\beta}(ij,q)$ is estimated to be 1∿2 per cent from comparison between the results obtained by using 235 meshes and by using 125 meshes.

We focus our attention to lattice vibrations along the x direction and hence numerical calculations of $\chi^{\alpha\beta}(ij,q)$ have been carried out for seven wave vectors, $q=(m/12,0,0)$ $(m=0-6)$, along the Δ line. Then, eigenvalues and eigenvectors of $\chi^{\alpha\beta}(ij,q)$ have been determined for each q. In Fig.3-1 we show all eigenvalues of $\chi^{\alpha\beta}(ij,q)$ at normal pressure by open circles. All of the obtained eigenvalues are negative, which means that electron-lattice interaction has a role of lowering phononen frequencies. The eigenvectors on the Δ line are classified into four irreducible representations, Δ_1, Δ_2, Δ_3 and Δ_4. Symmetry coordinates which belong to each irreducible representation are tabulated in Table 3-1. In Fig.3-2 we show in magnified scale three eigenvalues which correspond to three acoustical branches, LAx, TAy, and TAz, respectively. The symmetries of LAx, TAy, and TAz are Δ_1, Δ_4 and Δ_2, respectively. The eigenvectors of LAx mode consists mainly of two symmetry coordinates x_1+x_4 and x_2+x_3, but the

components of z_1-z_4 and z_2-z_3 are also included a little.

We have calculated the eigenvalues of $\chi^{\alpha\beta}(ij,\mathbf{q})$ also for 15 kbar. The results are shown by closed circles in Fig.3-2. As seen from the figure the magnitude of the eigenvalues become larger as the pressure is increased. Hence, $\chi^{\alpha\beta}(ij,\mathbf{q})$ plays a role of softening the phonon frequencies with increasing pressure. The change of eigenvalues of Δ_1-modes is relatively large compared with that of other modes, and in particular the LAx mode has the largest increase of the magnitude of eigenvalue among three acoustical modes. This fact strongly implies a possibility that only the LAx acoustic phonon shows softening as pressure is applied.

The large softening of the Δ_1-mode is related with the electronic band structure near the Fermi level. Because of the energy difference in the denominator of eq.(3.31) a main contribution to χ arises from couplings between HVB and LCB near Z point. If we consider a wave vector $\mathbf{q}$ on the Δ line and choose as $(n\mathbf{k})$ state the bottom of the conduction band at Z point, Z_4^-, then a large contribution arises if $(n'\mathbf{k}-\mathbf{q})$ state lies in HVB with U_2-symmetry along the U line. In this case there is a selection rule by group theoretical concideration mentioned in previous section and only the Δ_1-mode can connect those two electronic states, Z_4^-, and U_2. As seen from Fig.2-4 the energy difference $E(Z_4^-)$-$E(U_2)$ decreases considerably with increasing pressure. This is the main reason why the decreases of eigenvalues of the Δ_1-symmetry mode under pressure are large.

Validity of the above argument is confirmed by the following

analysis. First we have carried out numerical calculations of the magnitude of electron-lattice coefficient $|g_{12}^{\lambda}|$ where λ denotes a mode of atomic displacements modulated by the wave vector **q**, and 1 and 2 denote a pair of electronic states (n**k**) and (n'**k**-**q**). We have chosen as (n**k**) the bottom of the conduction band , Z_4^-. On the other hand, as (n'**k**-**q**) we have chosen following two bands near Fermi level along the U line:

(i) HVB with U_2-symmetry,

(ii) the second highest valence band with U_1-symmetry.

$|g_{12}^{\lambda}|$ is non-vanishing for λ with Δ_1-symmetry in the case (i) and for λ with Δ_2-symmetry in the case (ii) according to the selection rule. The values of $|g_{12}^{\lambda}|$ calculated for symmetry modes $\lambda=\Delta_1(x)\equiv x_1+x_4$ and $\lambda=\Delta_2(z)\equiv z_1+z_4$ in the cases of (i) and (ii) are shown in Fig.3-3a by solid line (normal presssure) and broken line (15kbar). We can see that $|g_{12}^{\lambda}|$ is large in the case (i) compared with that in the case (ii). However, the change of $|g_{12}^{\lambda}|$ due to pressure in the case (ii) is as large as that in the case (i). Therefore, there is no evidence that the change of $|g_{12}^{\lambda}|$ due to pressure can be a origin of large softening of Δ_1-phonons. Next we have taken energy denominator E_1-E_2 into consideration. Calculated $|g_{12}^{\lambda}|^2/(E_1-E_2)$ is shown in Fig.3-3b by solid line (normal pressure) and broken line (15kbar). As is obvious from the figure, the change of $|g_{12}^{\lambda}|^2/(E_1-E_2)$ due to pressure is considerably large in the case (i) compared with that in the case (ii). Thus, it has been

clearly shown that the large decrease of eigenvalues of Δ_1-symmetry modes caused by pressure is a result of the pressure-induced narrowing of the energy gap.

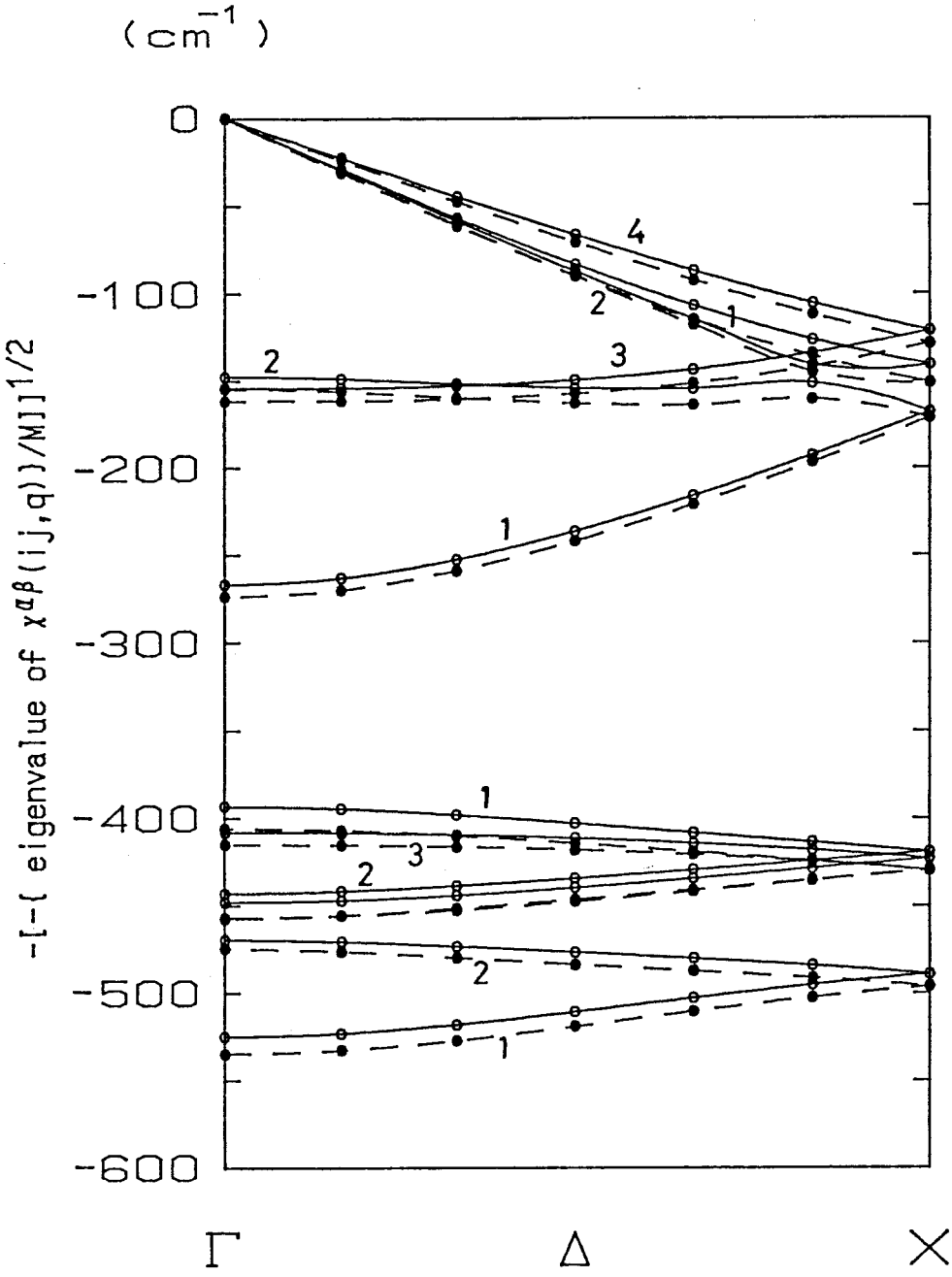

Fig.3-1 The eigenvalues of $\chi^{\alpha\beta}(ij,\mathbf{q})$ for wave vectors along the Δ line. In this figure we have plotted $-\sqrt{(-\text{eigenvalue})/M}$ where M denotes the mass of P atom. Note that the eigenvalues are negative. The numbers, 1, 2, 3 and 4, denote the symmetry: 1; Δ_1, 2; Δ_2, 3; Δ_3, 4; Δ_4. The open and closed circles are obtained by diagonalizing $\chi^{\alpha\beta}(ij,\mathbf{q})$ calculated from eq.(3.31) whereas the full and dotted curves are obtained by using $\chi^{\alpha\beta}(ij,\mathbf{q})$ calculated from eq.(4.4) (for details, see §4).

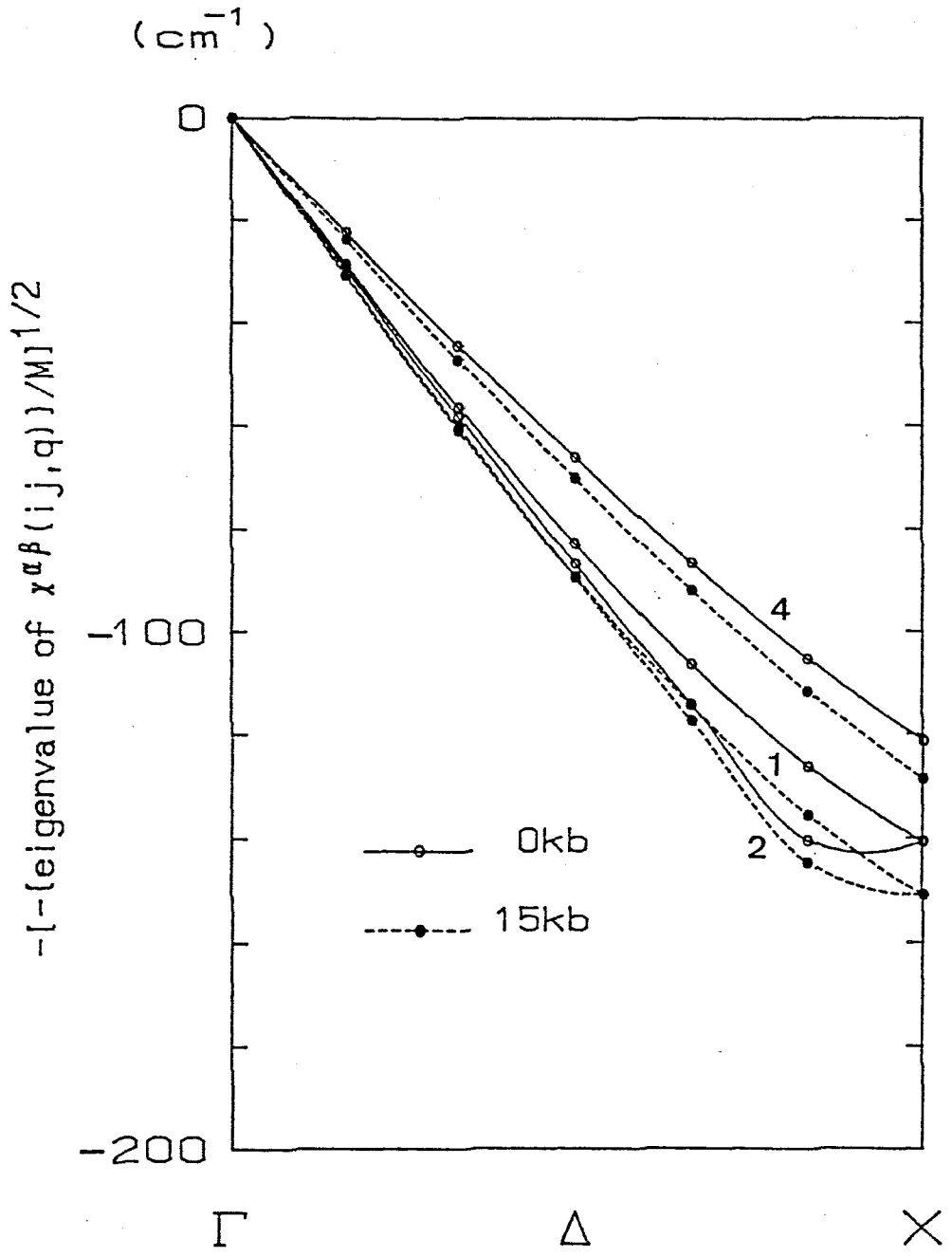

Fig.3-2 Enlarged figure of Fig.3-1 for three acoustic modes: 1(LAx), 2(TAz) and 4(TAy).

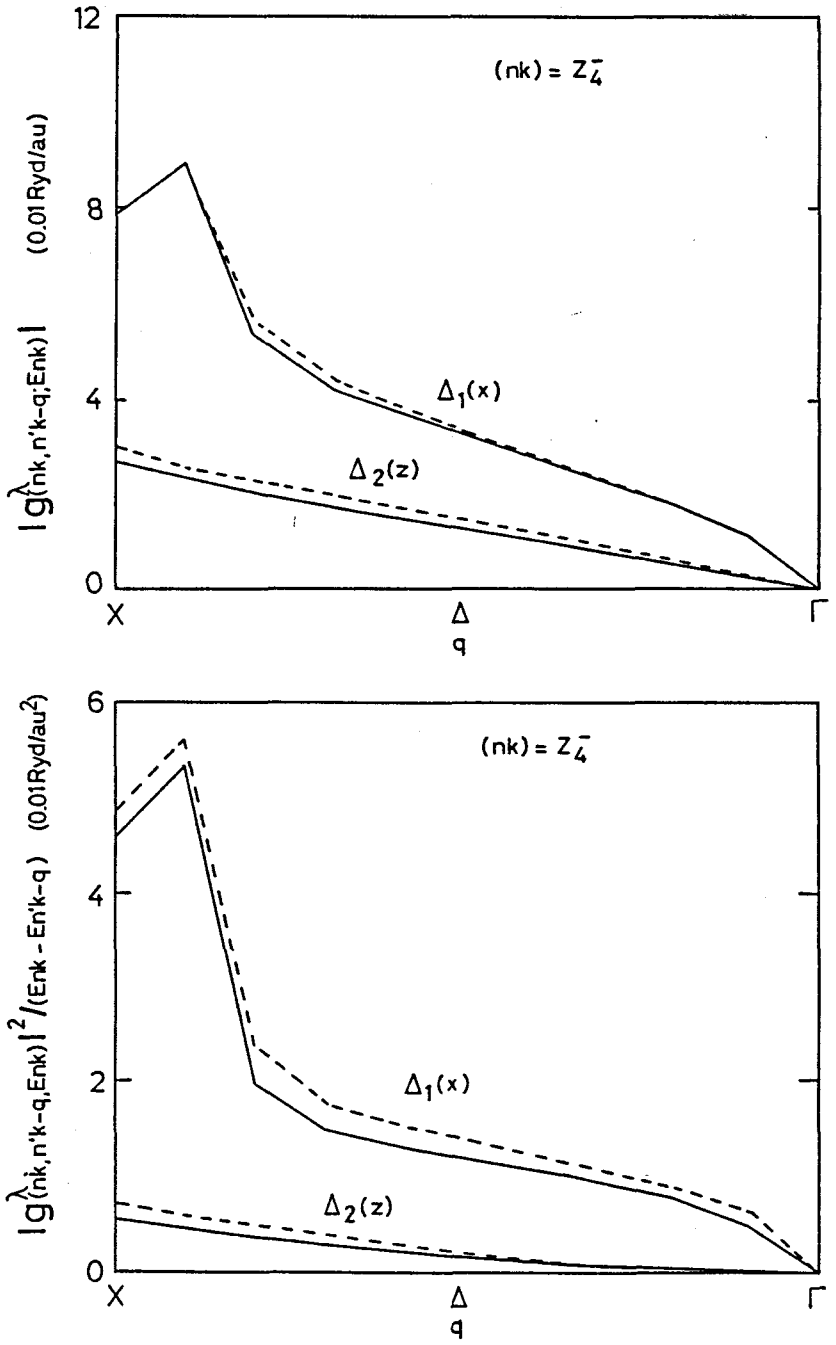

Fig.3-3 Wave vector dependence of (a) $|g^{\lambda}(\mathbf{nk},\mathbf{n'k-q},E_{\mathbf{nk}})|$ and (b) $|g^{\lambda}(\mathbf{nk},\mathbf{n'k-q},E_{\mathbf{nk}})|^2/(E_{\mathbf{nk}}- E_{\mathbf{n'k-q}})$ for $\lambda=\Delta_1(x)=x_1+ x_4$ and $\lambda=\Delta_2(z)=z_1+ z_4$. Electornic state $\mathbf{nk}$ is fixed at the lowest conduction band state Z_4^- and $\mathbf{n'k-q}$ moves along the highest valence band with U_2 symmetery for $\lambda=\Delta_1(x)$ and along the second highest valence band with U_1 symmetry for $\lambda=\Delta_2(z)$. Solid line: at 0 kbar (normal pressure). Broken line: at 15 kbar.

Table 3-1. Symmetry coordinates at the Γ point and on the Δ line.

Γ point $(2\Gamma_1^+ + 2\Gamma_2^+ + \Gamma_3^+ + \Gamma_4^+ + \Gamma_1^- + \Gamma_2^- + 2\Gamma_3^- + 2\Gamma_4^-)$

Γ_1^+: $x_1 - x_2 - x_3 + x_4$, $z_1 - z_2 + z_3 - z_4$

Γ_2^+: $x_1 - x_2 + x_3 - x_4$, $z_1 - z_2 - z_3 + z_4$

Γ_3^+: $y_1 - y_2 + y_3 - y_4$

Γ_4^+: $y_1 - y_2 - y_3 + y_4$

Γ_1^-: $y_1 + y_2 - y_3 - y_4$

Γ_2^-: $y_1 + y_2 + y_3 + y_4$

Γ_3^-: $x_1 + x_2 + x_3 + x_4$, $z_1 + z_2 - z_3 - z_4$

Γ_4^-: $x_1 + x_2 - x_3 - x_4$, $z_1 + z_2 + z_3 + z_4$

Δ line $(4\Delta_1 + 4\Delta_2 + 2\Delta_3 + 2\Delta_4)$

Δ_1: $x_1 + x_4$, $x_2 + x_3$, $z_1 - z_4$, $z_2 - z_3$

Δ_2: $x_1 - x_4$, $x_2 - x_3$, $z_1 + z_4$, $z_2 + z_3$

Δ_3: $y_1 - y_4$, $y_2 - y_3$

Δ_4: $y_1 + y_4$, $y_2 + y_3$

§4 Interplanar Forces Caused by Electron-Lattice Interaction

4-1 Interatomic forces and interplanar forces

In general $\chi^{\alpha\beta}(ij,q)$ can be expressed as the Fourier transform of effective interatomic forces[29)]

$$\chi^{\alpha\beta}(ij,q) = \sum_{\ell} F_{\chi}^{\alpha\beta}(\ell i,\ell' j)\exp\{iq\cdot(R_{\ell i}-R_{\ell' j})\}, \tag{4.1}$$

and inversely $F_{\chi}^{\alpha\beta}(\ell i,\ell' j)$ is expressed as

$$F_{\chi}^{\alpha\beta}(\ell i,\ell' j) = \frac{1}{N}\sum_{q} \chi^{\alpha\beta}(ij,q)\exp\{-iq\cdot(R_{\ell i}-R_{\ell' j})\}. \tag{4.2}$$

Further, we can express the change of electronic free energy due to atomic displacements as:

$$\Delta F_1 = \frac{1}{2}\sum_{\alpha\beta}\sum_{\ell i}\sum_{\ell' j} F_{\chi}^{\alpha\beta}(\ell i,\ell' j)\delta R_{\ell i}^{\alpha}\delta R_{\ell' j}^{\beta} . \tag{4.3}$$

From eq.(4.3) we can easily see that $-F_{\chi}^{\alpha\beta}(\ell i,\ell' j)$ represents an effective interatomic force acting on the atom $(\ell' j)$ along the β-direction when the atom (ℓi) is displaced by a unit length along the α-direction, and vice versa.

In general ΔF_1 must be invariant under symmetry operations of the crystal. From this requirement we can obtain a number of mutual relations among $F_{\chi}^{\alpha\beta}(\ell i,\ell' j)$'s. Further, we can determine the tensor form of $F_{\chi}^{\alpha\beta}(\ell i,\ell' j)$ for a given pair of atoms by considering the symmetry operations of the crystal that keep the

pair invariant. In Appendix B we give detailed consideration of the crystal symmetry of BP and determine explicitly tensor forms of the effective force for several kinds of atomic pairs.

If a crystal contains many ions in the primitive unit cell and its crystal symmetry is low, we have a number of independent elements of force constant tensors even if we consider forces only between near neighboring atoms. BP is an example of such crystals. In case we focus our attention on phonon diespersions along a particular direction in the q-space as in the present study, it is convenient to introduce interplanar forces[31] instead of interatomic forces. It is noted that the lattice dynamics for wave vectors along a particular direction can be completely determined by giving forces between planes perpendicular to that direction because all the same kind of atoms on one of such planes vibrate in the same phase. Hence the crystal vibrations can be described as vibrations of a linear chain of planes moving as rigid units. In this picture, $\chi^{\alpha\beta}(ij,q)$ can be expressed as one-dimensional Fourier transform of effective interplanar forces:

$$\chi^{\alpha\beta}(ij,q) = \sum_{p} K_{\chi}^{\alpha\beta}(pi,p'j)\exp\{iq(R_{pi}-R_{p'j})\}, \qquad (4.4)$$

where p or p' denotes a unit cell in the linear chain of planes, $(R_{pi}-R_{p'j})$ represents the distance between the p-th plane of i atoms and p'-th plane of j atoms. The effective interplanar force $K_{\chi}^{\alpha\beta}(pi,p'j)$ is obtained by inverse Fourier transformation of $\chi^{\alpha\beta}(ij,q)$. It can be expressed also in terms of interatomic

forces as follows:

$$K_{\chi}^{\alpha\beta}(pi,p'j) = \sum_{\ell}^{\text{plane}(pi)} F_{\chi}^{\alpha\beta}(\ell i,\ell' j), \tag{4.5}$$

where the atom $(\ell' j)$ is on the plane $(p'j)$ and the summation over ℓ is confined on the plane (pi). It is clear form eq.(4.5) that $-K_{\chi}^{\alpha\beta}(pi,p'j)$ represents the force acting on an atom on the plane $(p'j)$ along the β-direction when the plane (pi) is displaced by a unit length along the α-direction.

If we confine ourselves to the [100] direction of BP, each atomic plane contains only one kind of phosphorus atom, 1, 2, 3, and 4, and the form of interplanar force tensors is determined by symmetry consideration as follows (see Appendix B):

$$K_{\chi}^{\alpha\beta}(p,0) = \begin{pmatrix} a & 0 & b \\ 0 & c & 0 \\ b & 0 & d \end{pmatrix}, \quad \text{(for p=0, 1, 5, and 7)} \tag{4.6}$$

$$K_{\chi}^{\alpha\beta}(p,0) = \begin{pmatrix} a & 0 & b \\ 0 & c & 0 \\ -b & 0 & d \end{pmatrix}, \quad \text{(for p=2, 4, and 8)} \tag{4.7}$$

$$K_{\chi}^{\alpha\beta}(p,0) = \begin{pmatrix} a & 0 & b \\ 0 & c & 0 \\ d & 0 & e \end{pmatrix}. \quad \text{(for p=3A, 6A, and 9A)} \tag{4.8}$$

Here we have omitted for simplicity the site index i (or j) of atoms: a plane of atom 1 has been chosen as the plane 0, and the plane 1 is a plane of atom 2, the plane 2 is a plane of atom 3, the planes 3A and 3B are planes of atom 4, and so on (see Fig.4-1). The interplanar force tensors for p=3B and 6B are

related to those for p=3A and 6A, respectively, as follows:

$$K_{\chi}^{\alpha\alpha}(3B,0) = K_{\chi}^{\alpha\alpha}(3A,0), \quad (\alpha=x,\ y,\ z) \tag{4.9a}$$

$$K_{\chi}^{zx}(3B,0) = -K_{\chi}^{xz}(3A,0), \quad K_{\chi}^{xz}(3B,0) = -K_{\chi}^{zx}(3A,0), \tag{4.9b}$$

$$K_{\chi}^{\alpha\alpha}(6B,0) = K_{\chi}^{\alpha\alpha}(6A,0), \quad (\alpha=x,\ y,\ z) \tag{4.10a}$$

$$K_{\chi}^{zx}(6B,0) = K_{\chi}^{xz}(6A,0), \quad K_{\chi}^{xz}(6B,0) = K_{\chi}^{zx}(6A,0) \tag{4.10b}$$

The relation for p=9B and 9A are the same as those for p=3B and 3A. Because of the crystal symmetry σ_y (i.e. reflection in the plane y=0), off-diagonal xy, yx, yz, and zy elements vanish exactly. Interplanar force tensors $K_{\chi}^{\alpha\beta}(p',p'')$ between arbitraly planes, p' and p", can be easily obtained from the knowledge of $K_{\chi}^{\alpha\beta}(p,0)$ by considering the symmetry of the crystal.

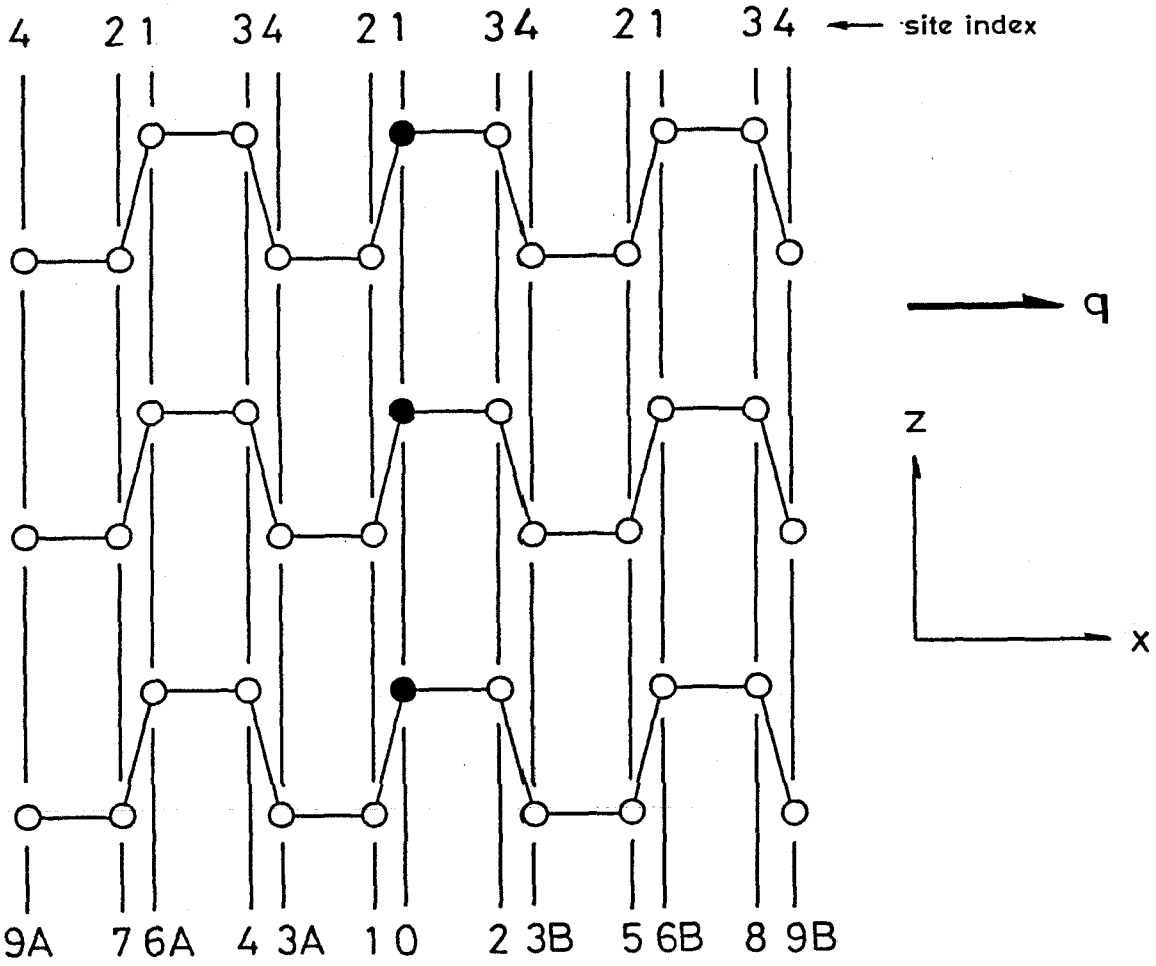

Fig.4-1 The sequence of atomic planes perpendicular to the [100] direction.

4-2 Effective interplanar forces corresponding to $\chi^{\alpha\beta}(ij,q)$

Instead of performing inverse Fourier Transformation of eq.(4.5) we have determined the interplanar forces $K_{\chi}^{\alpha\beta}(p,0)$ by a least sqares fitting (LSF) procedure so as to reproduce $\chi^{\alpha\beta}(ij,q)$ for $q=\Gamma$, $(1/2)\Gamma X$, and X.

The number of independent matrix elements $\chi^{\alpha\beta}(ij,q)$ for above three q-vectors is 50 (11 from Γ, 13 from X, and 26 from $(1/2)\Gamma X$). This is a sufficient number of data to determine the interplanar forces up to the ninth neighboring plane because there are 43 independent force constants within the ninth neighboring plane.

For convenience we introduce three kinds of vector, $\{\chi_\rho\}$, $\{K_\mu\}$ and $\{X_\rho\}$ $(\rho=1,\cdots,50,\ \mu=1,\cdots,43)$:

χ_ρ; independent matrix elements $\chi^{\alpha\beta}(ij,q)$ calculated from eq.(3.31) for $q=\Gamma$, $1/2\Gamma X$ and X.

K_μ; independent interplanar force constants up to the ninth neighboring plane,

X_ρ; independent matrix elements $\chi^{\alpha\beta}(ij,q)$ calculated from eq.(4.5) in terms of K_μ for $q=\Gamma$, $1/2\Gamma X$ and X.

Obviously, X_ρ is expressed in linear combination of K_μ as

$$X_\rho = \sum_\mu C_{\rho\mu}\cdot K_\mu \ , \qquad (\rho=1,\cdots,50\ ;\mu=1,\cdots,43) \qquad (4.11)$$

where coefficients $C_{\rho\mu}$ are known quantities. Then, the variance is defined by

$$V = \sum_{\rho} W_{\rho}(X_{\rho}-\chi_{\rho})^2 = \sum_{\rho} W_{\rho}[\sum_{\mu} C_{\rho\mu}K_{\mu} - \chi_{\rho}]^2, \qquad (4.12)$$

where W_{ρ} denotes the weight. Now, $\{K_{\mu}\}$ can be determined by the minimization condition for the variance V, which is expressed as

$$\sum_{\mu} A_{\nu,\mu} K_{\mu} = D_{\nu} , \qquad (\nu=1,\cdots,43) \qquad (4.13)$$

where

$$A_{\nu,\mu} = \sum_{\rho} C_{\rho\nu}W_{\rho}C_{\rho\mu} , \text{ and } \quad D_{\nu} = \sum_{\rho} W_{\rho}C_{\rho\nu}\chi_{\rho} . \qquad (4.14)$$

On the basis of the above LSF method we have determined the effective interplanar force constants at normal pressure and 15 kbar. We have used the uniform weight (W_{ρ}=const). Solid and dashed curves in Figs.3-1 and 3-2 represent the results of diagonalization of $\chi^{\alpha\beta}(ij,q)$ obtained from eq.(4.4) using such determined interplanar force constants. As seen from the figure, $\chi^{\alpha\beta}(ij,q)$ calculated from eq.(3.31) have been reproduced almost completely.

In Fig.4-2 we show the determined values of $-K_{\chi}^{\alpha\beta}(p,0)$ at normal pressure. Characteristic features of the effective interplanar forces are summarized as follows:

(1) Almost all the forces have negative values, which means that the electron-lattice interaction tends to destabilize the bonds.

(2) Force constants of far neighboring planes are certainly small, but $\chi^{\alpha\beta}(ij,q)$ obtained from eq.(3.31) are reproduced

poorly if we neglect these far neighboring forces. In this sense the effective force is fairly long-ranged.

(3) Magnitude of $-K_{\chi}^{xx}(p,0)$ is remarkably large for the second neighboring plane (p=2) reflecting strong covalent bonding between the plane 0 and the plane 2. It shoud be also noted that the effective force of the fourth neighboring planes (p=4) is considerably large compared with those of other far neighboring planes.

(4) $-K_{\chi}^{yy}(p,0)$ shows a distance-dependence similar to that of the xx-component, but its magnitude is smaller than that of the xx-component.

(5) The zz-component shows a distance-dependence different from that of the xx- or yy-component. The magnitue of $-K_{\chi}^{zz}(p,0)$ is the largest for the first neighboring plane which is connected to the plane 0 by covalent bonds orientating parallel to $\tau_1-\tau_2$.

(6) Off-diagonal xz- and zx-compoments are quite small except for the first neighboring plane. For this reason the mixing of the displacements along the x- and z-directions is considerably small in the LAx and TAz eigenvectors of $\chi^{\alpha\beta}(ij,q)$.

Next we have investigated effects of pressure on the effective interplanar forces. The changes of interplanar forces due to pressure

$$\Delta[-K_{\chi}^{\alpha\beta}(p,0)] \equiv [-K_{\chi}^{\alpha\beta}(p,0)]_{15kbar} - [-K_{\chi}^{\alpha\beta}(p,0)]_{0kbar}$$

are ploted in Fig.4-3. Effects of pressure on each component of $-K_{\chi}^{\alpha\beta}(p,0)$ are summarized as follows:

(a) All of $\Delta[-K_{\chi}^{xx}(p,0)]$ are found to be negative, i.e. the magnitude of the xx-component is increased by pressure. It should be noted that the relaticve increase of the magnitude is particularly large for p=4.

(b) The magnitude of $\Delta[-K_{\chi}^{yy}(p,0)]$ is almost the same as that of the xx-component for p=1 and 2. For p=4 and 5, however, the magnitude of $\Delta[-K_{\chi}^{yy}(p,0)]$ is about a half of that of $\Delta[-K_{\chi}^{xx}(p,0)]$.

(c) The magnitude of $\Delta[-K_{\chi}^{zz}(p,0)]$ is particularly large for p=1. However, this change cannot affect strongly the frequencies of the LAz mode of long wave length, as will be discussed in the next section.

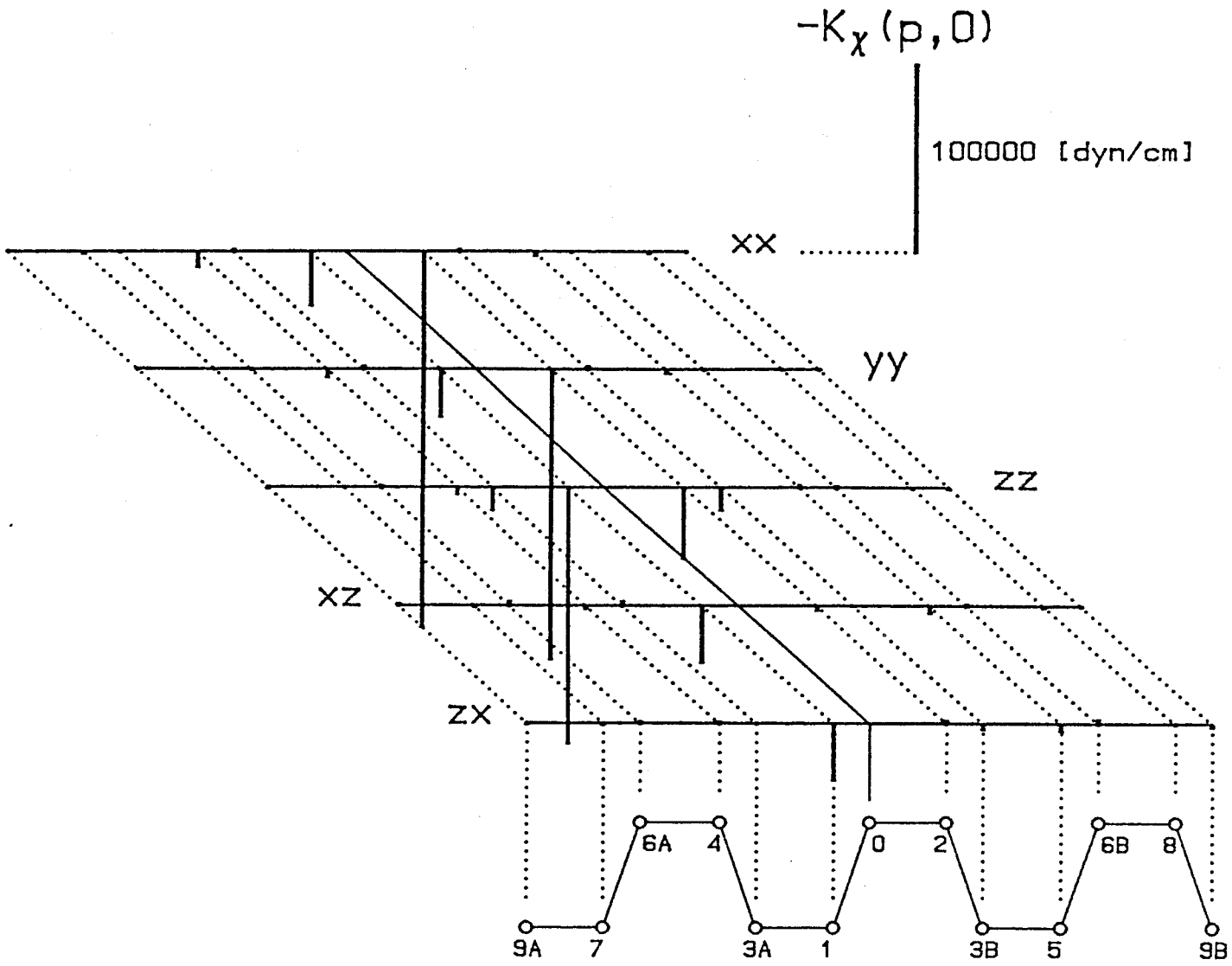

Fig.4-2 The effective interplanar force constants $-K_\chi^{\alpha\beta}(p,0)$ corresponding to the generalized electronic susceptibility $\chi^{\alpha\beta}(ij,q)$.

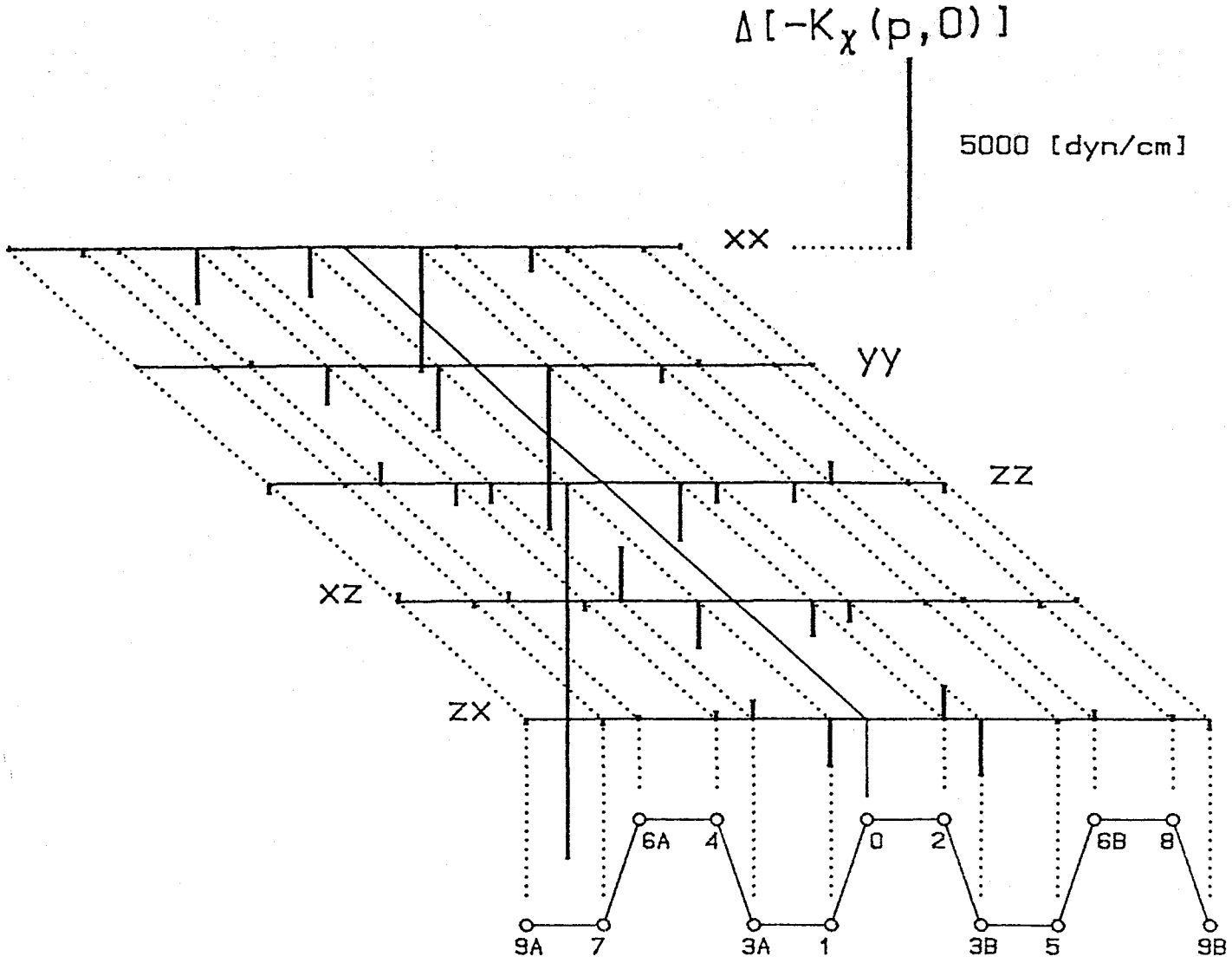

Fig.4-3 Difference between two effective interplanar force constants at 15 kbar and 0 kbar: $-\Delta K_{\chi}^{\alpha\beta}(p,0) \equiv [-K_{\chi}^{\alpha\beta}(p,0)]_{15\ \text{kbar}} - [-K_{\chi}^{\alpha\beta}(p,0)]_{0\ \text{kbar}}$.

§5 Lattice Dynamics

From the results of calculation of the generalized electronic susceptibility $\chi^{\alpha\beta}(ij,\mathbf{q})$ of BP we have pointed out in §3 that the electron-lattice interaction can give rise to large softening of the LAx phonon frequency as pressure is applied. As mentioned at the end of subsection 3-1, however, the true phonon frequency is determined by the total dynamical matrix $D^{\alpha\beta}(ij,\mathbf{q}) = \chi^{\alpha\beta}(ij,\mathbf{q}) + R^{\alpha\beta}(ij,\mathbf{q})$. Hence, to see whether the LAx mode can actually show softening as pressure is applied we have to calculate the phonon dispersion along the [100] direction by taking account of short-range repulsive part $R^{\alpha\beta}(ij,\mathbf{q})$.

We express $R^{\alpha\beta}(ij,\mathbf{q})$ in terms of short-range interplanar force constants $K_R^{\alpha\beta}(pi,p'j)$ in the same manner as eq.(3.4). Then, the total interplanar force constants $K^{\alpha\beta}(pi,p'j)$ are given by

$$K^{\alpha\beta}(pi,p'j) = K_\chi^{\alpha\beta}(pi,p'j) + K_R^{\alpha\beta}(pi,p'j). \tag{5.1}$$

and the dynamical matrix $D^{\alpha\beta}(ij,\mathbf{q})$ is expressed as the Fourier transform of $K^{\alpha\beta}(pi,p'j)$:

$$D^{\alpha\beta}(ij,\mathbf{q}) = \sum_p K^{\alpha\beta}(pi,p'j)\exp\{iq(R_{pi}-R_{p'j})\}. \tag{5.2}$$

Now, the phonon frequencies are determined by solving the secular equation

$$\det\left| D^{\alpha\beta}(ij,\mathbf{q}) - M\omega^2 \right| = 0, \qquad (5.3)$$

where M denotes the mass of the phosphorus atom.

At symmetry points or on symmetry lines the dynamical matrix D can be represented in a irreducible form (i.e. a block diagonalized form) and then the determinant in eq.(5.3) can be factorized. For example, D is decomposed into two 2×2 matrices and eight 1×1 matrices at the Γ point and into two 4×4 matrices and two 2×2 matrices on the Δ line.

5-1 Lattice dynamics at normal pressure

We first calculate the phonon dispersion curves at normal pressure. For that purpose we have to determine the short-range interplanar force constants $K_R^{\alpha\beta}(p,0)$ at normal pressure. We have assumed $K_R^{\alpha\beta}(p,0)=0$ for $p\geq 4$ except $K_R^{zz}(4,0)$. Then, the total number of independent short-range force constants is 13. These independent force constants have been determined by a procedure of least-squares fits (LSF) so as to reproduce thirteen phonon frequencies (eight optical modes at Γ, two at X, and three acoustical modes at (1/4,0,0)) obsreved by Raman scattering,[17] by infrared reflection,[16] and by inelastic neutron scattering.[13] These experimental data are listed in Table 5-1 and ploted in Fig.5-1 by closed circles. The force constant $K_R^{zz}(4,0)$ had to be included in order to reproduce the phonon frequency of the Γ_3^- mode.

Eigenvectors of four optical modes, Γ_3^+, Γ_4^+, Γ_3^- and Γ_4^-, are determined uniquely from symmetry. Hence, the phonon frequencies of these modes are expressed explicitly in the form of linear combination of the interplanar force constants. By making use of these linear relations we have reproduced exactly the frequencies of the Γ_4^+, Γ_3^- and Γ_4^- modes. As for the Γ_3^+ mode we did not fix its frequency at the observed value, 197 cm^{-1}.[17] The reason is that if we reproduce completely the frequency of the Γ_3^+ mode the frequency of the TAy branch at the X point is then determined always to be lower by about 20 cm^{-1} than the observed value, 146 cm^{-1}.[13] We have tried to reproduce the

frequency of the TAy branch as well as possible with sacrifice of the frequency of the Γ_3^+ mode. Furthermore, we have given special weight on the three acoustical modes at q=(1/4,0,0) so as to reproduce the frequencies of these modes with the smallest variance. The final values of those phonon frequencies optimized in this way are shown in column 5 of Table 5-1.

In Fig.5-1 we show by solid curves the phonon dispersion curves calculated by using $K_R^{\alpha\beta}(p,0)$ determined above and $K_\chi^{\alpha\beta}(p,0)$ obtained in §4. The whole dispersion along the Δ line consists of six high-energy branches with energies higher than $350cm^{-1}$, and six low-energy branches with energies lower than $250cm^{-1}$ including three acoustical branches, LAx, TAy and TAz. The characteristic shape of the LAx branch as well as the features of the TAz and the TAy branches are in good agreement with the experimental results by Yamada et al.[13)]

The short-range interplanar forces $K_R^{\alpha\beta}(p,0)$ and the total interplanar forces $K^{\alpha\beta}(p,0)$ are illustrated in Fig.5-2 and 5-3, respectively. Comparing Figs.4-1, 5-2, and 5-3 we can see a large cancellations between $K_\chi^{\alpha\beta}(p,0)$ and $K_R^{\alpha\beta}(p,0)$. Since we have assumed $K_R^{\alpha\beta}(p,0)=0$ for $p\geq 4$, $K^{\alpha\beta}(p,0)$ is equal to $K_\chi^{\alpha\beta}(p,0)$ for $p\geq 4$. The total interplanar force constants $K^{\alpha\beta}(p,0)$ can be classified into three groups according to their magnitudes and each group plays a charateristic role in determining the phonon frequencies as follows:

(1) Group L: Forces with magnitude larger than 13×10^4 dyn/cm. This group determines mainly the energies of the six

high-energy branches.

(2) Group M: Forces with magnitude of $1\times10^4\sim4\times10^4$ dyn/cm. This group determines mainly the energies of the six low-energy branches.

(3) Group S: Forces with magnitude smaller than 1×10^4 dyn/cm. This group modifies slightly the energies of the six low-energy branches.

Since the puckered layer is constructed by the covalent bonds, both xx- and yy-components of the total interplaner forces take their largest value (belong to group L) for p=2, whereas the zz-component takes its largest value (group L) for p=1.

The normal coordinate of the Γ_3^- mode is given by $z_1+z_2-z_3-z_4$ and hence the frequency of this mode is determined only by the zz-components of the forces as follows:

$$\omega(\Gamma_3^-) = [2\{-K^{zz}(2,0)-2K^{zz}(3A,0)-K^{zz}(4,0)\}/M]^{1/2} \qquad (5.4)$$

where we have neglected $K^{zz}(p,0)$ with $p\geqq6$. In the right-hand side of eq.(5.4) a considerable cancellation occurs between the negative force (group M) for p=2 and the positive forces (group M) for p=3A (see Fig.5-3). This is a reason why the zz-component of the short-range force for p=4 had to be taken into account as an adjustable parameter.

Off-diagonal xz- or zx-components of the total forces take their largest value (group M) for p=1. It should be noted that these off-diagonal forces play a significant role in determining

the curvature of the characteristic shape of the LAx branch, as explained below. If we neglect all of the off-diagonal forces in the present case , the lowest optical branch and the acoustical branch with symmetries Δ_1 and Δ_2 become as shown by solid curves in Fig.5-3. Here the squared frequency $\omega^2(\mathbf{q})$ of the LAx mode or the TAz mode can be written as

$$\begin{aligned} M\omega^2(q) = & -4K(3A)\sin^2(\pi q/2)-4K(6A)\sin^2(\pi q)-S \\ & +[S^2-4\{K(1)K(2)+K(1)K(4)+K(2)K(5)\}\sin^2(\pi q/2) \\ & -4\{K(1)K(5)+K(2)K(4)\}\sin^2(\pi q) \\ & -4K(4)K(5)\sin^2(3\pi q/2)]^{1/2} \end{aligned} \qquad (5.5)$$

where $S\equiv K(1)+K(2)+K(4)+K(5)$ and $K(p)$ represents $K^{xx}(p,0)$ for the LAx mode and $K^{zz}(p,0)$ for the TAz mode. The dotted curves which are plotted in the extended zone and meet with the LAx and the TAz branches at the X point, respectively, indicate the energies of "extended" acoustical branches calculated from eq.(5.5) by extending the wave vector q to $\Gamma'=(1,0,0)$ beyoned the zone boundary X. It should be noted that the symmetry of the mode changes from Δ_1 (Δ_2) to Δ_2 (Δ_1) as coming from the first Brillouin zone (Γ-X) into the extended zone (X-Γ') along a acoustical branch defined by eq.(5.5). Thus, the lowest optical branch which meets the TAz branch at the X point and crosses with the LAx branch near (2/3)ΓX has the same symmetry as that of the LAx mode, i.e. Δ_1 symmetry. Therefore, if we take account of off-diagonal forces , this accidental degeneracy at the crossing

between the two branches is removed. As the result we obtain such a characteristic shape of the LAx branch. It should be noted that the energy of the Γ_3^- mode (136 cm^{-1}) shown in Fig.5-3 is not affected by the off-diagonal forces.

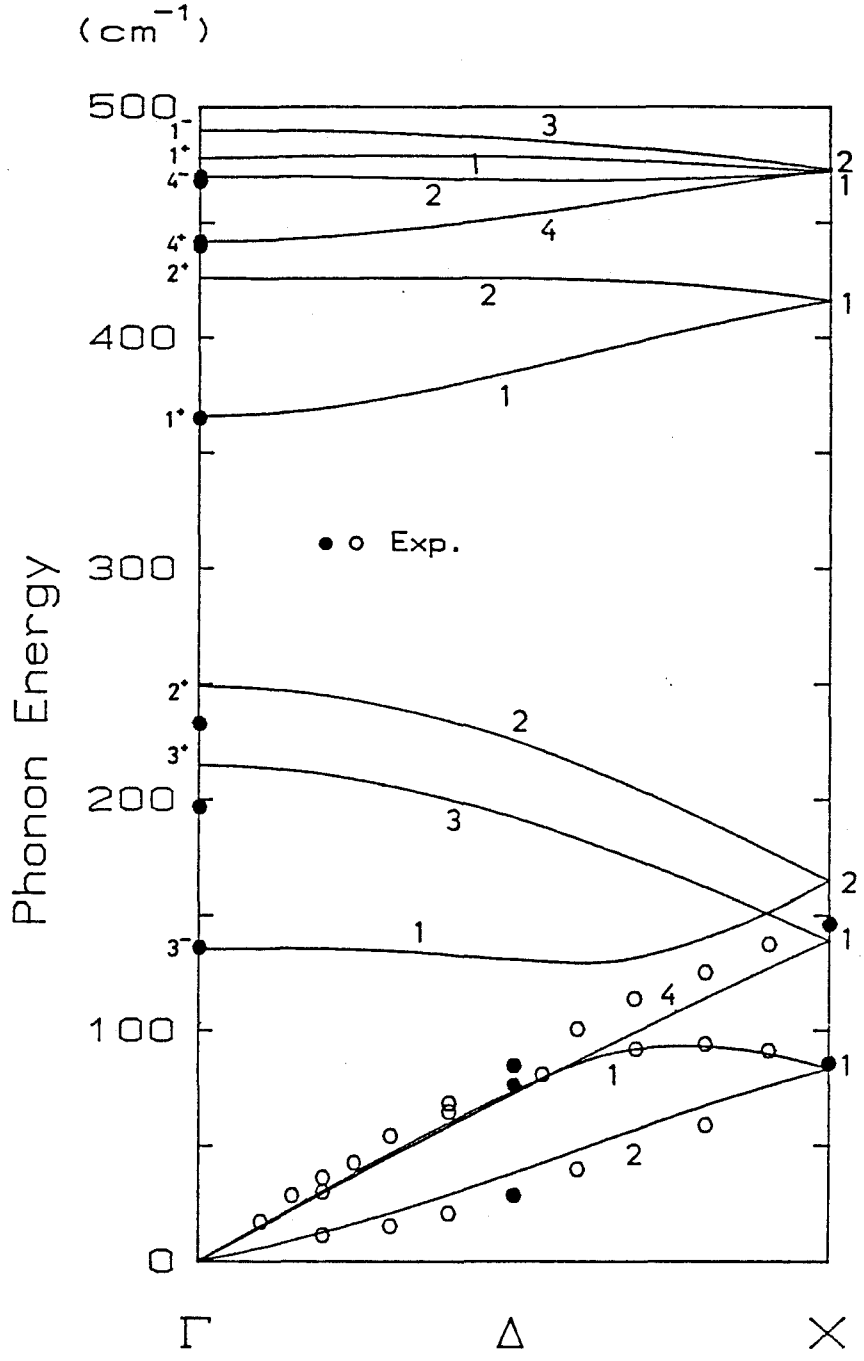

Fig.5-1 The phonon dispersion curves at 0 kbar (normal pressure). Experimental data are taken from Ref.13. Data represented by closed circles are used for the least-squares fitting procedure to determine the short-range interplanar forces.

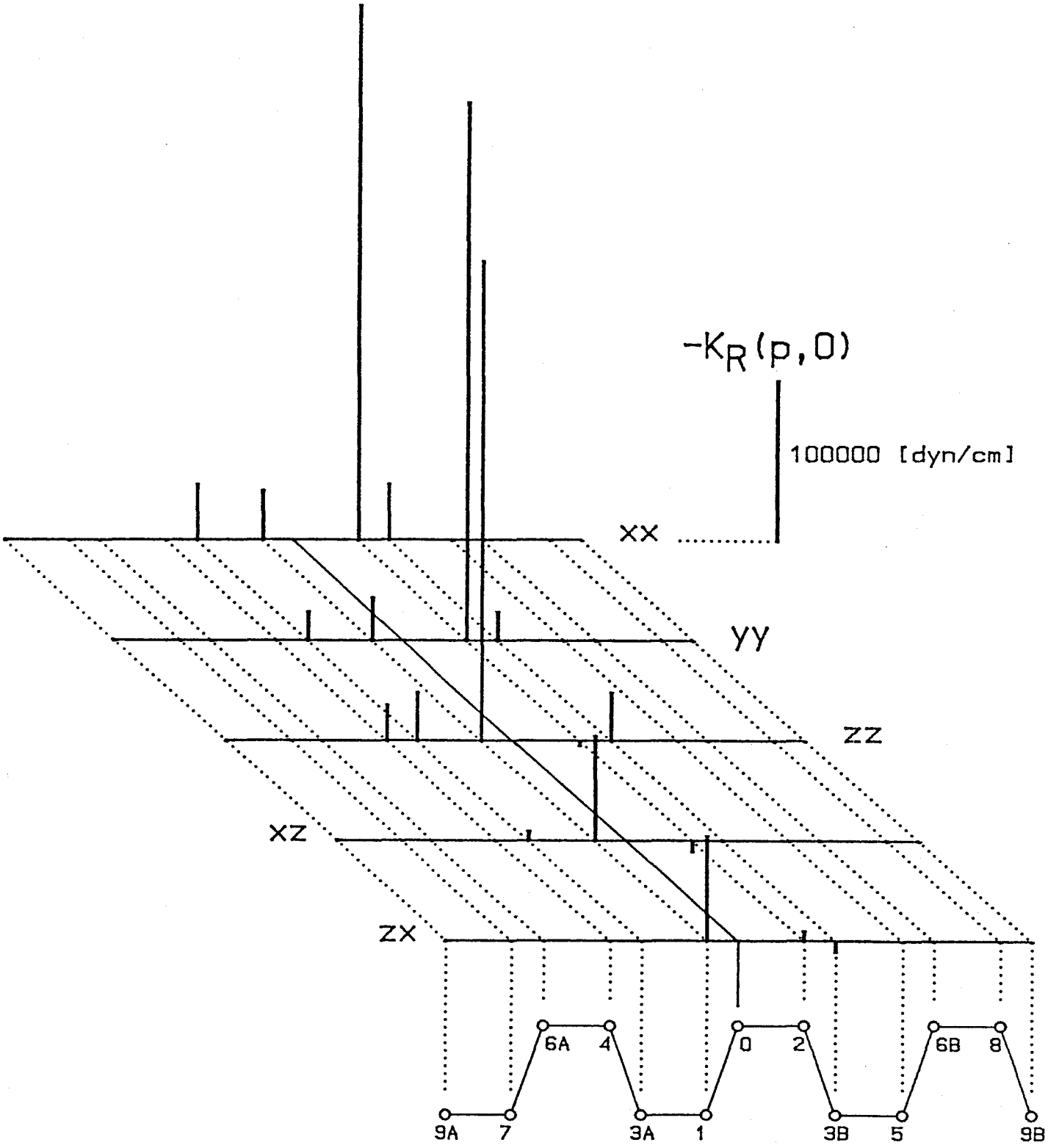

Fig.5-2 The short range repulsive interplanar force constants $-K_R^{\alpha\beta}(p,0)$.

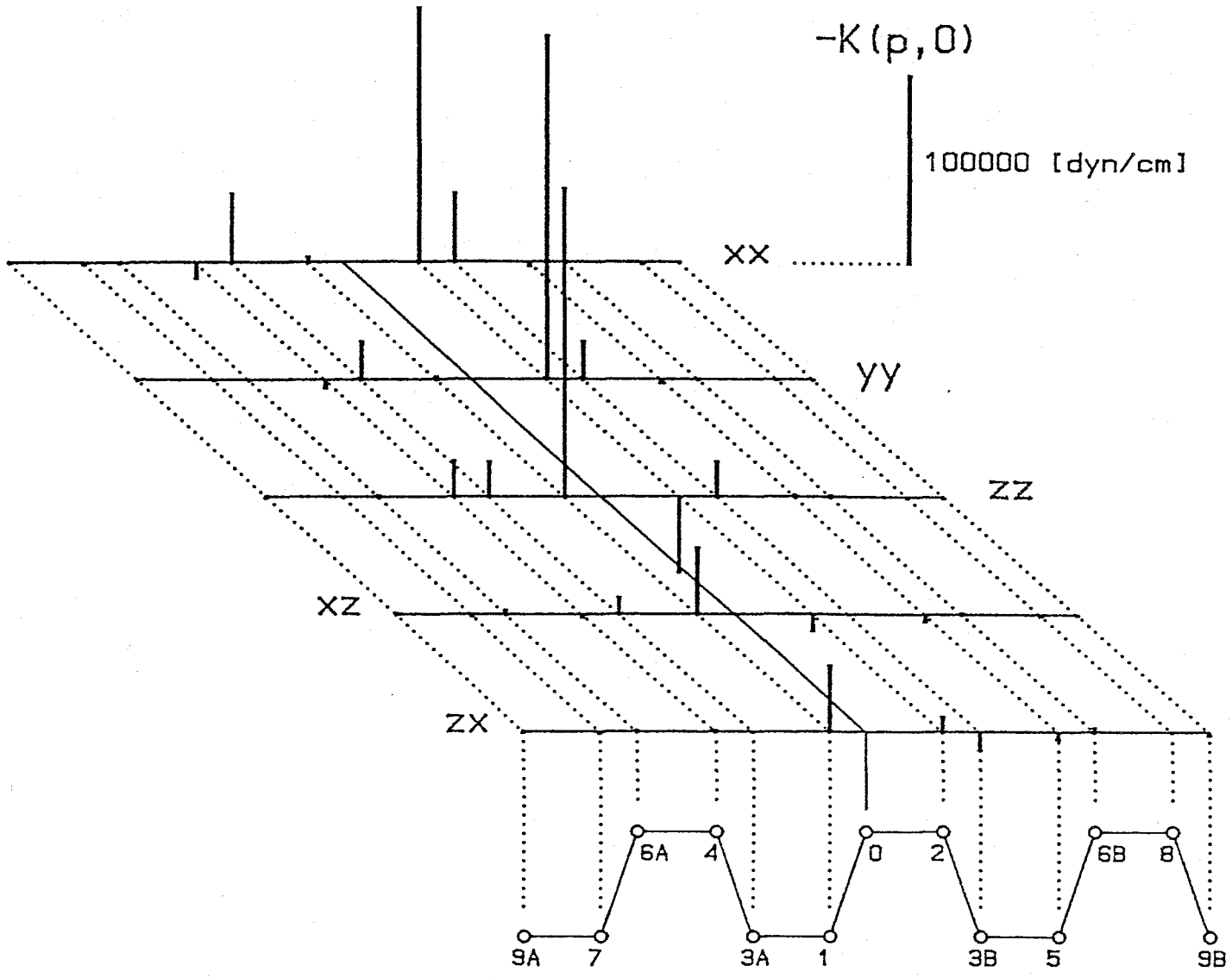

Fig.5-3 The total interplanar force constants $-K^{\alpha\beta}(p,0) = -[K_{\chi}^{\alpha\beta}(p,0) + K_{R}^{\alpha\beta}(p,0)]$.

5-2 Pressure effects - Softening of LAx-phonon

In order to see clearly effects of the change of $K_{\chi}^{\alpha\beta}(p,0)$ due to pressure on the lattice dynamics we have first calculated the phonon dispersion curves by using $K_{\chi}^{\alpha\beta}(p,0)$ at 15 kbar and $K_{R}^{\alpha\beta}(p,0)$ determined for normal pressure in the previous subsection. The results are shown by dotted curves in Fig.5-5. For comparison, the phonon dispersidon curves at normal pressure are also depicted by full curves. As expected in §3 every modes shows softening of frequency due to pressure. Among three acoustical branches the LAx branch certainly shows the largest softening in the region except near the Γ point. The frequency of the TAz mode with long wave-length (i.e. with a wave vector near the Γ point) is considerably small at normal pressure and its frequency is very sensitive to change of the forces. Therefore it becomes imaginary at 15 kbar.

In real situation the short range forces $K_{R}^{\alpha\beta}(p,0)$ also depend on pressure and we may expect that the magnitude of $K_{R}^{\alpha\beta}(p,0)$ increases with increasing pressure. At present, however, we have no way to evaluate the pressure dependence of $K_{R}^{\alpha\beta}(p,0)$. Therefore, we have assumed simply that magnitudes of $K_{R}^{\alpha\beta}(p,0)$ increase at the same rate, ε, as pressure is applied. The dotted curves in Fig.5-6a show phonon dispersion curves obtained by using $K_{\chi}^{\alpha\beta}(p,0)$ at 15 kbar and short-range force constants larger by 5% (ε=0.05) than those at normal pressure. Fig.5-6b shows the phonon dispersion curves of the LAx and TAz modes in enlarged scale. As seen form Figs.5-6a and 5-6b the LAx mode

does show softening whereas othere phonon modes show hardening except the TAy mode whose frequency is almost unchanged. Experimentally there is no observation about the pressure dependence of the TAy mode. Experimental results by Yamada et al.[13] are shown in Fig.5-6b by open circles (0 kbar) and by closed circles (15 kbar). We can see a qualitative agreement between the theoretical and experimental results.

It should be emphasized that far-neighboring interplanar forces caused by electron-lattice interaction is indispensable to explaining the observed pressure-dependence of phonon frequencies. In particular, large increase of the magnitude of $K_{\chi}^{xx}(4,0)$ caused by pressure plays a vital role in pressure-induced softening of the LAx mode. If we neglect all of off-diagonal components of the forces and take account of the forces up to the sixth neiboring plane, then the squared frequency of the LAx mode with long wave-length is written as

$$M\omega^2(q) \simeq -[K(3A)/4 + K(6A) + \gamma\{K(1)+K(5)\}/8 + \gamma K(4)/2]q^2 \qquad (5.6)$$

where K(p) stands for $K^{xx}(p,0)$, and $\gamma \equiv K(2)/\{K(1)+K(2)+K(4)+K(5)\}$. Eq.(5.6) is obtained by expanding eq.(5.5) with respect to q around the Γ point. The value of γ is nearly equal to unity because the magnitude of $K(2) \equiv K^{xx}(2,0)$ is very large compared with those of K(1), K(4) and K(5) (see Fig.5-3). Therefore the right-hand side of eq.(5.6) is much affected by the change of $K(4) \equiv K^{xx}(4,0)$ and $K(6A) \equiv K^{xx}(6A,0)$. In the present case the value of $K(6A) = K_{\chi}^{xx}(6A,0)$ and its pressure dependence are very small (see

Figs.4-2 and 4-3). Dashed curves in Fig.5-4 show the dispersion curves obtained by using $K^{xx}(4,0)$ at 15 kbar and the other force constants at normal pressure with neglect of off-diagonal xz- and zx-components. It is clearly seen that the considerable softening of the LAx mode can be caused by the change of the fourth neighboring interplanar force due to pressure.

According to our consideration about the origin of the characteristic shape of the LAx branch, it can be understood that the pressure dependence of the forces which give rise to the hardening of the TAz mode is also responsible to the hardening of the LAx mode which have appeared near the zone boundary.

Sugai et al.[16] have found from the Raman scattering experiment that three Raman active modes Γ_1^+ (467cm^{-1}, 362 cm^{-1}), and Γ_4^+ (439 cm^{-1}) show the hardenings by magnitudes of 2 cm^{-1}, 10 cm^{-1}, and 4 cm^{-1}, respectively, as pressure of 15 kbar is applied. As seen from Fig.5-6a, the hardenings of these modes are qualitatively reproduced by our calculation though the calculated frequencies are somewhat larger than measured ones. Our calculation predicts also that the infrared active Γ_3^- mode will show hardening by magnitude of a few cm^{-1} as pressure of 15 kbar is applied. Thus far, however, there has been no measurement on the pressure dependence of this frequency.

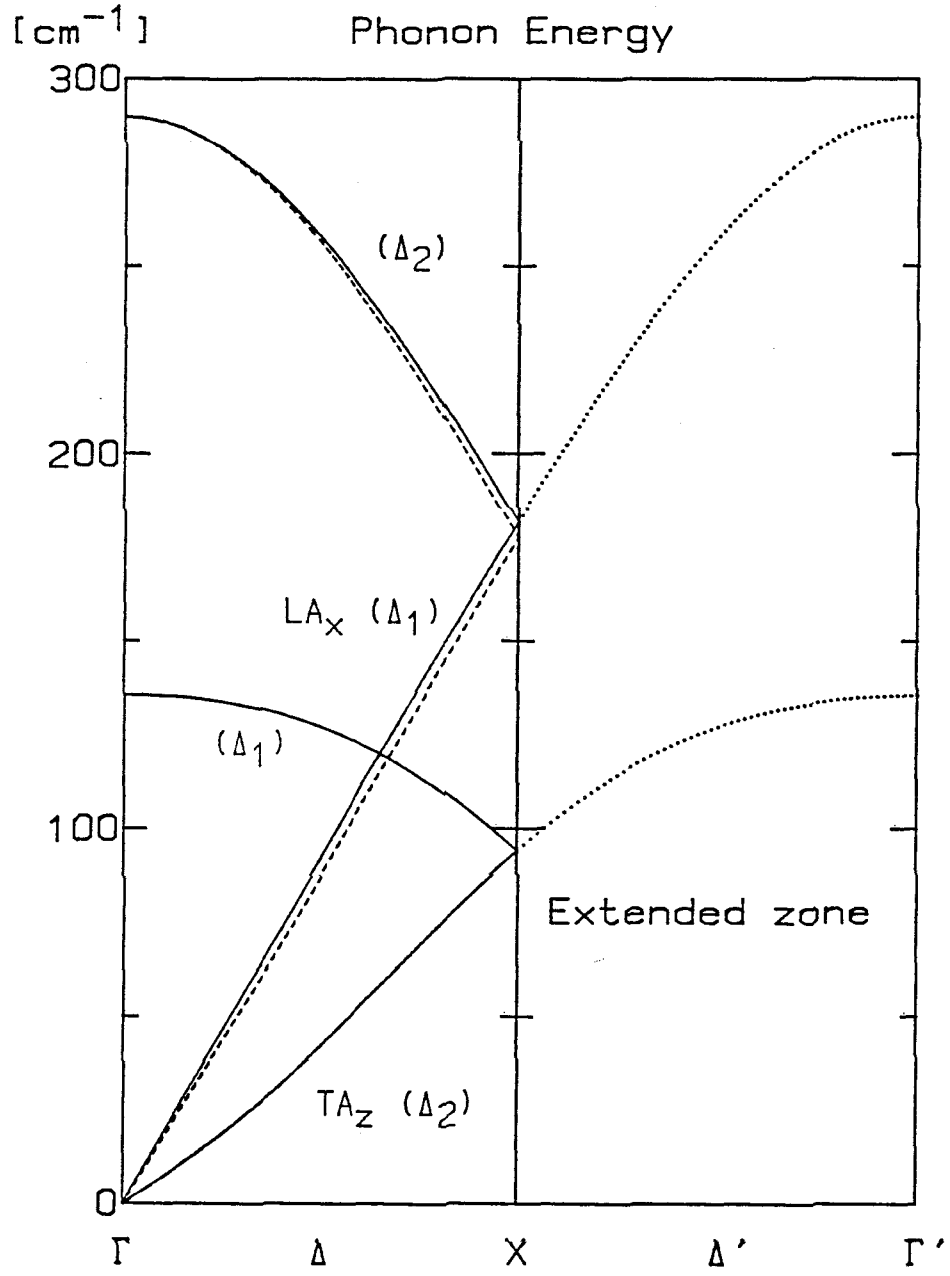

Fig.5-4 The phonon dispersion curves of the LAx and TAz modes when the off-diagonal xz- and zx-components of interplanar forces are neglected. The broken curves represent the dispersion obtained by using $K^{xx}(4,0)$ at 15 kbar and other forces at 0 kbar.

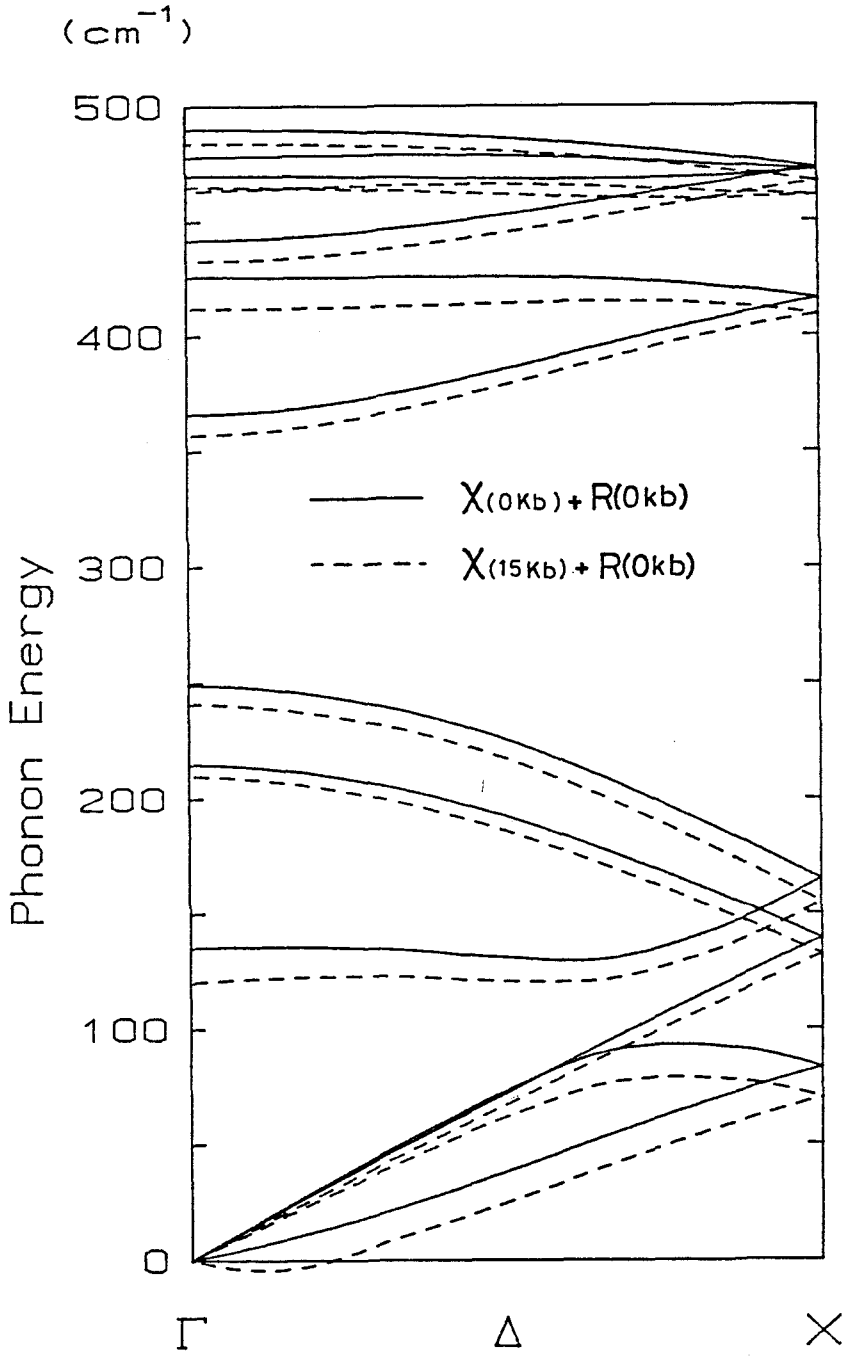

Fig.5-5 The phonon dispersion curves calculated by using χ[0 kbar] and R[0 kbar] (full curves) and by using χ[15 kbar] and R[0 kbar] (broken curves).

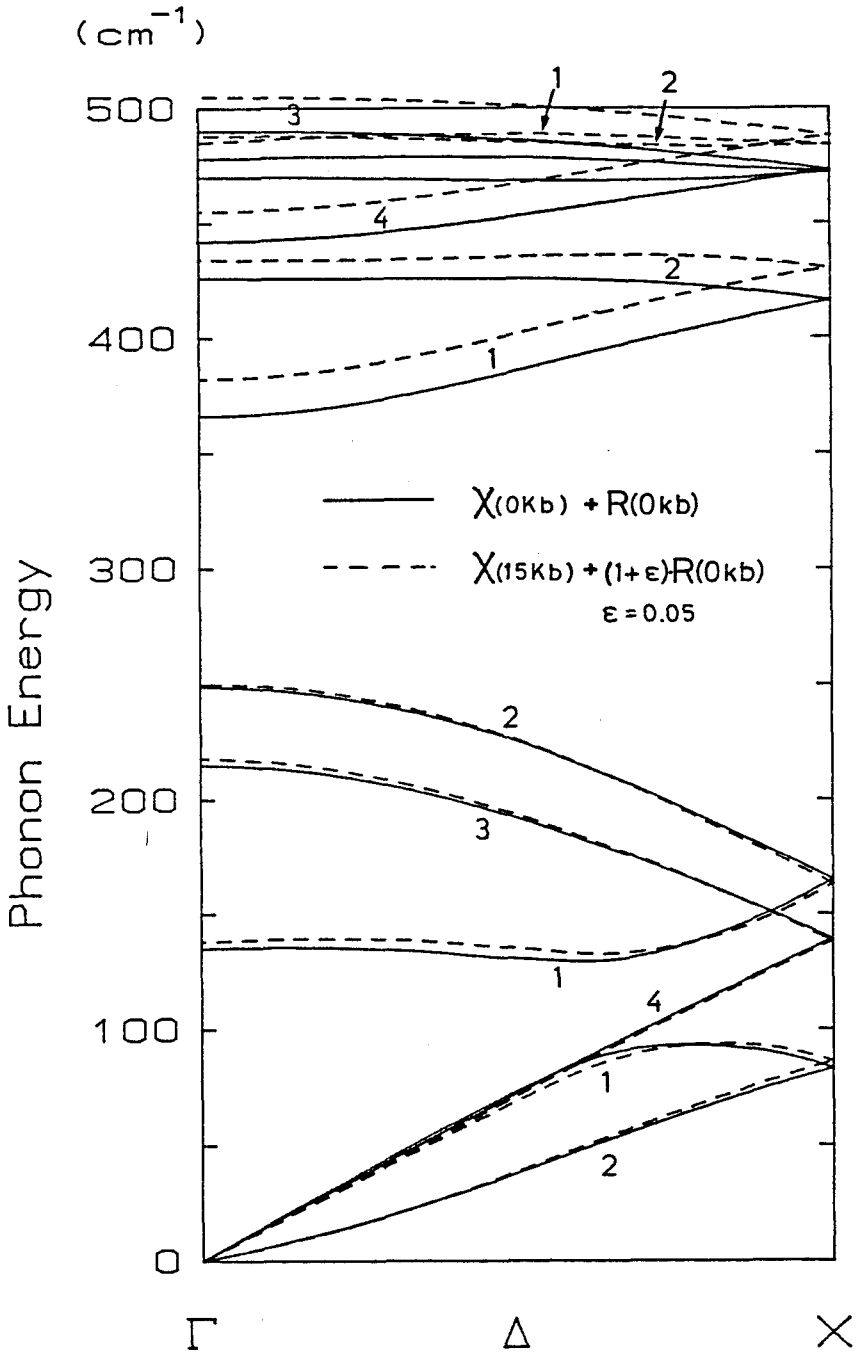

Fig.5-6a The phonon dispersion curves calculated by using χ[0 kbar] and R[0 kbar] (full curves) and by using χ[15 kbar] and 1.05×R[0 kbar] (broken curves). The numbers, 1, 2, 3 and 4, denote the symmetry: 1; Δ_1, 2; Δ_2, 3; Δ_3, 4; Δ_4.

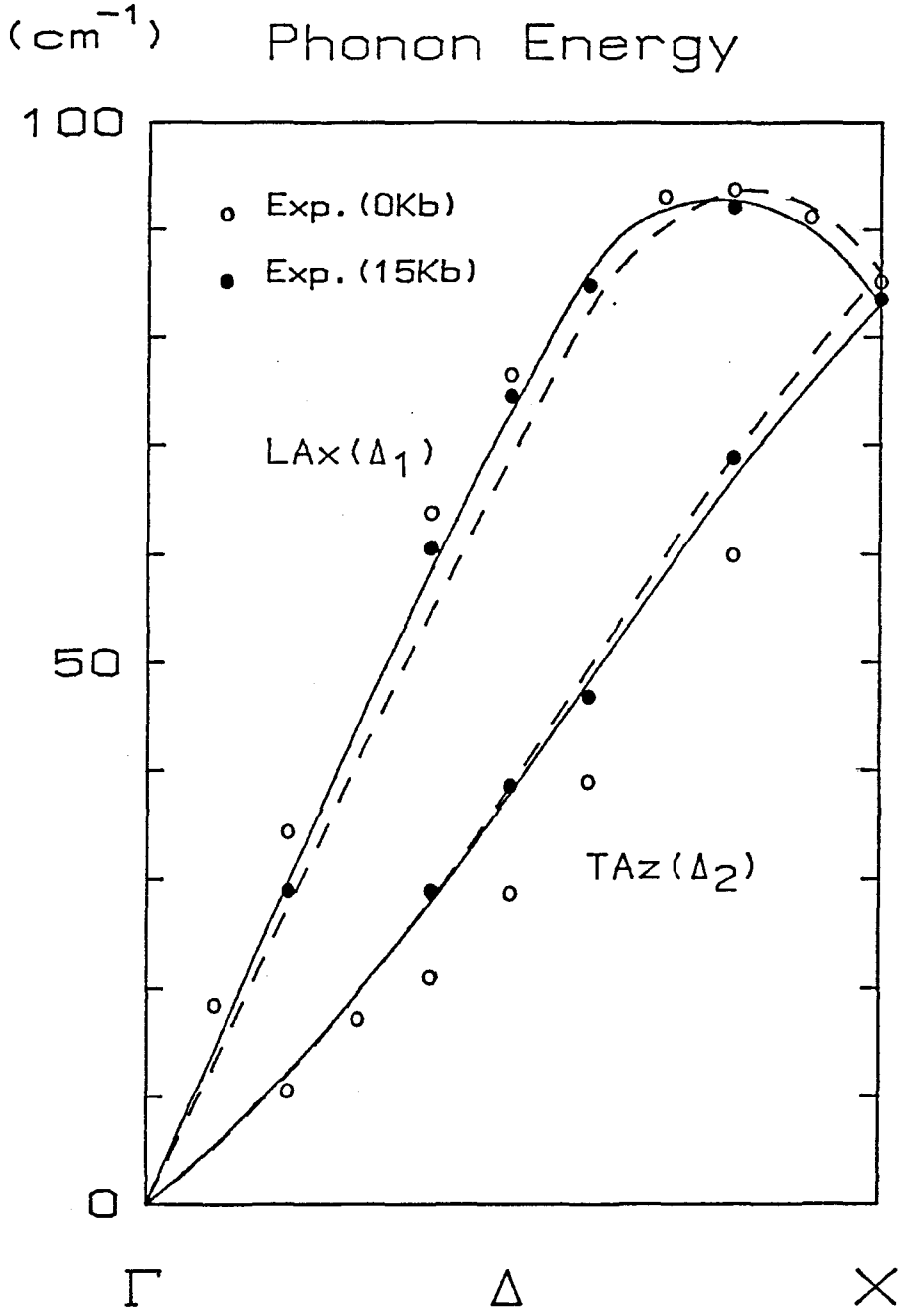

Fig.5-6b The phonon dispersion curves of the LAx and TAz modes which are drawn by enlarging Fig.5-6a. Full curves: at 0 kbar; broken curves: at 15 kbar. Experimental data are taken from Ref.13.

Table 5-1. Thirteen phonon frequencies used for the LSF determination of the short-range interplanar forces.

No.	Irred. Rep.	Phonon frequency (cm^{-1})		
		Experiment		Calculation
1	Γ_1^+	R	365	365.7
2	Γ_1^+	R	470	478.7
3	Γ_2^+	R	233	248.7
4	Γ_2^+	R	440	425.6
5	Γ_3^+	R	197	215.0
6	Γ_4^+	R	442	442.0
7	Γ_3^-	IR	136	136.0
8	Γ_4^-	IR	470	470.0
9	X_1	N	85	83.1
10	X_2	N	146	139.0
11	Δ_1^*	N	76	73.0
12	Δ_2^*	N	28	37.0
13	Δ_4^*	N	84	72.0

* $q=(1/2)\Gamma X$

R: Raman scattering (Sugai and Shirotani)[16)]

IR: Infrared reflection (Sugai and Shirotani) 16)

N: Inelastic neutron scattering (Yamada et al.)[13)]

§6. Supplementary Remarks and Conclusion

As mentioned in §1 lattice dynamics of BP at normal pressure has been studied thus far on the basis of two phenomenological models: one is the valence force field model (VFFM) by Kaneta et al.[14] and the other the bond charge model(BCM) by Kaneta and Morita.[15]

The VFFM has been widely used to calculate molecular vibrations and lattice vibrations of covalent crystals of the group IV.[32] Kaneta et al.[14] introduced four lattice dynamical variables within a puckered layer: the changes of the two kinds of bond lengths for the nearest and next nearest neighboring atoms, δr and $\delta r'$, and the changes of the two kinds of bond angles, $\delta\theta$ and $\delta\theta'$. In the scheme of interatomic forces this model of Kaneta et al. takes account of interatomic interactions up to the fifth neighbors in a layer. As for the interaction between the nearest neighboring puckered layers they assumed axially symmetric interatomic forces up to third neighbors. In the scheme of interplanar forces along the [100] direction this model takes account of interplanar interactions only up to third neighbors.

This VFFM can reproduce almost all the observed phonon frequencies at normal pressure. However, it has two disadvantageous points. The first one is that it cannot reproduce the frequency of the Γ_3^- mode in a satisfactory way. As long as the interlayer interaction is very weak, the

frequencies of the Γ_3^- and Γ_3^+ modes are almost determined only by a single parameter, $K_{\theta'}$, which is the coefficient of $(\delta\theta')^2$ in the VFF, and then it is easily shown that the frequency of the Γ_3^- mode ia always higher than that of Γ_3^+ mode. Experimentally the frequency of the Γ_3^- mode ($136cm^{-1}$)[16] is much smallar than that of the Γ_3^+ mode ($197\ cm^{-1}$).[17] If we assume unusually large interactions between the layers, we may reproduce both frequencies of the Γ_3^- and Γ_3^+ modes. If we do so, however, we cannot reproduce other phonon frequencies at all. The second disadvantageous point is that it cannot explain the characteristic pressure dependences of phonon frequencies. In fact, we have tried to explain the observed pressure effects on the basis of the force constant model with use of interplanar forces only up to the third neighboring planes, which is equivalent to the VFFM with respect to the lattice vibration along the [100] direction. As the result we have found that we can never explain the experimental results. This fact also suggests strongly the necessity of far-neighboring interplanar forces in order to explain the observed pressure dependences of phonon frequencies.

Recently, Kaneta and Morita[15] have used the BCM to improve lattice dynamical calculation of BP at normal pressure. In this model, point bond charges which move adiabatically with the ions are introduced at the midpoint of each pair of covalently bonding ions. The first disadvantageous point in the VFFM is then removed, because the BCM has new additional degrees of freedom

with respect to the point bond charge so that the vibration of the Γ_3^- mode can be described without changing BC-ion-BC angle, θ'. There has been no attempt to calculate lattice dynamics of BP at 15 kbar on the basis of this BCM. Hence, it is not clear whether the BCM can explain the observed pressure dependences of phonon frequencies.

We have calculated the generalized electronic susceptibility $\chi^{\alpha\beta}(ij,q)$ of BP and the corresponding interplanar forces $K_\chi^{\alpha\beta}(pi,p'j)$ by using the electron-lattice interaction derived microscopically on the basis of realistic tight-binding calculation of the band structure. With respect to the short range repulsive part $R^{\alpha\beta}(ij,q)$ of the dynamical matrix we have treated it phenomenologically. In this sense, our calculation of lattice dynamics of BP is not fully microscopic. The point we would like to stress is that we have succeeded for the first time in presenting a partly microscopic model of lattice dynamics which can explain well the characteristic pressure dependences of phonon frequencies observed in BP.

The results we obtained in the present study are summarized as follows:

(1) Effective interplanar forces caused by electron-lattice interaction is fairly long-range in black phosphorus because of its small energy gap.

(2) These effective interplanar forces play a role of softening phonon frequencies as pressure is applied.

(3) The softening is the largest for the LAx (Δ_1-symmetry) mode. This consequence comes from the facts: (i) the energy gap decreases considerably by pressure and (ii) only the Δ_1-mode can couple the conduction band bottom (Z_4^-) with the highest valence band states (U_2-symmetry) near the Z point.

(4) These effective interplanar forces combined with short-range repulsive forces appropriately chosen can explain qualitatively the characteristic pressure dependences of phonon frequencies, i.e. only the LAx mode shows softening as pressure is applied whereas other modes show hardening.

(5) It is the effective force $K_\chi^{xx}(4,0)$ (fourth neighboring interplanar force) that plays a most crucial role in pressure-induced softening of the LAx mode.

Appendix A. Slater-Koster representation of differential coefficients of overlap integral

We summarize here the differential coefficients of overlap integrals with respect to the Cartesian coordinates of atom.

The overlap integral between an orbital ν centered at origin and an orbital centered at $(x,y,z) = R(\ell,m,n)$, i.e. distance R along direction (ℓ,m,n), can be represented as

$$S_{\mu\nu}(x,y,z) = \sum_j C_{\mu\nu,j}\{\ell,m,n\}\cdot(\mu\nu;j) \qquad (A.1)$$

where $(\mu\nu;j)$ stands for Slater-Koster's (S-K) two center integral, which is a function of interatomic distance R, index j specifies a type of bond, namely $j=\sigma,\pi,\delta,\cdots$, $C_{\mu\nu,j}\{\ell,m,n\}$ is a function of direction cosines, ℓ,m,n. The S-K representation of overlap integrals for s and p orbitals are presented in Table A-1.

In order to treat (ℓ,m,n,R) as a set of independent variables, we introduce an artificial variable $u=(\ell^2+m^2+n^2)^{1/2}$, which is unity in actual. Then alternative sets of independent variables (x,y,z,u) and (ℓ,m,n,R) are related as

$$x=\ell R,\ y=mR,\ z=nR,\ u=(\ell^2+m^2+n^2)^{1/2}\ . \qquad (A.2)$$

The inverse relation is

$$\ell=xu/(x^2+y^2+z^2)^{1/2},\ m=yu/(x^2+y^2+z^2)^{1/2},\ n=zu/(x^2+y^2+z^2)^{1/2},$$

$$R=(x^2+y^2+z^2)^{1/2}/u. \qquad (A.3)$$

Making use of eq.(A.3), the partial differential operaters with respect to the Cartesian coordinates x,y, and z, can be expressed as

$$\partial_x = [(1-\ell^2)\partial_\ell - \ell m\partial_m - \ell n\partial_n]/R + \ell\partial_R , \qquad (A.4a)$$

$$\partial_y = [-m\ell\partial_\ell + (1-m^2)\partial_m - mn\partial_n]/R + m\partial_R , \qquad (A.4b)$$

$$\partial_z = [-n\ell\partial_\ell - nm\partial_m + (1-n^2)\partial_n]/R + n\partial_R , \qquad (A.4c)$$

where u is unity, and the notation ∂_q (q=x,y,z,ℓ,m,n,R) means the partial differntial operator with respect to q. Note that we can simply differentiate $C_{\mu\nu,j}\{\ell,m,n\}$ as if ℓ, m, and n are the independent variables, when we operate eqs.(A.4a,b,c) to right-hand side of eq.(A.1). The result is, for example,

$$S'^{x}_{\mu\nu}(R) \equiv \partial_x S_{\mu\nu}(x,y,z)$$

$$= \sum_j [\{(1-\ell^2)\partial_\ell C_{\mu\nu,j} - \ell m\partial_m C_{\mu\nu,j} - \ell n\partial_n C_{\mu\nu,j}\}\frac{(\mu\nu;j)}{R} - \ell C_{\mu\nu,j}\frac{d(\mu\nu;j)}{dR}]. \qquad (A.5)$$

Similar relations for $S'^{y}_{\mu\nu}(R)$, and $S'^{z}_{\mu\nu}(R)$ can be obtained by using eqs.(A.4b) and (A.4c), respectively. S-K representation for the differential coefficients of overlap integrals for s and p orbitals are presented in Table A-2.

Table A-1. S-K representation of overlap integrals for s and p orbitals.

$$S_{ss} = (ss\sigma)$$

$$S_{sx} = \ell(sp\sigma)$$

$$S_{xx} = \ell^2(pp\sigma) + (1-\ell^2)(pp\pi)$$

$$S_{xy} = \ell m(pp\sigma) - \ell m(pp\pi)$$

In present study, S-K two center integrals are eveluated by the Slater orbitals (see §2-2) as follows:

$$(ss\sigma)=[1+s+(7/15)s^2+(2/15)s^3+(2/75)s^4+(1/225)s^5+(1/1575)s^6]e^{-s}$$

$$(pp\sigma)=[1+p+(9/25)p^2+(2/75)p^3-(34/1575)p^4-(13/1575)p^5 -(1/525)p^6]e^{-p}$$

$$(pp\pi)=[1+p+(34/75)p^2+(3/25)p^3+(31/1575)p^4-(1/525)p^5]e^{-p}$$

$$(sp\sigma)=A_{05}+A_{14}-A_{16}-2A_{23}-A_{25}+2A_{34} ,$$

$$A_{nm}= I_n(u)J_m(v)+I_m(u)J_n(v),$$

$$I_n(u)=\sum_k^n [n!/(n-k)!]e^{-u}/u^{k+1}, \quad J_m(v)= -\frac{1}{2}[I_m(v)+(-1)^m I_m(-v)]$$

where $s=\alpha_{3s}R$, $p=\alpha_{3p}R$, $u=(s+p)/2$, and $v=(s-p)/2$, α_{3s} and α_{3p} are the Clementi's exponent.

Table A-2. S-K representation of differential coefficients of overlap integrals for s and p orbitals.

$$S'^{x}_{ss} = \ell(ss\sigma)'$$

$$S'^{x}_{sx} = (1-\ell^2)(sp\sigma)/R + \ell^2(sp\sigma)'$$

$$S'^{y}_{sx} = -m\ell(sp\sigma)/R + m\ell(sp\sigma)'$$

$$S'^{x}_{xx} = 2\ell(1-\ell^2)[(pp\sigma)-(pp\pi)]/R - \ell^3(pp\sigma)' + \ell(1-\ell^2)(pp\pi)'$$

$$S'^{y}_{xx} = -2\ell^2 m[(pp\sigma)-(pp\pi)]/R + m(pp\pi)'$$

$$S'^{x}_{xy} = (1-2\ell^2)m[(pp\sigma)-(pp\pi)]/R - \ell^2 m[(pp\sigma)'-(pp\pi)']$$

$$S'^{z}_{xy} = -2\ell mn[(pp\sigma)-(pp\pi)]/R + \ell mn[(pp\sigma)'-(pp\pi)']$$

where $(\mu\nu j)'$ stands for $d(\mu\nu j)/dR$.

Appendix B. Derivation of the general form of interatomic forces and interplanar forces in BP

Interatomic forces

The change of the total interatomic potential energy due to the displacements, $\{\delta R^{\alpha}_{\ell i}\}$, of atoms from their equillibrium posotions is written, in the harmonic approximation, as follows:

$$\Delta V = (1/2) \sum_{\ell i} \sum_{\ell' j} \sum_{\alpha\beta} F^{\alpha\beta}(\ell i, \ell' j) \delta R^{\alpha}_{\ell i} \delta R^{\beta}_{\ell' j} \tag{B.1}$$

where the force constant $F^{\alpha\beta}(\ell i, \ell' j)$ is equal to $F^{\beta\alpha}(\ell' j, \ell i)$. For brevity, we rewrite eq.(B.1) as

$$\Delta V(\{\delta R_L\}) = (1/2) \sum_{L} \sum_{M} {}^{t}(\delta R_L) \mathbf{F}(L,M) \delta R_M \ , \tag{B.2}$$

where we have introduced the vector notations

$$\delta R_L \equiv {}^{t}(\delta R^{x}_{L} , \delta R^{y}_{L} , \delta R^{z}_{L}) \tag{B.3}$$

for the displacements, and tensor notations

$$\mathbf{F}(L,M) = \begin{pmatrix} F^{xx}(L,M) & F^{xy}(L,M) & F^{xz}(L,M) \\ F^{yx}(L,M) & F^{yy}(L,M) & F^{yz}(L,M) \\ F^{zx}(L,M) & F^{zy}(L,M) & F^{zz}(L,M) \end{pmatrix} \tag{B.4}$$

for the force constants, L and M are the contracted symbols for atomic sites ℓi and $\ell' j$, respectively.

Let us consider a symmerty operation, $\Gamma \equiv \{\gamma | b\}$, of the space

group, where γ is a point group oparation (identity, rotation, reflection, or inversion) and **b** is a translational vector. Suppose that the symmetry operation Γ replaces atoms located at L,M,$\cdots$, by atoms located at $\tilde{L},\tilde{M},\cdots$, respectively. Since Γ is a symmetry operation of the crystal, the atomic displacements δR_L, δR_M, $\cdots$, in the expression (B.2) must be replaced by $\gamma\delta R_{\tilde{L}}$, $\gamma\delta R_{\tilde{M}}$, $\cdots$, respectively, without a change of the form of the total potential energy, ΔV, namely,

$$\Delta V(\delta R_L,\delta R_M,\delta R_N,\cdots) = \Delta V(\gamma\delta R_{\tilde{L}},\gamma\delta R_{\tilde{M}},\gamma\delta R_{\tilde{N}},\cdots). \qquad (B.5)$$

Using eq.(B.2), right-hand side of eq.(B.5) can be written as

$$\Delta V(\{\gamma\delta R_{\tilde{L}}\}) = (1/2)\sum_L\sum_M {}^t(\delta R_{\tilde{L}})\,{}^t\gamma F(L,M)\gamma\delta R_{\tilde{M}}$$

$$= (1/2)\sum_L\sum_M {}^t(\delta R_L)[{}^t\gamma F(\Gamma L,\Gamma M)\gamma]\delta R_M \qquad (B.6)$$

where symbols ΓL and ΓM denote atomic sites to which atoms are moved by operation Γ from atomic sites L and M, respectively. It is clear, through eq.(B.5), that eq.(B.6) is an alternative expression of eq.(B.2). Thus following relation holds for each symmetry operation:

$$\mathbf{F}(L,M) = {}^t\gamma\mathbf{F}(\Gamma L,\Gamma M)\gamma\ . \qquad (B.7)$$

Such relations reduce the number of independent elements of the force constant tensors. The translational operation $\Gamma=\{E|Rm\}$ requires

$$\mathbf{F}(\ell i,\ell' j) = \mathbf{F}(\ell+mi,\ell+mj). \qquad (B.8)$$

Next we consider a pair of atoms. As a matter of convenience, here we define two terms, "equivalent" and "transposed" : if an atomic pair (L,M) and another atomic pair (L',M') are connected by a translational operation, such atomic pairs are called "equivalent" pairs. The force constant tensors for the equivalent pairs are equal to each other, by eq.(B.8). By exchanging the order of atoms in a pair (L,M), we get (M,L) which is a "transposed" pair of (L,M). The force constant tensor for a transposed pair (M,L) can be obtained by transposing that for pair (L,M) as

$$\mathbf{F}(M,L) = {}^{t}\mathbf{F}(L,M). \qquad (B.9)$$

In general, a pair (L,M) will be moved by symmetry operations Γ to a pair (ΓL,ΓM) which is

(1) equivalent to (L,M), or
(2) equivalent to (M,L), or
(3) otherwise.

In case of (1), following restriction F(L,M) must be imposed on a force constant tensor,

$$\mathbf{F}(L,M) = {}^{t}\gamma\mathbf{F}(\Gamma L,\Gamma M)\gamma = {}^{t}\gamma\mathbf{F}(L,M)\gamma \ . \qquad (B.10)$$

In case of (2), similarly,

$$F(L,M) = {}^{t}\gamma F(M,L)\gamma = {}^{t}\gamma {}^{t}F(L,M)\gamma \ . \qquad (B.11)$$

It can easily be proved that more information other than eqs.(B.10), (B.11) cannot be obtained from the case (3).

A pair of the nearest neighboring atoms, which are indicated by 1 and 3 in Fig.2-1, is transposed by a symmetry operation $\{C_{2z}|\tau\}$. Therefore, the interatomic force for this pair satisfies $F(1)=C_{2z}F(1)C_{2z}$. Thus the form of this tensor can be written as

$$F(1)=\begin{pmatrix} a & u & v \\ u & b & w \\ -v & -w & c \end{pmatrix}. \qquad (B.12)$$

Eq.(B.12) can also be obtained by considering the symmetry operation $\{\sigma_z|\tau\}$.

A pair of the second neighboring atoms, which are indicated by 1 and 2 in Fig.2-1, is moved to the pair equivalent to itself by a reflection, $\{\sigma_y|0\}$, and transposed by the inversion $\{I|0\}$ or a rotation $\{C_{2y}|\tau\}$. Therefore, the force constant tensor for this pair satisfies $F(2)=\sigma_y F(2)\sigma_y = I\,{}^{t}F(2)I$. Thus the forme of this tensor can be written as

$$F(2)=\begin{pmatrix} a & 0 & v \\ 0 & b & 0 \\ v & 0 & c \end{pmatrix}. \qquad (B.13)$$

A pair of third neighboring atoms, which are indicated by 1

and 1' in Fig.2-1, is transposed by a reflection $\{\sigma_y|0\}$. Thus, $\mathbf{F}(3)=\sigma_y{}^t\mathbf{F}(3)\sigma_y$ must be satisfied, and therefore,

$$\mathbf{F}(3)=\begin{pmatrix} a & u & v \\ -u & b & w \\ v & -w & c \end{pmatrix}. \tag{B.14}$$

The force constant tensor for a pair of fourth neighboring atoms, which are indicated by 1 and 3' in Fig.2-1, has the same form as eq.(B.12).

The force constant tensor for a pair of fifth neighboring atoms, which are indicated by 1 and 4 in Fig.2-1, has most general form with nine independent elements.

Interplanar forces

The interplanar force constant tensors for atomic planes perpendicular to [100] direction inherit their charactors from constituent interatomic force constant tensors. The definition, eq.(4.5), can be rewitten as

$$\mathbf{K}(P,P') = \sum_{L}^{P} \mathbf{F}(L,M), \tag{B.15}$$

where M is arbitrary atomic site included in plane P', the summataion with respect to L is confined on plane P. From eq.(B.7), we have

$$\sum_{L}^{P} \mathbf{F}(L,M) = {}^t\gamma[\sum_{L}^{P} \mathbf{F}(\Gamma L,\Gamma M)]\gamma . \tag{B.16}$$

Let us consider a symmetry operation Γ that moves atoms

(a) from plane P to P, and from P' to P', or

(b) from plane P to P', and from P' to P.

In the case of (a), ΓL and ΓM can be replaced by L and M, respectively, in eq.(B.16). Then we have

$$\mathbf{K}(pi,p'j) = {}^{t}\gamma\, \mathbf{K}(pi,p'j)\gamma \ , \tag{B.17}$$

where i and j specify the kind of atoms (1,2,3, or 4) incuded in plane P at p-th unit cell and plane P' at p'-th unit cell, respectively. In the case of (b), ΓL and ΓM can be replaced by M and L, respectively, in eq.(B.16). Then we have

$$\mathbf{K}(pi,p'j) = {}^{t}\gamma\,{}^{t}\mathbf{K}(pi,p'j)\gamma \ . \tag{B.18}$$

Since σ_y moves atoms within a plane, eq.(B.17) says that all of the interplanar force constant tensors are unchanged when they are transformed by σ_y, namely,

$$\mathbf{K}(pi,p'j) = \sigma_y \mathbf{K}(pi,p'j)\sigma_y \ . \tag{B.19}$$

Therefore, off-diagonal xy,yx,zy, and yz components vanish exactly, namely,

$$\mathbf{K}(pi,p'j) = \begin{pmatrix} a & 0 & d \\ 0 & b & 0 \\ d' & 0 & c \end{pmatrix} . \tag{B.20}$$

Making use of eqs.(B.17),(B.18), and the relations

$$K(pi,p'j) = {}^{t}K(p'j,pi), \tag{B.21}$$

$$K(pi,p'j) = K(p+mi,p'+mj), \tag{B.22}$$

we can fined the form of the interplanar force tensors. In case of i=2 and j=1, we can chose inversion operator I as Γ, and obtain $K^{xz}(p2,p'1) = K^{zx}(p2,p'1)$. In cace of i=3 and j=1, we can chose $\{\sigma_x|\tau\}$ with appropriate primitive translation $\{E|R_m\}$ as Γ, and obtain $K^{xz}(p3,p'1) = -K^{zx}(p3,p'1)$. In case of i=1 and j=1, and in case of i=4 and j=1, we find no relation between off-diagonal components, d and d', in eq.(B.20).

Condition of infinitesimal translation invariance

Suppose that whole crystal is displaced by infinitesimal vector. It is obvious that arbitrary plane (p'j) dose not accept the force, namely,

$$\sum_{p}\sum_{i} K(pi,p'j) = \sum_{i}\sum_{p} K(pi,0j) = 0 . \tag{B.23}$$

Let us define following tensor:

$$K[i,j] \equiv \sum_{p} K(pi,0j). \tag{B.24}$$

Since the inversion I transpose atoms 1 and 2, atoms 3 and 4, we obtain; $K[1,1]=K[2,2]$, $K[3,3]=K[4,4]$, $K[2,1]=K[1,2]= {}^{t}K[2,1]$,

$\mathbf{K}[3,4]=\mathbf{K}[4,3]={}^{t}\mathbf{K}[3,4]$. On the other hand, a reflection $\{\sigma_x|\tau\}$ transpose atoms 1 and 3, atoms 2 and 4, thus using eqs.(B.16), (B.21), we obtain:

$$\mathbf{K}[3,1] = {}^{t}\sigma_x\mathbf{K}[1,3]\sigma_x = \sigma_x{}^{t}\mathbf{K}[3,1]\sigma_x. \tag{B.25}$$

This means $K^{xz}[3,1]=-K^{zx}[3,1]$. Further, a reflection $\{\sigma_z|\tau\}$, which transpose atoms 1 and 4, atoms 2 and 3, leads to

$$\mathbf{K}[4,1] = {}^{t}\sigma_z\mathbf{K}[1,4]\sigma_z = \sigma_z{}^{t}\mathbf{K}[4,1]\sigma_z. \tag{B.26}$$

This means $K^{xz}[4,1]=-K^{zx}[4,1]$. By substituting obtained relations of $\mathbf{K}[i,j]$ into eq.(B.23), we can find the conditions of infinitesimal translation invariance as follows:

$$K^{xx}[1,1] + K^{xx}[2,1] + K^{xx}[3,1] + K^{xx}[4,1] = 0, \tag{B.27a}$$

$$K^{yy}[1,1] + K^{yy}[2,1] + K^{yy}[3,1] + K^{yy}[4,1] = 0, \tag{B.27b}$$

$$K^{zz}[1,1] + K^{zz}[2,1] + K^{zz}[3,1] + K^{zz}[4,1] = 0, \tag{B.27c}$$

$$K^{xz}[1,1] + K^{xz}[2,1] + K^{xz}[3,1] + K^{xz}[4,1] = 0, \tag{B.27d}$$

$$K^{xz}[1,1] + K^{xz}[2,1] - K^{xz}[3,1] - K^{xz}[4,1] = 0. \tag{B.27d'}$$

Note that eqs.(B.27d),(B.27d') require

$$K^{xz}[1,1] + K^{xz}[2,1] = 0, \tag{B.28a}$$

$$K^{xz}[3,1] + K^{xz}[3,1] = 0. \tag{B.28b}$$

The restoring force K(pi,pi) can be defined by eqs.(B.27a-d').

REFERENCES OF PART I

1. I. Shirotani, R. Maniwa, H. Sato, A. Fukizawa, N. Sato, Y. Maruyama, T. Kajiwara, H. Inokuchi and S. Akimoto: Nippon Kagaku Kaishi (1981) No.10, 1604 [in Japanese].
2. S. Endo, Y. Akahama, S. Terada and S. Narita: Jpn. J. Appl. Phys. 21 (1982) L482.
3. R.W. Keyes: Phys. Rev. 92 (1953) 580.
4. D. Warschauer, J. Appl. Phys. 34 (1963) 1853.
5. J. Donohue, The Structure of the Elements, (Wiley, New York, 1974).
6. A. Brown and S. Rundqvist: Acta Cryst. 19 (1965) 684.
7. J.C. Jamieson: Science 139 (1963) 1291.
8. T. Kikegawa and H. Iwasaki: Acta Cryst. B39 (1983) 158.
9. I.V. Berman and N.B. Brandt: ZhETF Pis'ma 7 (1968) 412.
10. H. Kawamura, I. Shorotani and K. Tachikawa: Solid State Commun. 49 (1984) 879.
11. H. Kawamura, I. Shirotani and K. Tachikawa: Solid State Commun. 54 (1985) 775.
12. J. Wittig, B. Bireckoven and T. Weidlich: Solid State Physics under High Pressure; Recent Advance with Anvil Devices, ed. by S. Minomura (KTK Scientific Publisher, Tokyo 1985) p.217.
13. Y. Yamada, Y. Fujii, Y. Akahama, S. Endo, S. Narita, J.D. Axe and D.B. McWhan: Phys. Rev. B30 (1984) 2410.
14. C. Kaneta, H. Katayama-Yoshida and A. Morita: J. Phys. Soc. Jpn. 55 (1986) 1213.

15. C. Kaneta and A. Morita: J. Phys. Soc. Jpn. 55 (1986) 1224.
16. S. Sugai and I. Shirotani: Solid State Commun. 53 (1985) 753.
17. S. Sugai, T. Ueda and K. Murase: J. Phys. Soc. Jpn. 50 (1981) 3356.
18. K. Paukov: Zh. Fiz. Khim. 43 (1969) 1385.
19. L. Cartz, S.R. Srinivasa, R.J. Riedner, J.D. Jorgensen and T.G. Worlton: J. Chem. Phys. 71 (1979) 1718.
20. J.C. Slater, G.F. Koster and J.H. Wood: Phys. Rev. 126 (1962) 1307.
21. H. Asahina, K. Shindo and A. Morita: J. Phys. Soc. Jpn. 51 (1982) 1192.
22. Y. Takao, H. Asahina and A. Morita: J. Phys. Soc. Jpn. 50 (1981) 3362.
23. Y. Harada, K. Murao, I. Shirotani, T. Takahashi and Y. Maruyama: Solid State Commun. 44 (1982) 877.
24. Y. Hayashi, T. Takahashi, H. Asahina, T. Sagawa, A. Morita and I. Shirotani: Phys. Rev. B30 (1984) 1891.
25. T. Takahashi, H. Tokailin, S. Suzuki, T. Sagawa and I. Shirotani: Phys. Rev. B29 (1984) 1105; J. Phys. C 18 (1985) 825.
26. R. Hoffman: J. Chem Phys. 39 (1963) 1397.
27. F. Herman and S. Skillman: Atomic Structure Calculations (Prentice-Hall, N.J. 1963).
28. Y. Akahama, S. Endo and S. Narita: Physica 139&140B (1986) 397.

29. K. Motizuki and N. Suzuki: Structural Phase Transition of Layered Transition-Metal Compounds, ed. K. Motizuki (D. Reidel Publishing Co.) pp.1-134 (in press).
30. J.Ashkenazi, M. Dacorogna and M. Peter: Solid State Commun.29 (1979) 181.
31. K. Kunc and P.G. Dacosta: Phys. Rev. B32 (1985) 2010.
32. A.W. Solbrig, Jr.: J. Phys. Chem. Solids 32 (1971) 1761.

PART II

ELECTRONIC BAND STRUCTURE AND SUPERCONDUCTIVITY IN SIMPLE-CUBIC PHOSPHORUS

§1. Introduction

Black phosphorus studied in part I reveals successive structural transformation as pressure is applied. Around 55 kbar the crystal structure transforms from orthorhombic (A11) to rhombohedral (A7) structure and above 110 kbar it becomes the simple-cubic structure.[1] The simple-cubic phosphorus is metallic and its electronic band structure has been studied thus far on the basis of the pseudopotential method.[2,3]

The occurence of superconductivity in metallic phosphorus has received considerable attention, as pressure induced superconductivity.[4-8] Recently several experimental studies of the pressure dependence of the superconducting transition temperature, Tc, have been reported.

Wittig et al.[4] have found an interesting behavior of Tc as a function of pressure: Tc exhibits two distinct maxima at 120 kbar and 230 kbar both being separated by a pronounced minimum at 170 kbar. Similar results have been obtained by Akahama et al.[7] Moreover, they have found that Tc decreases linearly with pressure above 230 kbar.

Kawamura et al. have reported[5,6] anomalous pressure dependence of Tc: Tc versus pressure curve strongly dedpends on a path. Two different path A and B were considered. In path A the pressure is applied at room temperature and then the temperature is cooled down to liquid helium temperature. Experiments by Wittig et al. and by Akahama et al. have been done also by using this path A. In path B the sample is cooled down to 4.5 K

without applying pressure and then the pressure is increased. In the case of path A Kawamura et al. have found that Tc is almost constant (6K) as a function of pressure, which contradicts the results obtained by Wittig et al. and by Akahama et al. In the case of path B, on the other hand, Tc rapidly increases from 5 K to 11 K as pressure increases from 130 kbar to 290 kbar. From these results they speculated that the orthorhombic phase and the simple-cubic phase coexist in samples prepared by using the path B. This speculation has been confirmed by X-ray diffraction measurements at liquid nitrogen temperature.[6)]

In the present stage, however, there is no clear understanding of the superconductivity of phosphorus under pressure, even of pure simple-cubic phosphorus.

Our purpose is to study microscopically the superconductivity of the pure simple-cubic phosphorus, on the basis of the BCS-type mechanism with strong electron-phonon coupling. We pay our attention also to the pressure effect on Tc.

In §2 the electronic band structure is calculated by the self-consistent APW method. Density of states (DOS) and the Fermi surfaces are obtained. In §3 the electron-lattice matrix elements are calculated on the basis of the rigid muffin-tin approximation. In §4 the electron-phonon mass enhancement parameter λ is estimated by using the obtained electron-lattice matrix elements, the calculated DOS at the Fermi level, and the phonon frequencies estimated by using the measured bulk modulus. We calculate the superconducting transition temperature T_c in accordance with McMillan-Allen-Dynes equation. Pressure effects of Tc is discussed. Finally, §5 is devoted to summary.

§2. APW Calculation of Electronic Band Structure

2-1 Band structure

The augmented plane wave (APW) method has been widely applied to calculate the Bloch functions as well as the electronic energy bands of crystals in which the crystal potential can be successfully approximated by a muffin-tin (MT) potential.

The simple-cubic phosphorus is one of the crystals with the highest symmetry, even though the coordination number is 6, so that the crystal potential around a lattice point cannot be considered to have much larger non-spherical components than that for the other elemental crystals with higher coordination number. Thus we can expect that this crystal is a good example for the band calculation based on the APW method with the MT approxmation.

Fig.2-1 shows the first Brillouin zone of the simple-cubic lattice. Four symmetry points, Γ, X, M and R, and six symmetry lines, Δ, Z, T, Λ, Σ and S, are presented in a tetrahedal irreducible zone.

We have calculated the electronic band structures of simple-cubic phosphorus using a semi-relativistic version of the APW method which includes the mass-velocity and Darwin corrections exactly but neglects the spin-orbit interaction.[9] The exchange-correlation potential is constructed using the Gunnarsson-Lundqvist form[10] of the local density approximation, and the electron charge density of the crystal is determined

self-consistently within the MT approximation. Actual calculations have been performed for two lattice constants, a = 2.369 A and 2.298 A, which were determined by the X-ray diffraction experiments at 132 kbar and at 304 kbar respectively.[1] The MT radius, r_{MT}, is chosen to be a half of the lattice constant for both pressure. The ratio of the volume of the MT sphere to the primitive cell volume is 0.52: this is relatively small compared with that for hcp or fcc lattice (0.74), and even for bcc lattice (0.68).

The first step in APW band calculation is a self-consistent determination of the energy levels and the charge density of an isolated atom. The electron configuration of a single P atom is $1s^2 2s^2 2p^6 3s^2 3p^3$, and we have obtained the following atomic energy levels (in unit of Ryd.):

1s : -152.722,

2s : -12.859, 2p : -9.286,

3s : -1.125, 3p : -0.514.

Because the energy levels of 1s, 2s, and 2p electrons are sufficiently deep compared with those of 3s and 3p electrons, we treat 1s, 2s, and 2p shells as a frozen core whose charge density is a source of the core potential for the band electrons. The charge density constructed by 3s and 3p electrons are used as a starting valence charge density of the self-consistent calculation.

In the next step, the sampling k-points are appropriately

chosen in the Brillouin zone and iteration of the APW calculation is performed until the energy eigenvalues and the charge density of the crystal converge. The eigenvalues have converged within 1 mRyd in our case.

In order to clarify whether the self-consistent eigenvalues depend on a choice of a set of sampling k-points or do not, we performed calculations for two different sets of k-points described as follows:

(i) 22 k-points with high symmetry, i.e. the symmetry points Γ, R, X, and M, and 3 k-points (3/10, 5/10, and 7/10 position) on each symmetry line of Λ, S, Z, Σ, T, and Δ.

(ii) 20 special-points for the simple cubic structure, i.e. those k-points in an irreducible zone written as $\pi(l,m,n)/8a$, where l, m, and n are odd integers such as 1, 3, 5, and 7. (The special point method was first proposed by Chadi and Cohen.[11])

For the set (i), the first 8 iterations were carried out using Γ, and R points, and X, and M points were added in the next 9 iterations. All the midpoints of 6 symmetry lines were taken into account in the next 10 iterations. Finally, after 3 iterations with use of all of 22 k-points the eigenvalues converged within the required accuracy. For the set (ii), iterations were carried out using 20 special-points from the first time and the energy eigenvalues and the valence charge density converged well after only 10 iterations. In both

calculations, the angular momentum component of the states of a valence electron in the MT sphere has been taken into account up to $\ell=5$, and the cutoff wave vector of APW has been taken to be $3.1(2\pi/a)$ which correspond to the wave vector of a free electron with the kinetic energy of 12∿13 Ryd. The agreement between the self-consistent eigenvalues obtained from the sets (i) and (ii) is fairly well, but the energy values in the latter case are about 6 mRyd smaller than those obtained from the set (i). This fact implies that we can obtain good eigenvalues and wave functions by the use of relatively small number of k-points if we employ an appropriate set of special-points. Therefore, in the following calculations, we employ the self-consistent crystal potential obtained by using the 20 special-points.

Fig.2-2a shows $4\pi r^2$ times the total charge density, $\rho(r)$, and its core electron and valence electron components inside the MT sphere at 132 kbar, and Fig.2-2b shows those at 304 kbar. For both pressure the core electrons localize inside $r=0.5r_{MT}$ and valence electrons mainly exist outside it. The number of the valence electrons inside the MT sphere is found to be 3.6265 at 132 kbar and 3.5381 at 304 kbar; a slightly larger number of electrons are extended to the interstitial region at higher pressure.

Fig.2-3a shows the energy bands at 132 kbar along the symmetry lines in the Brillouin zone. The features of these bands below the Fermi level, which is indicated by the horizontal line at 0.62 Ryd, are similar to those of free electrons in the empty lattice.

From the features of dispersion curves and the decomposition of the wave function inside the MT sphere into the ℓ-componemts (i.e. angular momentum components), we have obtained following informations:

(1) The lowest band almost completely consists of 3s state except for the states near the R point. The lowest 3-fold degenearte state at R has a pure 3p character.

(2) The second and the third bands are degenerate along the T and Λ lines. These bands almost completely consists of 3p states. As expected from Fig.2-3a, the second band provides Fermi surface of the hole-pocket type that surounds Γ point. On the other hand, the third band provides Fermi surface of the open-type, which inevitably contacts with the above hole surface at a point on the Λ line because the second and third bands are degenerate on the Λ line.

(3) The fourth band provides two kinds of Fermi surfaces of the electron-pocket type: one surrounds the R point and the other surrounds the M point. The state of the fourth band at the R point consists of 3s state. As coming apart from the R point along the Λ, S, or T lines, the 3p components increase. The state of the fourth band at the M point has pure 3d character.

On account of the high symmetry of the simple cubic structure, 3p orbitals cannot hybridize with 3s or 3d orbitals at symmetry points Γ, X, R, and M. According to the consideration

based on the tight-biding model, the characters of several low energy states at symmetry points can be interpreted in terms of the atomic orbital as follows :

Γ point: 3s <bonbing>, 3p (3-fold) / 3d (2-fold), ...,
X point: 3s, $3p_x$ / $3p_y$ and $3p_z$ (2-fold), ...,
M point: 3s, $3p_x$ and $3p_y$ (2-fold), 3d / ...,
R point: 3p (3-fold), 3s <anti-bonding> / 3d (2-fold), ...

where the energy of the state increases from left to right, and the position of the Fermi energy is indicated by a slash, / . Because the 3s band lie well below the Fermi level almost in the whole B.Z., the 3s-electrons hardly contribute to the bonding. The bonds are composed mainly by the 3p-electrons with a little 3d contribution.

Fig.2-3b shows the energy bands at 304 kbar. Comparing this with Fig.2-3a, one can find the broadening of the band widths. This is due to an increase of the transfer integrals owing to a decrease of the lattice constant. The second and the third bands show a slight broadening of the band widths, but the positions at which these bands cross the Fermi level along the symmetry lines are almost unchanged by pressure in the range of 132-304 kbar. We note that with increasing pressure the electron-pocket centered at the R point vanishes and the electron-pocket centered at the M point expands remarkably. The characteristic vanishing of the electron-pocket at the R point is due to the increase of the energy separation between the lowest 3-fold degenerate 3p

state and the anti-bonding 3s state: this increase of energy separation is due to the broadening of the 3s and 3p bands. Similarly, the expansion of the electron-pocket centered at the M point can be interpreted as due to the broadening of the 3d band.

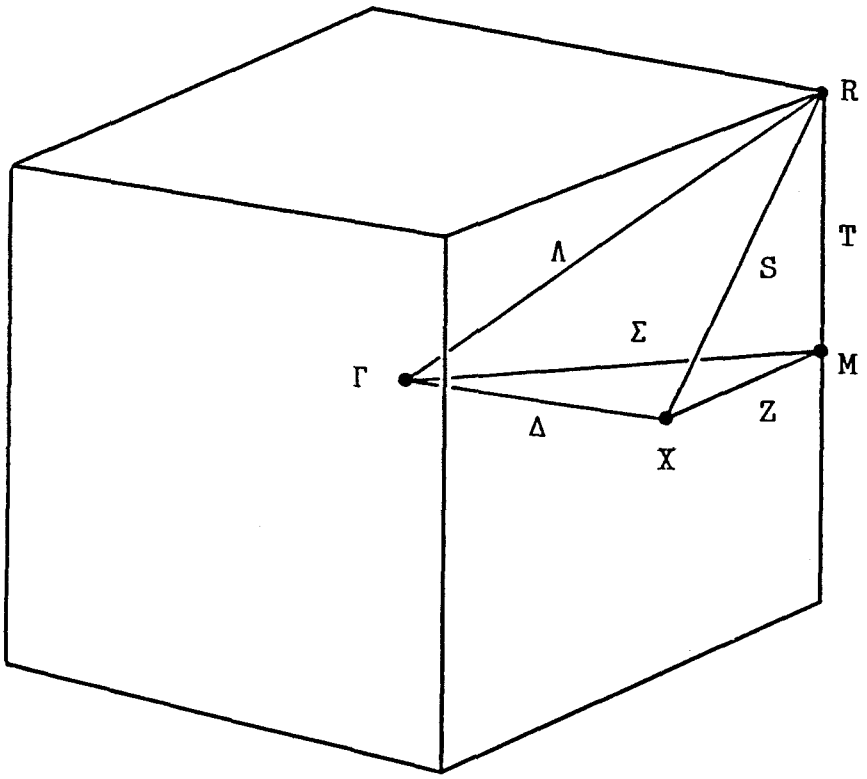

Fig.2-1 The Brillouin zone of simple cubic lattice.

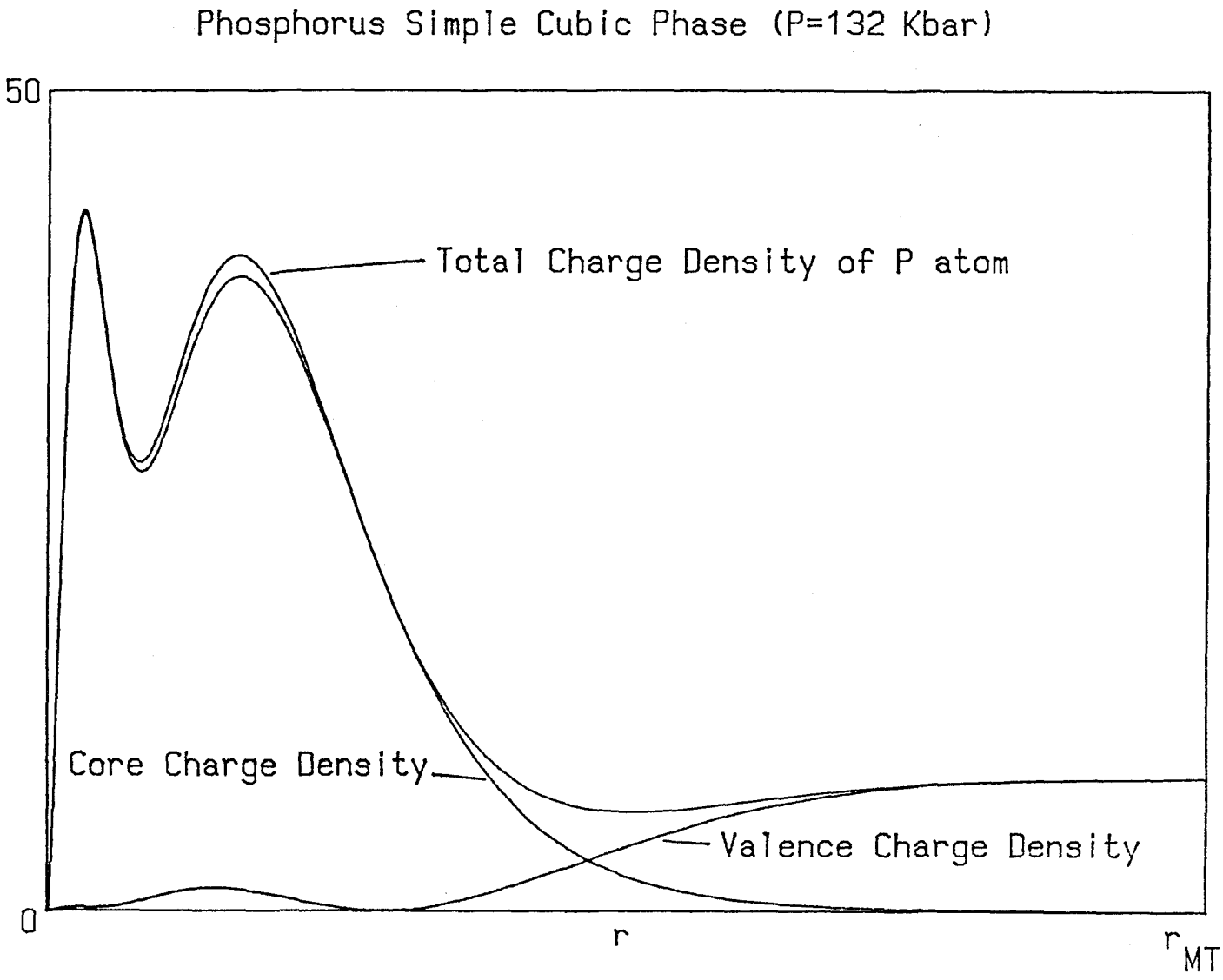

Fig.2-2a $4\pi r^2$ times the total charge density inside the muffin-tin sphere for 132 kbar. The core electron and the valence electron components are also shown.

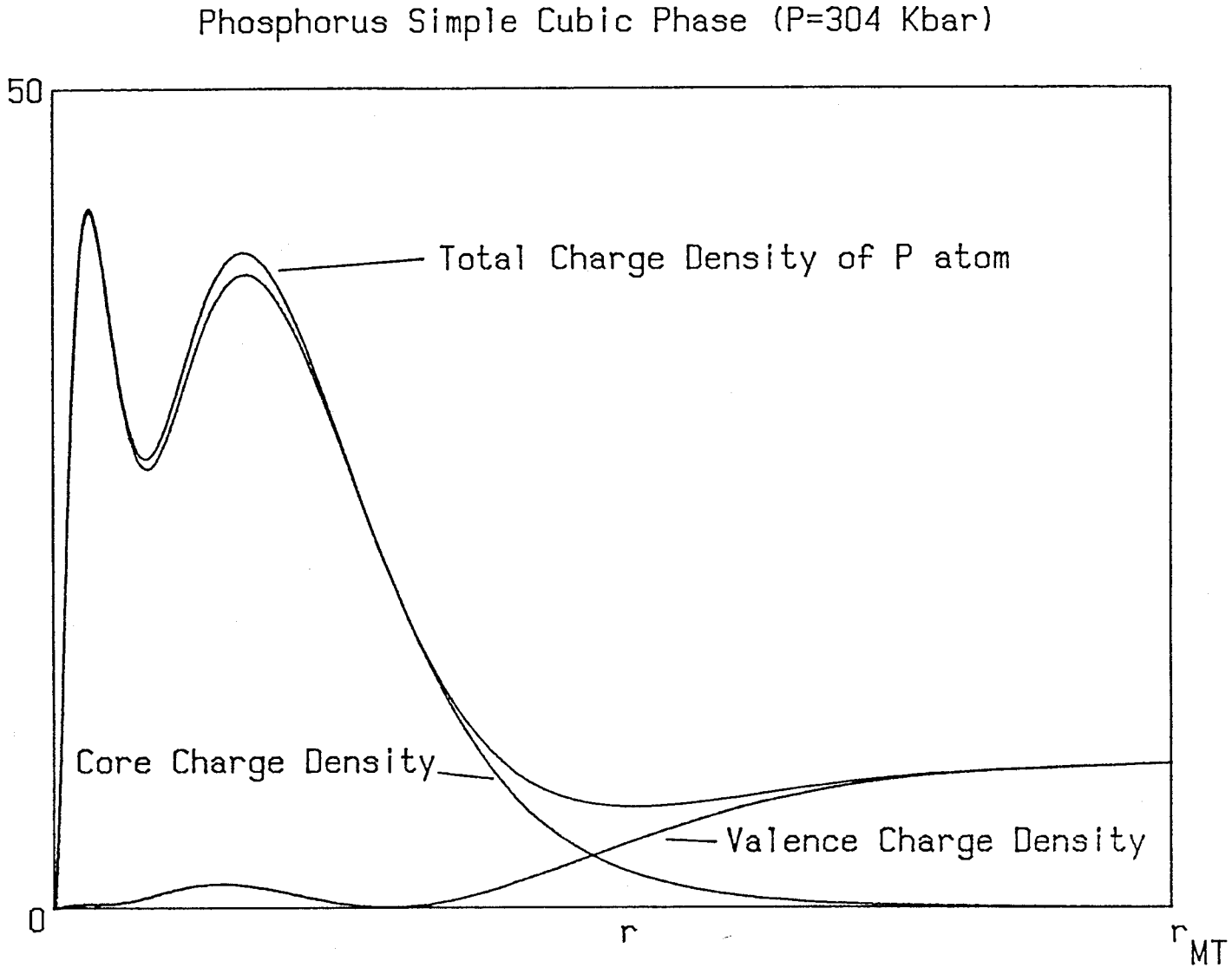

Fig.2-2b $4\pi r^2$ times the total charge density inside the muffin-tin sphere for 304 kbar. The core electron and the valence electron components are also shown.

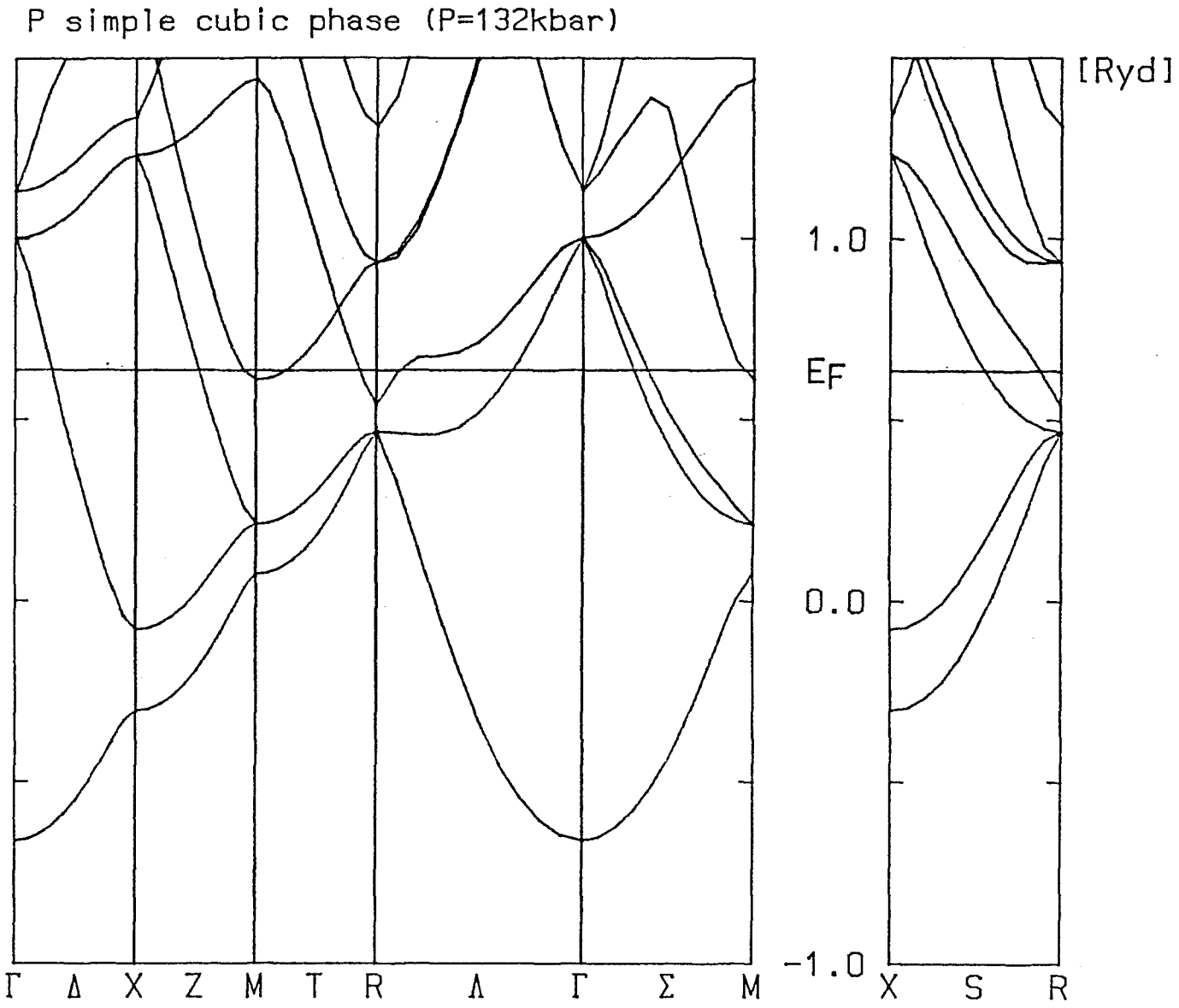

Fig.2-3a The energy dispersion curves of simple cubic phosphorus at 132 kbar. The Fermi level is indicated by a horizontal line at 0.62 Ryd.

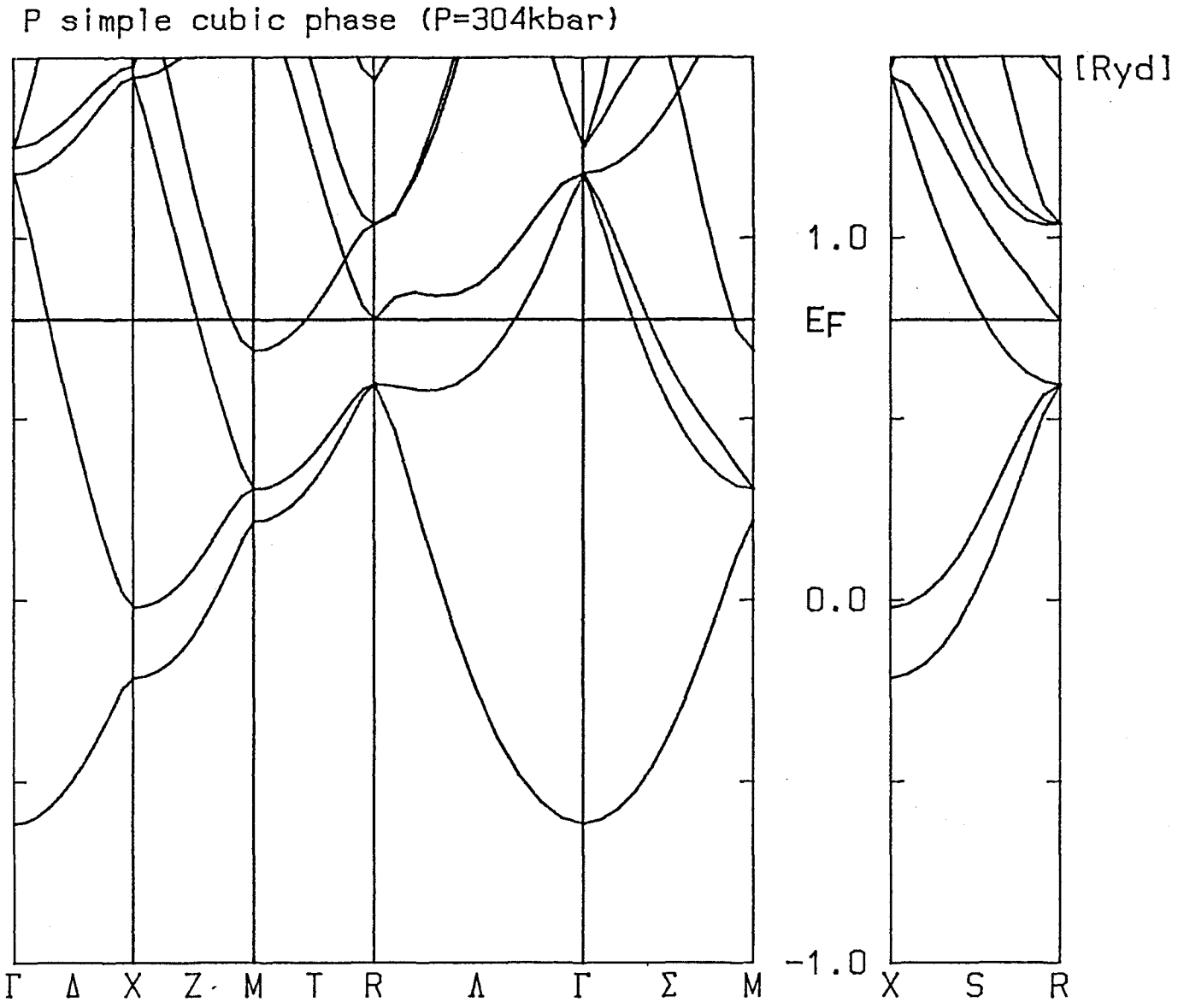

Fig.2-3b The energy dispersion curves of simple cubic phosphorus at 304 kbar. The Fermi level is indicated by a horizontal line at 0.76 Ryd.

2-2 Density of states

We have calculated the energy eigenvalues for 165 k-points in the irreducible zone. These values were then interpolated by spline funtions[12] to calculate the Fermi level (E_F) as well as the density of states (DOS). Actual calculation of the DOS has been done by the tetrahedron method[13] with use of 12,341 k-points in the irreducible zone.

Fig.2-4a shows the results of calculation at 132 kbar. The full curve denotes the total DOS and the dotted curves represent the partial DOS which arises from each band, 1, 2, 3, 4, and 5. The total DOS at the Fermi level, E_F=0.62 Ryd, is found to be 2.10 states/Ryd·atom· spin, which agrees with the result obtained by ab initio psudopotential calculation.[3] This value of the total DOS is smaller than the DOS at the Fermi level for free electrons, 2.69 states/Ryd·atom·spin, which is calculated from the relation

$$D_{free}(E_F)= \{ \Omega/(2\pi)^2\}^{2/3}\cdot(3n/4)^{1/3} \quad \text{(states/Ryd·atom·spin)},$$

where the unit cell volume is Ω=89.8 a.u.^{3} at 132 kbar, and the number of valence electrons is n= 5.

Values of the partial and the total DOS at E_F are listed in the second column of Table 2-1. As seen from the table, the third band, which provides the large Fermi surface of the open-type, gives rise to the largest partial DOS at E_F. The partial DOS at E_F of the band 4 may be divided into two

contributions: one comes from the electron-pocket centered at the M point and the other from that centered at the R point. The latter contribution is considerably small compared with the former contribution.

Fig.2-4b shows the total and the partial DOS at 304 kbar. Values of the partial and the total DOS at E_F=0.76 Ryd are listed in the third column of Table 2-1. Comparing the results for 304 kbar and those for 132 kbar, we can find that the partial DOS at E_F of the second and the third bands decrease with increasing pressure: this tendency can be explained by the broadening of these two bands. On the other hand, the partial DOS at E_F of the fourth band increases remarkably to result in the net increase (1.4 %) of the total DOS at E_F as pressure increases from 132 kbar to 304 kbar.

It should be noted that in pressure range of 132-304 kbar the increase of the total DOS at E_F is quite small, but that remarkable changes are found in the partial DOS of the third and the fourth bands. The small value of DOS and the fairly high superconducting transition temperature, such as 5-11 K, suggest that the simple-cubic phosphorus is a system having the strong electron-phonon interaction.

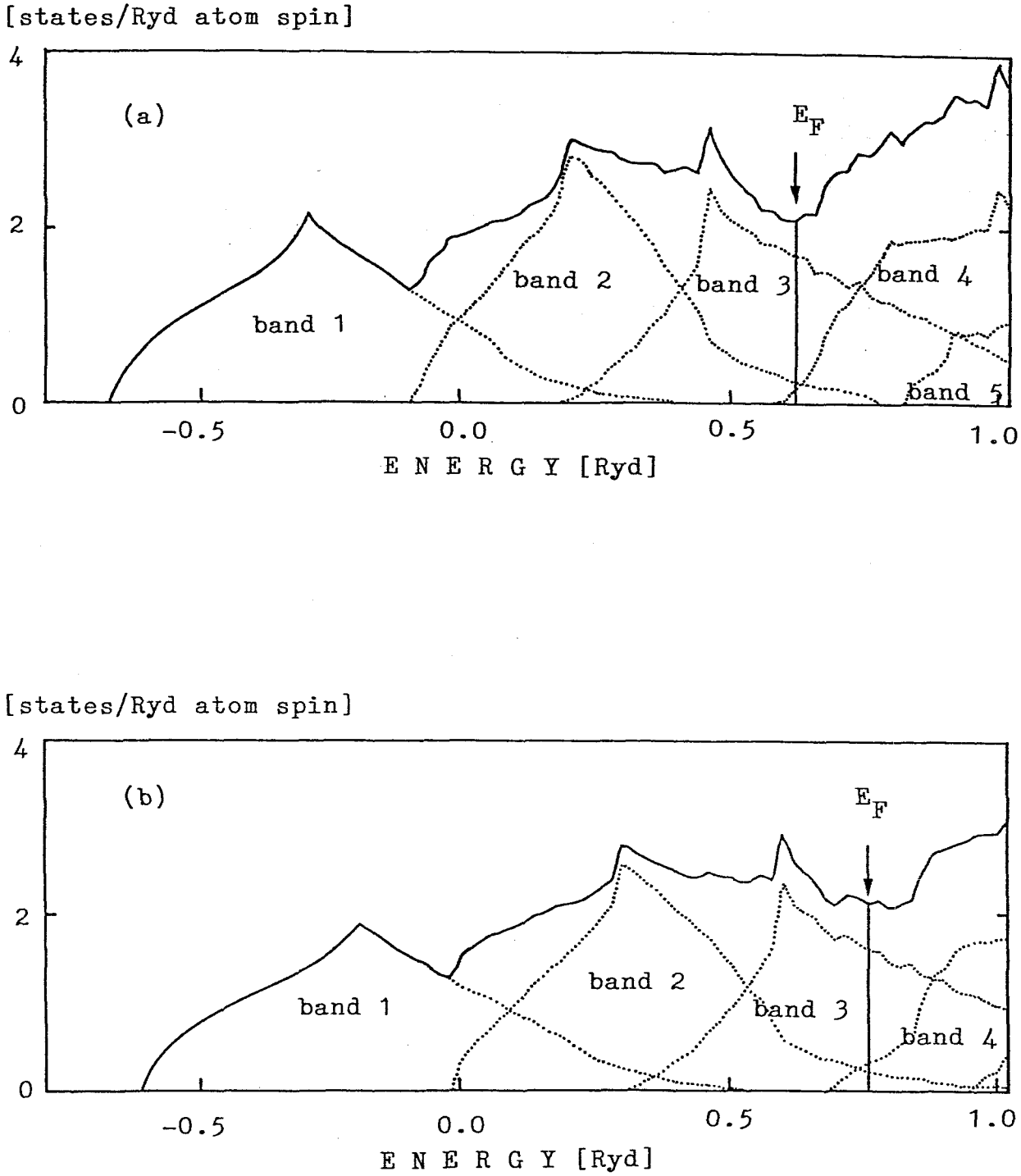

Fig.2-4 The electronic density of states (DOS) for (a) 132 kbar, and for (b) 304 kbar. Total DOS is plotted by solid curve and the contributions from bands 1∿5 are shown by dotted curves. The Fermi level is indicated by a vertical line.

Table 2-1. Partial and total DOS at Fermi level (in unit of per Ryd·atom·spin). Partial DOS arising from band 4 is decomposed into two contributions from states around the R point and from states around the M point.

band	Density of states $D(E_F)$	
	132 kbar	304 kbar
2	0.25	0.21
3	1.70	1.60
4	0.15	0.32
(4-R)	(0.03)	(0.0)
(4-M)	(0.12)	(0.32)
total	2.10	2.13

2-3 Fermi surfaces

Making use of energy eigenvalues obtained for 12,341 k-points in the irreducible zone by an interpolation method with use of spline functions, we have constructed the Fermi surfaces (FS) in the first Brillouin zone.

At 132 kbar, four types of FS are formed from bands 2, 3, and 4. The band 4 gives ries to two FS: one is centered at the R point and the other centered at the M point. The obtained Fermi surfaces are shown in Figs.2-5a, 2-5b and 2-5c. The features of these FS can be described as follows:

(1) FS-2: The FS formed by the band 2 (Fig.2-5a).
The length of edges of this dice-like-shaped FS is about $0.6\pi/a$. Electrons fill the outside of this FS.

(2) FS-3: the FS formed by the band 3 (Fig.2-5b).
This FS is open-type with six necks which intersect the faces of the zone boundary. The Brillouin zone is devided by this FS into two regions: the symmetry points Γ and X belong to the hole-region, and the symmetry points M and R belong to the electron-region.

(3) FS-4R: the FS centered at the R point formed by the band 4 (Fig.2-5c).
The inside of this FS is filled by electrons.

(4) FS-4M: the FS centered at the M point formed by the band 4 (Fig.2-5c).
The inside of this FS is filled by electrons.

When the pressure is increased up to 304 kbar, FS-2 and FS-3 remain almost unchanged, whereas FS-4R completely vanishes and FS-4M expands remarkablly as shown in Fig.2-6.

We can find in Kittel's text book[14] a typical shape of the FS for the simple cubic lattice. Fig.2-7 shows the FS in half-filled case for the simplest tight-binding band

$$E(\mathbf{k}) = -2T\{ \cos(k_x a) + \cos(k_y a) + \cos(k_z a)\}. \qquad (2.1)$$

This band shows a characteristic perfect-nesting with respect to the wave vector $\mathbf{Q} \equiv \Gamma R$ because the relation $E(\mathbf{k}) = -E(\mathbf{k}-\mathbf{Q})$ holds. Thus, this is a typical example of the electronic system that favors the Peierls instability.[15] Reflecting the fact that FS-3 of simple-cubic phosphorus is formed by nearly half-filled 3p-bands, there is no topological difference between the FS-3 and the typical FS shown in Fig.2-7 . In fact, FS-3 can be regarded as a certain modification, which arises from the anisotropy of the 3p orbitals, of the FS shown in Fig.2-6.

If the shapes of the hole-region and the electron-region of a particular band in the Brillouin zone are congruent each other, such a band is said to perfectly nest itself. It should be pointed out here that the band 3 has a property of nearly perfect nesting. This can be clearly seen by drawing FS-3 by choosing its center at the R point as shown in Fig.2-8. Comparing Fig.2-8 with Fig.2-5b, we can see a similarity between the two kind of FS-3. Thus, it has been shown that FS-3 nests itself and that the nesting vector is Q.

The nesting property of FS-3 mentioned above can also be confirmed by calculating the "band-decomposed" electronic susceptibility $\chi_0^{n,n'}(\mathbf{q})$ defined by

$$\chi_0^{n,n'}(\mathbf{q}) = \frac{2}{N} \sum_{\mathbf{k}} \frac{f(E_{n\mathbf{k}}) - f(E_{n'\mathbf{k}-\mathbf{q}})}{E_{n'\mathbf{k}-\mathbf{q}} - E_{n\mathbf{k}}}, \tag{2.2}$$

where $f(E_{n\mathbf{k}})$ denotes the Fermi distribution function. We have calculated $\chi_0^{n,n'}(\mathbf{q})$ at zero temperature using energy eigenvalues obtained for 8,000 k-points by the interpolation method. The results at 132 kbar are shown in Fig.2-9. As clearly seen, $\chi_0^{3,3}(\mathbf{q})$ has a large peak at $\mathbf{q}=\mathbf{Q}$ and $\chi_0^{3,3}(\mathbf{Q})$ is the largest among $\chi_0^{n,n'}(\mathbf{q})$. From these results we may expect a large frequency-softening of phonons at the R point. Precisely speaking, however, the frequency softening is determined not by $\chi_0^{n,n'}(\mathbf{q})$, but by the generalized electronic susceptibility $\chi^{\alpha\beta}(ij,\mathbf{q})$ which includes the electron-lattice coupling constants (see Part I). Therefore, in order to obtain a definite conclusion we need to investigate matrix elements of electron-lattice interaction for a pair of electronic states $|3\mathbf{k}\rangle$ and $|3\mathbf{k}-\mathbf{Q}\rangle$ with both $\mathbf{k}$ and $\mathbf{k}-\mathbf{Q}$ being on or near the FS-3. If these matrix elements are large or not so small, then we certainly expect a large frequency softening of phonons at the R point.

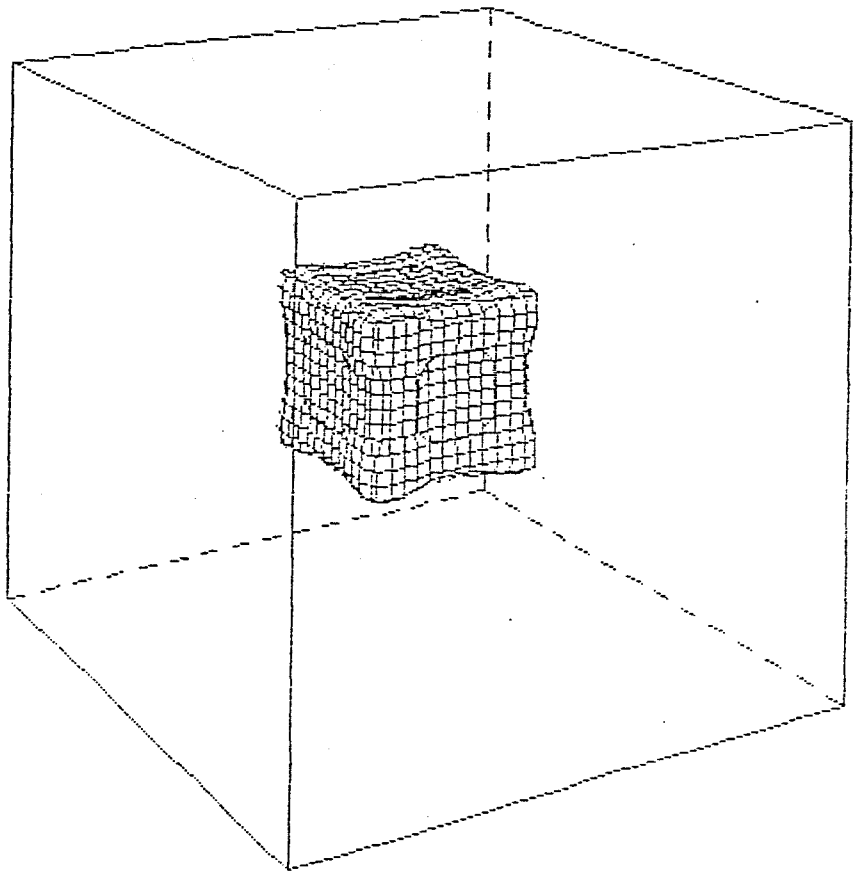

Fig.2-5a The Fermi surface formed by the band 2 (FS-2). The shape of this hole-surface is almost unchanged within pressure range of 132 ∿ 304 kbar.

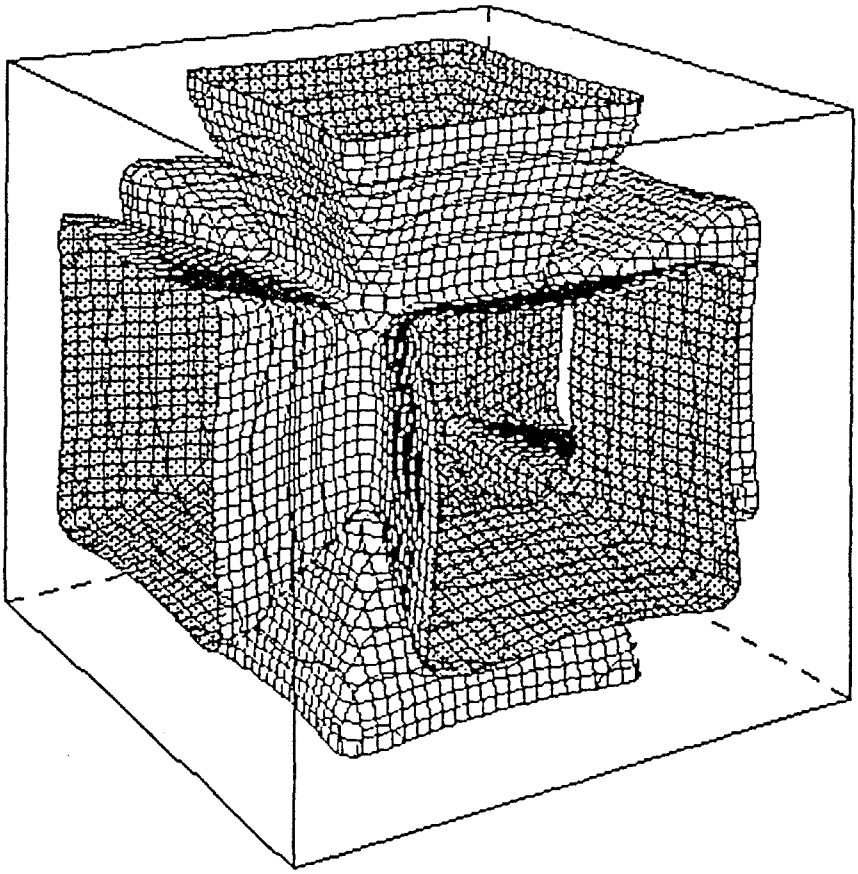

Fig.2-5b The open-type Fermi surface formed by the band 3 (FS-3). The hole region-side of this surface is shaded. The shape of this Fermi surface is almost unchanged within pressure range of 132 ∿ 304 kbar.

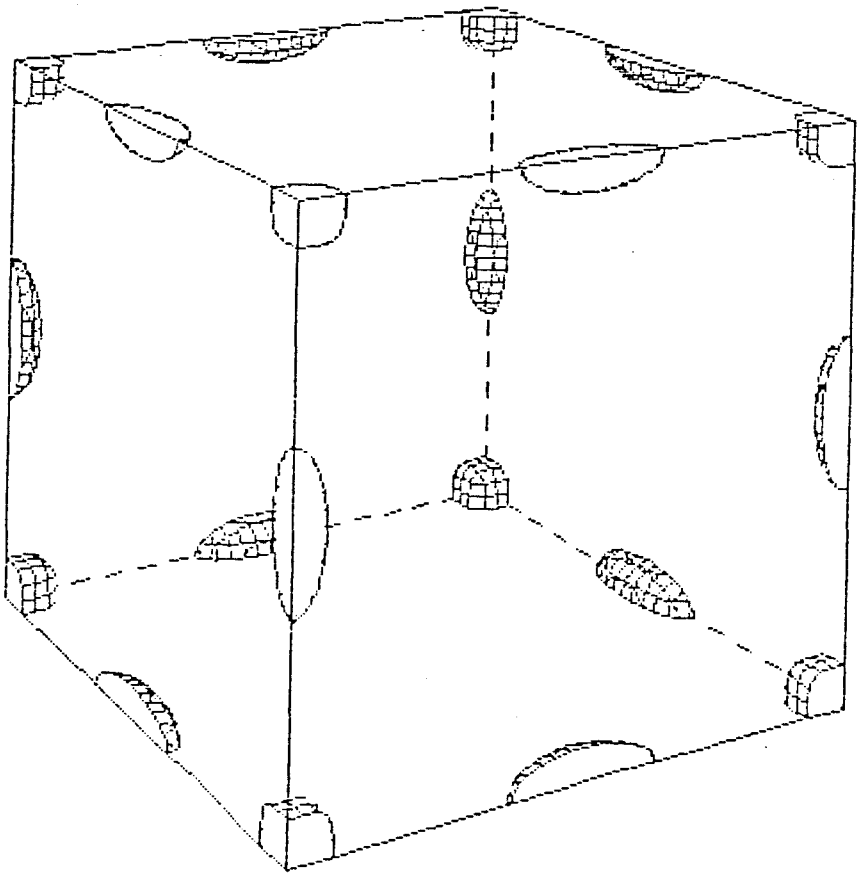

Fig.2-5c Two kinds of Fermi surfaces formed by the band 4 at 132 kbar. We can see 8 fragments of the electron-surfaces (FS-4R) centered at the R points and 12 fragments of the ellipsoidal electron-surfaces (FS-4M) centered at the M points.

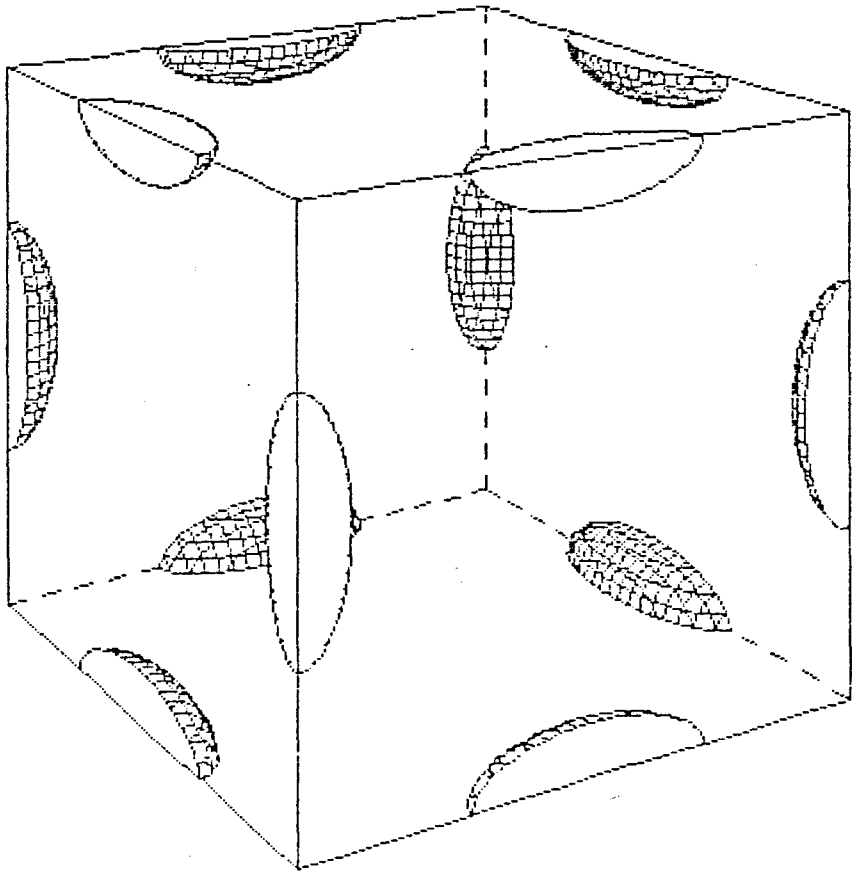

Fig.2-6 The Fermi surface FS-4M at 304 kbar. FS-4R is completely vanishing at this pressure.

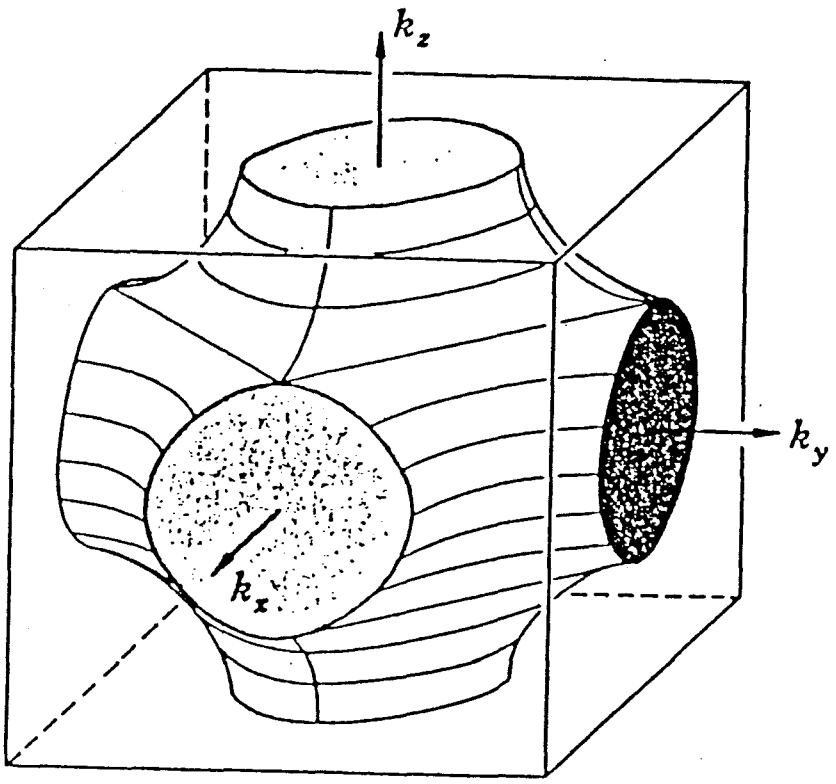

Fig.2-7 A typical example of the Fermi surface for simple cubic lattice found in Kittel's text book.

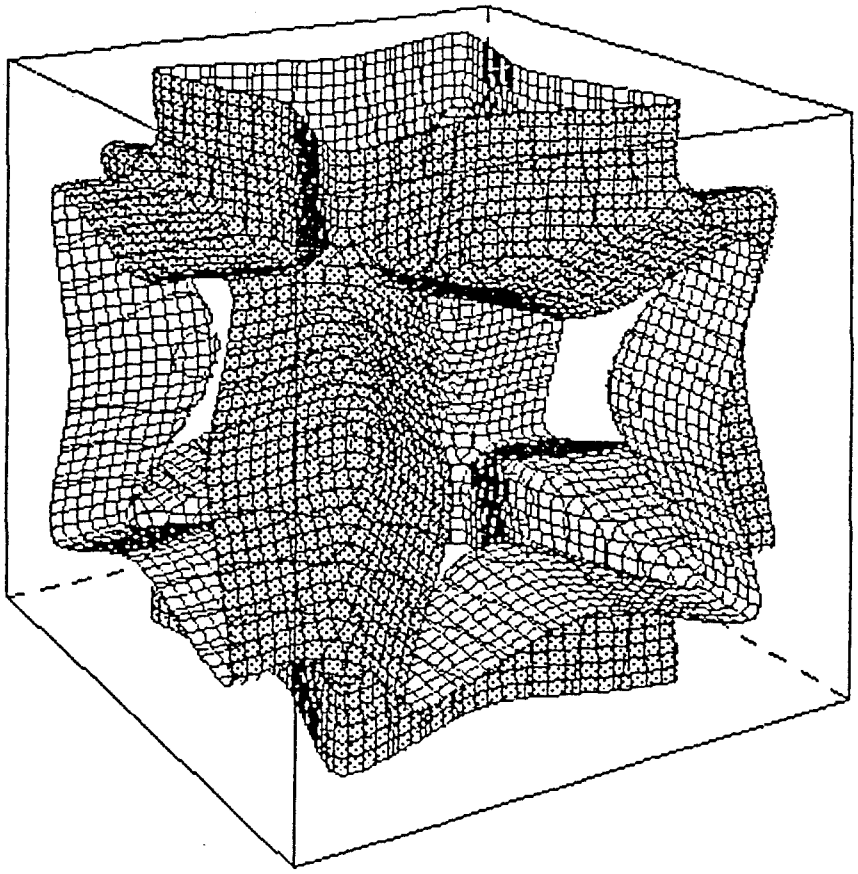

Fig.2-8 The open-type Fermi surface FS-3 displayed in the box which is centered at the R point. Here the 8 corners are the Γ point. The hole-region side is shaded.

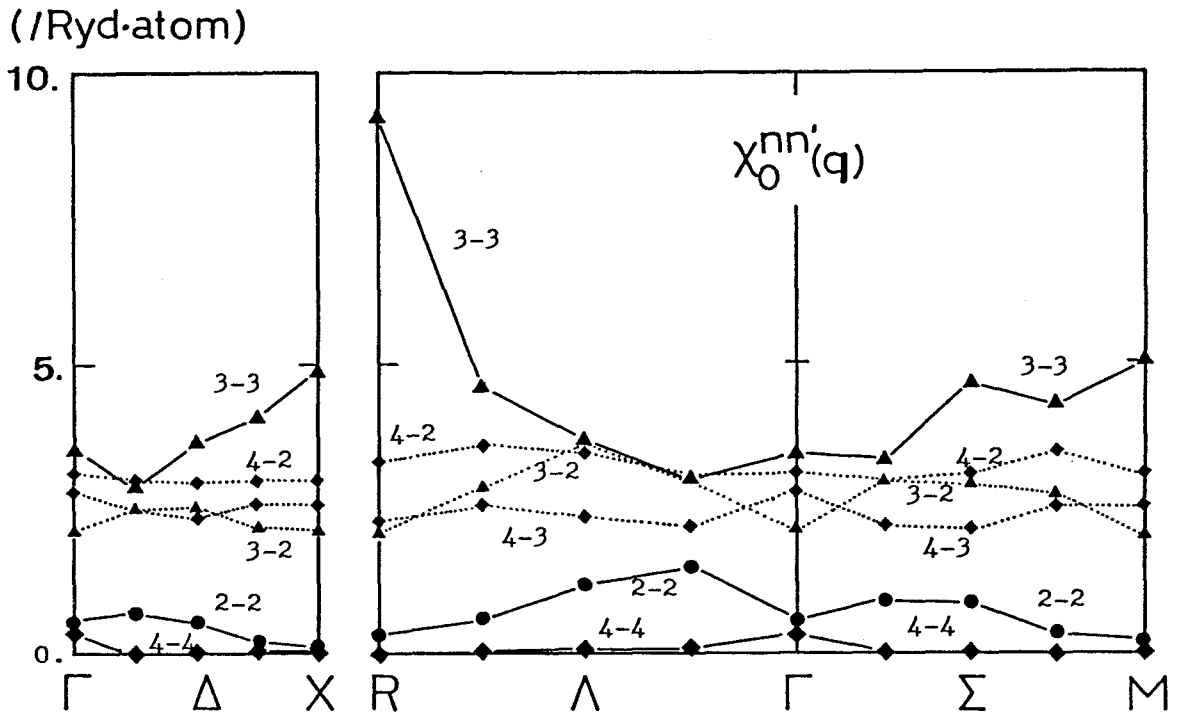

Fig.2-9 The "band-decomposed" electronic susceptibility $\chi_0^{nn'}(q)$ along the Δ, Λ, and Σ lines at 132 kbar. Band suffices are shown by the notation, n-n'.

§3. Electron-Lattice Interaction

3-1 Rigid muffin-tin approximation

The ab initio calculation of the electron-lattice interaction has long been a major problem in the solid state physics. On the basis of the adiabatic (Born-Oppenheimer) approximation, the matrix elements of the electron-lattice interaction, $\mathbf{I}(n\mathbf{k},n'\mathbf{k}') = (I^x(n\mathbf{k},n'\mathbf{k}'), I^y(n\mathbf{k},n'\mathbf{k}'), I^z(n\mathbf{k},n'\mathbf{k}'))$, are defined by

$$\mathbf{u}(\mathbf{q})\cdot\mathbf{I}(n\mathbf{k},n'\mathbf{k}') = \langle n\mathbf{k}|\delta U|n'\mathbf{k}'\rangle \ , \tag{3.1}$$

where δU is a change of the crystal potential $U(\mathbf{r})$ caused by the lattice displacement $\delta\mathbf{R}_\nu=\mathbf{u}(\mathbf{q})\exp(i\mathbf{q}\cdot\mathbf{R}_\nu)$. δU can be written explicitly as

$$\delta U(\mathbf{r}) = \mathbf{u}(\mathbf{q})\cdot\sum_\nu \exp(i\mathbf{q}\cdot\mathbf{R}_\nu)[\partial U(\mathbf{r})/\partial\mathbf{R}_\nu] \ . \tag{3.2}$$

where $\mathbf{R}_\nu$ denotes the position vector of the νth atom. Note that we consider the crystal containing only one atom in the unit cell. From now on $\mathbf{I}(n\mathbf{k},n'\mathbf{k}')$ will be called the electron-lattice matrix elements.

The rigid muffin-tin approximation (RMTA) is based on an assumption that the crystal perturbed by the displacement of the ions may be adequately described by a rigid displacement of the MT potential.[16-19] The form of the MT potential is written as

$$\begin{aligned} U(\mathbf{r}) &= V(|\mathbf{r}-\mathbf{R}_\nu|), && \text{for } \mathbf{r} \text{ inside MT}(\nu) \\ &= V_{const} \ , && \text{for } \mathbf{r} \text{ in intersticial region,} \end{aligned} \tag{3.3}$$

where MT(ν) means the MT sphere of the ν-th ion. Then the RMTA leads to the relations

$$\partial U/\partial R_\nu = (\partial|\mathbf{r}-\mathbf{R}_\nu|/\partial R_\nu)dV/d\rho = -\hat{\rho}V', \quad \text{for } \mathbf{r} \text{ inside MT}(\nu),$$

$$= 0, \quad \text{for elsewhere,} \tag{3.4}$$

where $\rho \equiv |\mathbf{r}-\mathbf{R}_\nu|$, $\hat{\rho} \equiv (\mathbf{r}-\mathbf{R}_\nu)/\rho$. In the RMTA, the effects of the electron screening and the change of potential due to the charge distribution outside the MT spheres are neglected.

The APW function for the eigenstate $|n\mathbf{k}\rangle$ is expressed as[20]

$$\Phi_{n\mathbf{k}}(\mathbf{r}) = \sum_i c_{n\mathbf{k},i}\chi(\mathbf{k}_i,\mathbf{r}) \tag{3.5}$$

$$\chi(\mathbf{k}_i,\mathbf{r}) = \frac{\exp(i\mathbf{k}_i\cdot\mathbf{R}_\nu)}{\sqrt{N\Omega}}\sum_{\ell=0}^{M} i^\ell(2\ell+1)j_\ell(k_iS)\cdot\frac{R_\ell(\rho,E_{n\mathbf{k}})}{R_\ell(S,E_{n\mathbf{k}})}\cdot P_\ell(\hat{\mathbf{k}}_i\cdot\hat{\rho}), \tag{3.6a}$$

for $\mathbf{r}$ inside MT(ν)

$$= \frac{1}{\sqrt{N\Omega}}\exp(i\mathbf{k}\cdot\mathbf{r}), \quad \text{for elsewhere} \tag{3.6b}$$

where Ω denotes the unit cell volume, j_ℓ is the spherical Bessel function of the ℓ-th order, P_ℓ represents the Legendre polynomial, $\mathbf{k}_i \equiv \mathbf{k}+\mathbf{G}_i$ with $\mathbf{G}_i$ being the i-th reciprocal lattice vector, and $\hat{\mathbf{k}}_i = \mathbf{k}_i/|\mathbf{k}_i|$. $R_\ell(\rho,E)$ is the radial wave function corresponing to the energy E, and S denotes the radius of the MT sphere. Substituting eqs.(3.2)-(3.6a) into eq.(3.1), we obtain the following expression for the electron-lattice matrix elemens:

$$I(n\mathbf{k},n'\mathbf{k}')=i\sum_{\ell} U(\ell,\ell+1,E)\ X_{\ell}(n\mathbf{k},n'\mathbf{k}'), \tag{3.7}$$

with

$$U(\ell,\ell+1,E) = \frac{\int_0^S R_{\ell}(\rho,E)V'R_{\ell+1}(\rho,E)\rho^2 d\rho}{\Omega\cdot R_{\ell}(S,E)R_{\ell+1}(S,E)}, \tag{3.8}$$

$$X_{\ell}(n\mathbf{k},n'\mathbf{k}')= \sum_{ij} c^{*}_{n\mathbf{k},i}c_{n'\mathbf{k}',j}\ \Lambda_{\ell}(\mathbf{k}_i,\mathbf{k}'_j). \tag{3.9}$$

where we have considered only the case of energy-conserving scattering of electrons by the lattice displacements, i.e. $E_{n\mathbf{k}}=E_{n'\mathbf{k}'}=E$. Λ_{ℓ} in eq.(3.9) is defined by

$$\Lambda_{\ell}(\mathbf{k}_i,\mathbf{k}'_j)=[\{j_{\ell}(k_iS)j_{\ell+1}(k'_jS)\int \hat{\rho}\ P_{\ell}(\hat{\mathbf{k}}_i\cdot\hat{\rho})P_{\ell+1}(\hat{\mathbf{k}}'_j\cdot\hat{\rho})d\hat{\rho}\ \} - \{\ \mathbf{k}_i \leftrightarrow \mathbf{k}'_j\ \}](2\ell+1)(2\ell+3), \tag{3.10}$$

where $d\hat{\rho}$ stands for $d(\cos\theta)d\phi$ and this integration can be performed analytically. The integration in eq.(3.8) can be easily performed by using radial Schrödinger equations for angular momenta ℓ and $\ell+1$[21], and $U(\ell,\ell+1,E)$ is obtained in a simple form as

$$U(\ell,\ell+1,E) = [(V_{MT}-E)S^2 - \{L_{\ell}(E)S-\ell\}\{L_{\ell+1}(E)S+\ell+2\}]/\Omega, \tag{3.11}$$

where V_{MT} denotes the MT potential on the surface of a MT sphere and $L_{\ell}(E)$ denotes logarithmic derivative defined by

$$L_{\ell}(E) = [d\log\{R_{\ell}(\rho,E)\}/d\rho]_{\rho=S}\ . \tag{3.12}$$

3-2 Electron-lattice matrix element

The electron-lattice interaction of the simple-cubic phosphorus is expected to be fairly strong from following two facts:

(i) The simple-cubic phosphorus is a superconductor with fairly high Tc in spite of the small DOS at the Fermi level.

(ii) It shows second-order-like structural phase transition into the A7 structure at ≈110 kbar as pressure is decreased. Since the A7 structure is described by condensation of the R-point phonon mode of the simple-cubic structure, it is speculated that this structural phase transition is drived by softening of the R-point phonon mode.

In McMillan's theory of superconductivity which will be explained in §4 electron-lattice matrix elements between arbitrary pair of electronic states on the Fermi surface can contribute to superconductivity. As discussed at the end of subsection 2-3, on the other hand, electron-lattice matrix elements between two electronic states on or near the FS-3 whose wave vectors are connected by $\mathbf{Q}=\pi(1,1,1)/a$ are expected to play an important role in frequency softening of the R-point phonon mode. Thus, it is interesting to investigate the electron-lattice matrix elements of simple-cubic phosphorus for various pair of electronic states on or near the Fermi surfaces.

First, we consider a pair of electronic states of the band

3: $|3\mathbf{k}\rangle$ and $|3\mathbf{k}'\rangle$ where $\mathbf{k}=\pi(2,1,0)/2a$ and $\mathbf{k}'=\pi(0,-1,-2)/2a$. These two states have the same energy, and k and k' are located very close to FS-3. Further, note that these wave vectors are connected by the wave vector of the R point, $\mathbf{Q}\equiv\pi(1,1,1)/a$, i.e. $\mathbf{k}-\mathbf{k}'=\mathbf{Q}$. The decompositions of the wawe functions inside the MT sphere have shown that these states are mainly composed by the p state (70%) and the remaining contributions come almost equally from the s- and d-states. At 132 kbar, the MT potential V_{MT} on the surface of a MT sphere has been determined to be -0.4676 Ryd. Now, using the determined transformation coefficients $c_{n\mathbf{k},i}$ and the calculated logarithmic derivatives $L_\ell(E)$, we have calculated $\mathbf{X}_\ell(3\mathbf{k},3\mathbf{k}')$ and $U(\ell,\ell+1,E)$ from eqs.(3.9) and (3.11). The results are shown in Table 3-1. Note that the x- and z-componets of $\mathbf{X}_\ell(3\mathbf{k},3\mathbf{k}')$ vanish exactly from symmetry. The value of $X^y_\ell(3\mathbf{k},3\mathbf{k}')$ decreases very rapidly as ℓ increases. Reflecting the nature of these two states large contributions come from p-d and s-p scattering. We finally obtain $I^y(3\mathbf{k},3\mathbf{k}') = 9.60$ eV/A.

Next, we have chosen the following typical four states out of electronic states of the bands 3 and 4 on the Fermi surfaces: $|3\mathbf{k}_1\rangle$, $|3\mathbf{k}_2\rangle$, $|4\mathbf{k}_3\rangle$, and $|4\mathbf{k}_4\rangle$. As shown in Fig.3-1, $\mathbf{k}_1$ and $\mathbf{k}_2$ lie on FS-3, $\mathbf{k}_3$ on FS-4M, and $\mathbf{k}_4$ on FS-4R. We have calculated the electron-lattice matrix elements for every pair out of these four states. Calculated $U(\ell,\ell+1,E)\cdot\mathbf{X}_\ell(n\mathbf{k},n'\mathbf{k}')$ for ℓ=0-4, and $I(n\mathbf{k},n'\mathbf{k}')$ are presented in Table 3-2. As seen from the table, the electron-lattice matrix element is considerably large for $(3\mathbf{k}_1, 4\mathbf{k}_3)$ and $(3\mathbf{k}_2, 4\mathbf{k}_3)$, i.e. the states on FS-3 are coupled strongly with those on FS-4M by the lattice displacements. For

these pairs the largest contributions are arising from the p-d scattering, whereas the s-p scattering hardly contributes because the electronic states of the band 4 near the M point almost completely consist of d state.

It is noted that the magnitude of the electron-lattice matrix element between $|3\mathbf{k}_1\rangle$ and $|3\mathbf{k}_2\rangle$ ($\mathbf{k}_1-\mathbf{k}_2=\pi(3,1,-3)/10a$) is smaller than that between $|3\mathbf{k}\rangle$ and $|3\mathbf{k}'\rangle$ ($\mathbf{k}-\mathbf{k}'=\mathbf{Q}=\pi(1,1,1)/a$). We further calculated the electron-lattice matrix elements for other various pairs of states $|3\mathbf{k}\rangle$ and $|3\mathbf{k}-\mathbf{q}\rangle$ on or near the FS-3. As the results, we found that the matrix elements take particularly large values for $\mathbf{q}=\mathbf{Q}$. Thus, in accordance with the discussion given at the end of subsection 2-3 we can conclude definitely that a large frequency softening of phonons at the R point will be caused by combined effects of the nesting property of the FS-3 and the strong electron-lattice interaction. We may suggest that the structural phase transition from the simple-cubic structure to A7 structure is related with this expected large frequency-sofetning of the R-point phonons.

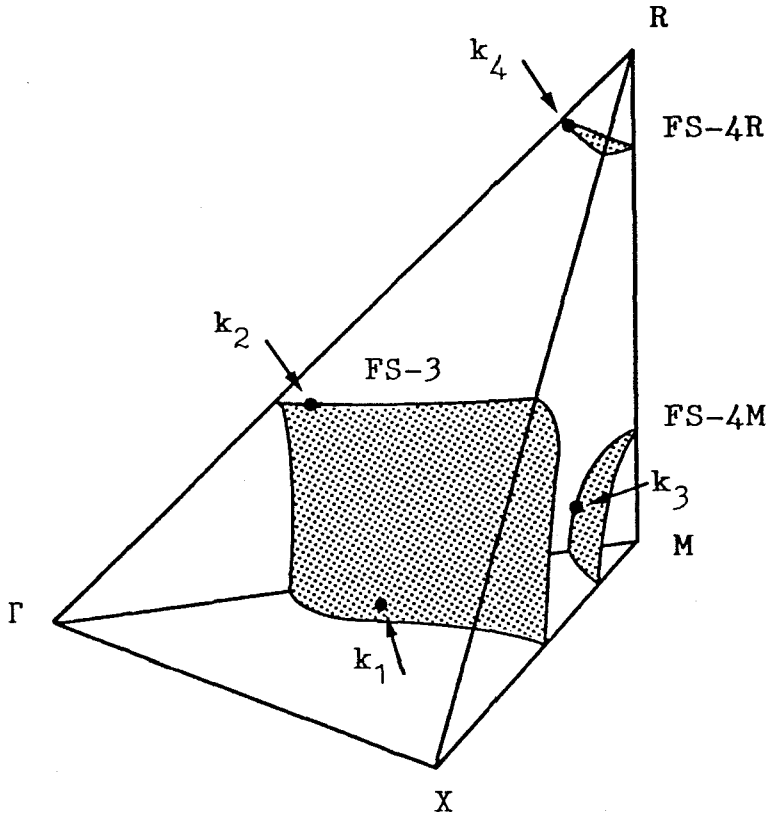

Fig.3-1 Typical four wave vectors chosen for calculating the electron-lattice matrix elements: k_1 and k_2 on FS-3, k_3 on FS-4M and k_4 on FS-4R.

Table 3-1. Electron-lattice matrix elements taken between two electronic states of the band 3, $|3\mathbf{k}\rangle$ and $|3\mathbf{k}'\rangle$, where $\mathbf{k}=\pi(2,1,0)/2a$ and $\mathbf{k}'=\pi(0,-1,-2)/2a$. Note that $\mathbf{k}-\mathbf{k}' = \mathbf{Q} = \pi(1,1,1)/a$.

ℓ		$U(\ell,\ell+1,E)$ [eV/A]	$X^y_\ell(3\mathbf{k},3\mathbf{k}')$	$U \cdot X$ [ev/A]
0	s-p	-2.21	1.337	-2.96
1	p-d	1.44	-4.461	-6.42
2	d-f	1.29	-0.229	-0.29
3	f-g	0.56	0.184	0.10
4	g-h	0.38	-0.052	-0.02

$|I^y(3\mathbf{k},3\mathbf{k}')| = 9.60$ ev/A

Table 3-2. Electron-lattice matrix elements taken between the following pairs of electronic states of the bands 3 and 4:

(1) $(3\mathbf{k}_1, 3\mathbf{k}_2)$, (2) $(3\mathbf{k}_1, 4\mathbf{k}_3)$, (3) $(3\mathbf{k}_1, 4\mathbf{k}_4)$, (4) $(3\mathbf{k}_2, 4\mathbf{k}_3)$, (5) $(3\mathbf{k}_2, 4\mathbf{k}_4)$, (6) $(4\mathbf{k}_3, 4\mathbf{k}_4)$,

where each wave vector is defined by

$\mathbf{k}_1=\pi(26,17,1)/40a$, $\mathbf{k}_2=\pi(14,13,13)/40a$,

$\mathbf{k}_3=\pi(38,38,8)/40a$, $\mathbf{k}_4=\pi(36,35,35)/40a$.

Note that $\mathbf{k}_1$ and $\mathbf{k}_2$ lie on FS-3, $\mathbf{k}_3$ on FS-4M and $\mathbf{k}_4$ on FS-4R.

(1)

ℓ		$U\cdot X_\ell^x$ [eV/A]	$U\cdot X_\ell^y$ [eV/A]	$U\cdot X_\ell^z$ [eV/A]
0	s-p	-1.12	0.68	0.45
1	p-d	-0.63	0.59	-0.44
2	d-f	-0.52	-0.06	0.30
3	f-g	0.02	-0.03	0.00
4	g-h	0.00	0.00	0.00
$\lvert I^\alpha(3\mathbf{k}_1,3\mathbf{k}_2)\rvert$		2.25	1.18	0.31

(2)

ℓ		$U\cdot X_\ell^x$	$U\cdot X_\ell^y$	$U\cdot X_\ell^z$
0	s-p	-0.14	-0.10	0.01
1	p-d	**5.17**	-0.24	-0.05
2	d-f	0.15	0.74	0.11
3	f-g	-0.01	0.00	0.00
4	g-h	0.00	0.00	0.00
$\lvert I^\alpha(3\mathbf{k}_1,4\mathbf{k}_3)\rvert$		**5.17**	0.40	0.07

Table 3-2. (continued)

(3)

ℓ		$U \cdot X_\ell^x$ [eV/A]	$U \cdot X_\ell^y$ [eV/A]	$U \cdot X_\ell^z$ [eV/A]
0	s-p	-0.44	2.22	-0.63
1	p-d	0.02	-0.85	0.26
2	d-f	-0.06	-0.40	-0.08
3	f-g	-0.06	-0.05	0.01
4	g-h	0.00	0.00	0.00
$\lvert I^\alpha(3\mathbf{k}_1, 4\mathbf{k}_4)\rvert$		0.54	0.92	0.44

(4)

ℓ		$U \cdot X_\ell^x$	$U \cdot X_\ell^y$	$U \cdot X_\ell^z$
0	s-p	-0.01	0.03	0.01
1	p-d	2.26	-4.92	0.02
2	d-f	0.00	-0.67	-0.01
3	f-g	0.00	0.01	0.00
4	g-h	0.00	0.00	0.00
$\lvert I^\alpha(3\mathbf{k}_2, 4\mathbf{k}_3)\rvert$		2.25	5.55	0.02

(5)

ℓ		$U \cdot X_\ell^x$	$U \cdot X_\ell^y$	$U \cdot X_\ell^z$
0	s-p	-2.26	1.05	1.05
1	p-d	0.33	-0.39	-0.39
2	d-f	0.23	-0.17	-0.17
3	f-g	0.03	-0.01	-0.01
4	g-h	-0.01	0.01	0.01
$\lvert I^\alpha(3\mathbf{k}_2, 4\mathbf{k}_3)\rvert$		1.68	0.49	0.49

Table 3-2. (continued)

(6)

ℓ		$U \cdot X_\ell^x$ [eV/A]	$U \cdot X_\ell^y$ [eV/A]	$U \cdot X_\ell^z$ [eV/A]
0	s-p	-0.31	-0.32	0.03
1	p-d	2.45	1.71	0.14
2	d-f	-0.21	-0.10	-0.12
3	f-g	-0.03	-0.02	0.00
4	g-h	0.00	0.00	0.00
$\lvert I^\alpha(4\mathbf{k}_3, 4\mathbf{k}_4)\rvert$		1.90	1.27	0.05

§4. Superconducting Transition Temperature T_c

4-1. Electron-phonon mass enhancement parameter λ

McMillan[22] has proposed a semi-empirical equation to determine the superconducting transition temperarture T_c by using the strong-coupled theory of superconductivity. Later, Allen and Dynes[23] have proposed the following improved equation for T_c by modifying the McMillan's equation:

$$k_B T_c = \frac{\langle\omega\rangle}{1.2} \exp\left\{ \frac{-1.04(1+\lambda)}{\lambda-\mu^*(1+0.62\lambda)} \right\} . \tag{4.1}$$

Here $\langle\omega\rangle$ denotes a kind of averaged phonon frequency, μ^* represents the effective electron-electron repulsion constant, and λ is the so-called electron-phonon mass enhancement parameter defined by

$$\lambda \equiv 2\int_0^\infty d\omega \frac{\alpha^2F(\omega)}{\omega} , \tag{4.2}$$

where $\alpha^2F(\omega)$ represents the spectral function of the electron-lattice interaction and can be written as

$$\alpha^2F(\omega) \equiv D(E_F) \frac{1}{2M\omega} \ll \sum_\gamma |\varepsilon_{\gamma \mathbf{k}-\mathbf{k}'} \cdot \mathbf{I}(n\mathbf{k},n'\mathbf{k}')|^2 \delta(\omega-\omega_{\gamma \mathbf{k}-\mathbf{k}'}) \gg_{FS} . \tag{4.3}$$

In the above equation $D(E_F)$ is the electronic DOS (per atom·spin)

at the Fermi level, $\omega_{\gamma q}$ and $\varepsilon_{\gamma q}$ denote the frequency and the polarization vector, respectively, of a phonon of wave vector q and mode γ, M is the mass of the ion, and $\langle\langle f(nk,n'k')\rangle\rangle_{FS}$ means that the average of an arbitraly function f which depends on a pair of states $(nk,n'k')$ is taken over the FS, namely,

$$\langle\langle f(nk,n'k')\rangle\rangle_{FS} \equiv \frac{\sum_{nkn'k'} \delta(E_{nk}-E_F)\delta(E_{n'k'}-E_F) f(nk,n'k')}{\sum_{nkn'k'} \delta(E_{nk}-E_F)\delta(E_{n'k'}-E_F)} . \tag{4.4}$$

We note that eq.(4.2) can be rewritten as

$$\lambda = D(E_F)\langle\langle \sum_{\gamma} \frac{|\varepsilon_{\gamma k-k'} \cdot I(nk,n'k')|^2}{M\omega^2_{\gamma k-k'}} \rangle\rangle_{FS} . \tag{4.5}$$

Further, if we neglect the mode dependence of the phonon frequencies, then eq.(4.5) can be transformed into a simplified form as

$$\lambda = D(E_F)\langle\langle \frac{|I(nk,n'k')|^2}{M\omega^2_{k-k'}} \rangle\rangle_{FS}, \tag{4.6}$$

by using the orthogonality relation of the phonon polarization vectors, i.e.

$$\sum_{\gamma} [\varepsilon^{\alpha}_{\gamma q}]^* \varepsilon^{\beta}_{\gamma q} = \delta_{\alpha\beta} . \tag{4.7}$$

The original definition of the averaged phonon frequency $\langle\omega\rangle$

given by Allen-Dynes is

$$\log\langle\omega\rangle \equiv \frac{\int_0^\infty d\omega\ \log\omega\ \frac{\alpha^2F(\omega)}{\omega}}{\int_0^\infty d\omega\ \frac{\alpha^2F(\omega)}{\omega}} = \frac{2}{\lambda}\int_0^\infty d\omega\ \log\omega\ \frac{\alpha^2F(\omega)}{\omega}\ . \qquad (4.8)$$

A central problem in evaluating the transition temperature is the estimation of λ, and the most difficult task in calculating λ from eq.(4.5) or eq.(4.6) is how to perform the averaging over the Fermi surface. Gaspari-Gyorffy[18] have proposed an approximate method for estimating λ, and their method has been widely applied, particularly to systems with complicated-shaped Fermi surfaces.[18,21] However, the shapes of the FS of the simple cubic phosphorus are not so complicated, and hence it is possible to perform the numerical average over the Fermi surfaces without great difficulty as described in the following.

In general, eq.(4.4) can be expressed in terms of the integrals over each FS as follows:

$$\langle\langle f(n\mathbf{k},n'\mathbf{k}')\rangle\rangle_{FS}$$

$$= \sum_{nn'}\int\frac{d^2k}{v_{n\mathbf{k}}}\int\frac{d^2k'}{v_{n'\mathbf{k}'}}\ f(n\mathbf{k},n'\mathbf{k}')\Big/\left(\sum_n\int\frac{d^2k}{v_{n\mathbf{k}}}\right)^2, \qquad (4.9)$$

where $v_{n\mathbf{k}} \equiv |\partial E_{n\mathbf{k}}/\partial k|$. If the Fermi velocity $v_{n\mathbf{k}}$ does not depend on wave vector $\mathbf{k}$ on each FS, eq.(4.9) can be further rewritten as

$$\langle\langle f(n\mathbf{k},n'\mathbf{k}')\rangle\rangle_{FS} = \sum_{nn'} \eta_n \eta_{n'} \frac{\sum_{\mathbf{k}_n}\sum_{\mathbf{k}'_{n'}} f(n\mathbf{k}_n,n'\mathbf{k}'_{n'})}{\sum_{\mathbf{k}_n}\sum_{\mathbf{k}'_{n'}} 1}, \qquad (4.10)$$

where $\mathbf{k}_n$ denotes a wave vector on the FS formed by the band n, and $\eta_n \equiv D_n(E_F)/D(E_F)$ with $D_n(E_F)$ being the partial DOS at the Fermi level arising from the band n. We employ eq.(4.10) in estimating the value of the electron-phonon mass enhancement parameter λ.

In order to estimate λ we need knowledge about phonons. However, there has been neither experimental nor theoretical study for lattice dynamics of simple-cubic phosphorus. Therefore we have calculated the phonon frequencies from bulk modulus by assuming a simple form of dispersion. Our recipe is summarized as follows:

(1) Evaluate the bulk modulus $B=-V(dP/dV)$ from Murnaghan equation of state,

$$P=(K_0/K')[(\Omega_0/\Omega)^{K'}-1], \qquad (4.11)$$

where Ω is the unit cell volume. The constants K_0, K', and Ω_0 have been determined by Kikegawa and Iwasaki[1] as: K_0=95 GPa, K'=2.1, Ω_0=15.2 A^3.

(2) Evaluate the longitudinal sound velocity v_s along the [100] direction from

$$v_s = \left[\frac{3B(1-\sigma)}{\rho(1+\sigma)} \right]^{1/2}, \tag{4.12}$$

where ρ is the mass density and σ denotes the Poisson's ratio defined by $\sigma \equiv C_{12}/(C_{11}+C_{12})$. Eq.(4.12) is obtained by using the relations, $v_s=(C_{11}/\rho)^{1/2}$ and $B=(C_{11}+2C_{12})/3$.

(3) Assume the following simple form of phonon dispersion:

$$\omega_{\mathbf{q}} = \omega_X[\sin^2(q_x a/2) + \sin^2(q_y a/2) + \sin^2(q_z a/2)]^{1/2}. \tag{4.13}$$

Then, we obtain the following relation

$$\omega_X = 2v_s/a. \tag{4.14}$$

In the above procedure the Poisson's ratio is an unknown parameter. In a fluid medium we obtain $\sigma=1/2$. This value is reduced in actual metals: for example, σ= 0.28 (Mo,W), 0.36∿0.37 (Al,Ni), 0.42∿0.46 (Cu,Ag,K,Na,Pb,Au,Li). Therefore, we have assumed the following three cases for the value of σ: (a) σ=0.36, (b) σ=0.40, and (c) σ=0.5. The values of the bulk modulus B evaluated at 132 kbar and 304 kbar are listed in column 3 of Table 4-1. The values of ω_X evaluated for each case assumed above are also listed in Table 4-1. Very recently Chang et al.[24] have calculated the phonon frequencies at several symmetry points in the Brillouin zone on the basis of the frozen-phonon method with use of the pseudopotential band calculation. The frequency of the longitudinal phonon at the X point obtained by

them is 4.19×10^{13} rad/s at 120 kbar and 5.16×10^{13} rad/s at 300 kbar, which are not far from the values of ω_X estimated by us.

By using eq.(4.13), eq.(4.6) can be rewritten as

$$\lambda = \frac{D(E_F)\xi}{M(\omega_X)^2}, \tag{4.15}$$

where ξ is defined by

$$\xi = \langle\langle \frac{|I(nk,n'k')|^2}{(\omega_{k-k'}/\omega_X)^2} \rangle\rangle_{FS} . \tag{4.16}$$

From now on ξ is called the strength of averaged electron-lattice matrix elements. It should be noted that ξ is independent of the value of ω_X.

Table 4-1. Bulk modulus B estimated by using Murnaghan equation (4.11). The value of ω_X has been evaluated from eqs.(4.12) and (4.14) for three cases with different value of Poisson's ratio σ; (a) σ=0.36, (b) σ=0.40, (c) σ=0.50.

P [kbar]	V [A^3]	B [GPa]	σ	ω_X[10^{13}rad/s]
132	13.3	126	(a)	5.72
			(b)	5.46
			(c)	4.82
304	12.0	156	(a)	6.26
			(b)	5.97
			(c)	5.27

4-2 Evaluation of T_c

In order to evaluate the transition temperature T_c from eq.(4.1) we first estimate the value of the electron-phonon mass enhancement parameter λ from eqs.(4.15) and (4.16).

To calculate ξ for 132 kbar, we have selected 336 k-points on the Fermi surfaces in the Brillouin zone: 48 k-points on FS-2, 144 k-points on FS-3, 48 k-points on FS-4R, and 96 k-points on FS-4M. The average over FS in eq.(4.16) have been performed by making use of eq.(4.10). All of possible pairs out of the above k-points are taken into account in the calculation. The value of ξ obtained for 132 kbar and the contribution to ξ from each FS are presented in Table 4-2. Large contributions arise from the scattering between the states on FS-3 and those on FS-3, FS-2 or FS-4M.

The calculation of ξ for 304 kbar has been carried out by using 288 k-points in the Brillouin zone: 48 k-points on FS-2, 144 k-points on FS-3, and 96 k-points on FS-4M. At this pressure FS-4R vanish completely. The results are presented also in Table 4-2. It must be noted that the contribution arising from the scattering between the states on FS-3 and those on FS-4M considerably increase with increasing pressure. This is due to the increase of the partial DOS arising from FS-4M. Even if we neglect the k-dependence of the phonon frequencies in eq.(4.13), similar dependence on pressure are obtained. Therefore the averaged electron-lattice matrix elements ξ are enhanced by the increase of the partial DOS arising from FS-4R, which consists of d-like states.

The electron-phonon mass enhancement parameter λ has been estimated for both pressure, 132 kbar and 304 kbar, by substituting ξ, $D(E_F)$, and ω_X into the right-hand side of eq.(4.15). The values of $D(E_F)$ are listed in Table 2-1. The value of ω_X has been evaluated from eqs.(4.12) and (4.14) for three cases with different value of Poisson's ratio σ (see Table 4-1). The value of λ estimated in this way are presented in Table 4-3. The value of λ ranges from $0.4 \sim 0.6$, and hence simple-cubic phosphorus is regarded as a superconductor with fairly strong electron-phonon coupling. As seen from Table 4-3 the value of λ is almost independent of pressure in spite of considerable increase of ξ with increasing pressure. This is because the increase of ξ is compensated by the increase of the phonon frequency ω_X.†

---

† Very recently, on the basis of total energy calculation by using the pseudpotential method Chang et al.[24] have calculated the phonon frequencies at the X and M points and the matrix elements of electron-phonon interaction associated with these phonons. Their results show also that the electron-lattice interaction is strong in simple-cubic phosphorus. Further, they have calculated the q-dependent electron-phonon mass enhancement parameter λ_q which may be defined by the same expression as eq.(4.5) provided that the average is taken for a fixed value of $\mathbf{k}-\mathbf{k}'=\mathbf{q}$. However, Chang et al. have not calculated the total λ and the transition temperature T_c. According to their results the values of λ_q obtained for $q=q_X$ and q_M show rather decreasing

trend with increasing pressure.

Now, the superconducting transition temperature Tc can be evaluated from McMillan-Allen-Dynes equation (4.1) if we know the values of μ^* and $\langle\omega\rangle$. We evaluate the value of the Coulomb repulsion parameter μ^* by using Bennemann-Garland's empirical formula:[25)]

$$\mu^* = 0.26N(E_F)/[1+N(E_F)], \tag{4.17}$$

where $N(E_F)$ denotes the electronic DOS at the Fermi level (in unit of per eV·atom). The original definition of $\langle\omega\rangle$ is the logarithmic average of phonon frequencies with respect to the spectral function $\alpha^2F(\omega)$ as expressed by eq.(4.8). For simplicity, however, we have evaluated $\langle\omega\rangle$ by using the phonon DOS $F(\omega)$ corresponding to our simplified phonon dispersion given by eq.(4.13) instaed of $\alpha^2F(\omega)$, i.e.

$$\log\langle\omega\rangle = \left\{ \frac{\sum_{\mathbf{q}} (\log\omega_{\mathbf{q}})/\omega_{\mathbf{q}}}{\sum_{\mathbf{q}} 1/\omega_{\mathbf{q}}} \right\} . \tag{4.18}$$

The summation over the Brillouin zone in the above equation has been carried out by using Monte Calro method with use of 5,000,000 sampling points. Then we have obtained $\langle\omega\rangle = 1.03\omega_X$.

We have evaluated the transition temperature T_c by using the values of λ, μ^* and $\langle\omega\rangle$ determined above. The results are shown in Table 4-3. As seen from the table, the value of T_c depends

somewhat on the choice of the value of σ. However, we would like to emphasize that the experimental value of T_c= 5∿11 K[4-8] has been reproduced in order of magnitude by our microscopic calculation based on the McMillan-Allen-Dynes theory. Therefore we are convinced that the superconductivity of simple-cubic phosphorus are well understood within the strong coupling theory of the BCS mechanism. If we assume that Poisson's ratio is independent of pressure, we expect that Tc increases only by ∿1K when pressure is increased from 132 kbar to 304 kbar. According to experimental results by Wittig et al.[4] and by Akahama et al.[7] the observed T_c shows larger pressure dependence. In order to discuss more precisely the pressure effect on T_c as well as the magnitude of T_c we need to study the lattice dynamics in detail. In particular it will be necessary to take account of softening behavior of phonons around the R point, which is expected as discussed in subsections 2-3 and 3-2.

Table 4-2. Calculated values of the strength of the electron-lattice interaction, ξ [eV^2/A^2]. ξ_{ij} [eV^2/A^2] represents the contribution from a pair of Fermi surfaces, FS-i and FS-j. ξ can be written as

$$\xi = \sum_i \sum_j \xi_{ij} \quad .$$

The weighting factor $W_{ij} \equiv \eta_i \eta_j$ arising from partial DOS is also presented.

FS		132 kbar		304 kbar	
i	j	W_{ij}	ξ_{ij}	W_{ij}	ξ_{ij}
2	2	0.014	0.58	0.010	0.45
3	2	0.094	4.75	0.075	4.18
3	3	0.653	14.76	0.561	14.25
4R	2	0.002	0.04	0.	0.
4R	3	0.013	0.30	0.	0.
4R	4R	0.000	0.02	0.	0.
4M	2	0.007	0.37	0.015	0.83
4M	3	0.048	2.42	0.113	5.61
4M	4R	0.001	0.02	0.	0.
4M	4M	0.003	0.00	0.023	0.06
total			ξ= 31.16		ξ= 35.99

Table 4-3. Values of λ and Tc evaluated for three cases with different value of Poisson's ratio: (a) σ=0.36, (b) σ=0.40, (c) σ=0.50. Coulomb repulsion parameter μ^* has been evaluated from Bennemann-Garland's empirical formula.

P [kbar]	μ^*	σ	λ	Tc [K]
132	0.10	(a)	0.44	3.3
		(b)	0.48	4.7
		(c)	0.62	9.8
304	0.10	(a)	0.45	3.7
		(b)	0.49	5.3
		(c)	0.63	11.0

§5. Summary

On the basis of the self-consistent APW method we calculated first the electronic band strucutre of simple-cubic phosphorus at 132 kbar (a=2.369 A) and at 304 kbar (a=2.298 A). Then, the electron-lattice interaction was studied within the rigid muffin-tin approximation, and the electron-phonon mass enhancement parameter λ was estimated with use of the calculated electron-lattice matrix elements and the phonon frequencies evaluated from the observed bulk modulus. Finally, the superconducting transition temperature T_c was evaluated in accordance with the McMillan-Allen-Dynes equation.

The results obtained in this part II are summarized as follows:

(a) The energy dispersion curves below the Fermi level are similar to those of free electrons in the empty lattice. The density of states at the Fermi level $D(E_F)$ is small and its pressure dependence is quite small: $D(E_F)$ = 2.10 per Ryd·atom·spin at 132 kbar and $D(E_F)$ = 2.13 per Ryd·atom·spin at 304 kbar.

(b) Four kinds of Fermi surfaces are obtained at 132 kbar.
   (1) FS-2: Dice-shaped hole pocket around the Γ point.
   (2) FS-3: Open-type Fermi surface with six necks which intersect the faces of the zone boundary.
   (3) FS-4R: Small electron pocket around the R point.
   (4) FS-4M: Ellipsoidal electron pocket around the M point.

At 304 kbar FS-4R vanishes completely and FS-4M is expanded remarkably whereas FS-2 and FS-3 are almost independent of pressure within this pressure range. The electronic states on FS-4M consist mainly of d-states.

(c) Simple-cubic phosphorus is a system with strong electron-lattice interaction. The strength of averaged electron-lattice matrix elements, ξ, shows a fairly large increase when pressure is increased: $\xi=31.16\ eV^2/A^2$ at 132 kbar and $\xi=35.99\ eV^2/A^2$ at 304 kbar. This increase is ascribed to expansion of FS-4M with increasing pressure. On the other hand, the estimated value of λ ($= 0.4 \sim 0.6$) is almost independent of pressure if we assume pressure-independent Poisson's ratio which was introduced to estimate the phonon frequencies.

(d) The superconducting transition temperature Tc is evaluated to be a few K $\sim$ 10 K, which agrees in order of magnitude with the observation. Detailed and more realistic study of the lattice dynamics is desired to discuss precisely the pressure effects on T_c as well as the magnitude of T_c.

(e) Large frequency softening of phonons at the R point is expected because of the nearly-perfect nesting property of the FS-3 as well as the strong electron-lattice interaction.

REFERENCES OF PART II

1. T. Kikegawa and H. Iwasaki: Acta Cryst. B39 (1983) 158.
2. T. Sasaki and A. Morita: presented at 40th Annual Conference of Physical Society of Japan, Kyoto (1985).
3. K.J. Chang and M.L. Cohen: Phys. Rev. B33 (1986) 6177.
4. J. Wittig, B.Bireckoven and T. Weidlich: Solid State Physics Under Pressure: Recent Advance with Anvil Devices, ed. by S. Minomura (KTK Scientific publisher, Tokyo, 1985), p,217.
5. H. Kawamura, I. Shirotani and K. Tachikawa: Solid State Commun. 49 (1985) 879.
6. H. Kawamura, I. Shirotani and K. Tachikawa: Solid State Commun. 54 (1985) 775.
7. Y. Akahama, S. Endo and E. Fujita: (private commun.)
8. I.V. Berman and N.B. Brandt: JETP Letter 7 (1968) 994.
9. D.D. Koelling and B.N. Harmon: J. Phys. C 10 (1977) 3101.
10. O. Gunnarsson and B.I. Lundqvist: Phys. Rev. B13 (1976) 4274.
11. D.J. Chadi and M.L. Cohen: Phys. Rev. B8 (1973) 5747.
12. We have used the computer subroutines of cubic spline of ACOS Advanced Scientific Library supported by NEC.
13. G. Lehmann and T.Taut: phys. stat. sol. (b) 54 (1972) 469.
14. C. Kittel: Introduction to Solid State Physics, 5th edition (Wiley, 1976) p. 260.
15. R.E. Peierls: Quantum Theory of Solids, (Oxford, 1968).
16. D.C. Golibersuch: Phys. Rev. 157 (1967) 532.
17. S.K. Shinha: Phys. Rev. 169 (1968) 477.

18. G.D. Gaspari and B.L. Gyorffy: Phys. Rev. Lett. 28 (1972) 801.

19. G.Grimvall: The Electron~Phonon Interaction in Metals, E.P. Wohlfarth, ed. (North-Holand, Amsterdam, 1981).

20. T.L. Loucks: Augmented Plane Wave Method, (W.A. Benjamin, Inc., New Tork, 1967).

21. R. Evans, G.D. Gaspari and B.L. Gyorffy: J. Phys. F 3 (1973) 39.

22. W.L. McMillan: Phys. Rev. 167 (1968) 331.

23. D.B. Allen and R.C. Dynes: Phys. Rev. B12 (1975) 905.

24. K.J. Chang and M.L. Cohen: Phys. Rev. B33 (1986) 7371.

25. K.H. Bennemann and J.W.Garland: Proc. of the Conf. on Superconductivity in d- and f-band Metals, Rochester, 1971, D.H. Douglas, ed. (AIP, New York, 1972) p. 103.

List of Publications

1. N. Suzuki and M. Aoki:

   Interplanar Forces of Black Phosphorus Caused by Electron-Lattice Interaction

   Solid State Commun. **61** (1987) 595-600.